



**HAL**  
open science

## Specific Recruitment of Phosphoinositide Species to the Plant-Pathogen

Li Qin, Zhuqing Zhou, Qiang Li, Chun Zhai, Lijiang Liu, Teagen Quilichini, Peng Gao, Sharon Kessler, Yvon Jaillais, Raju Datla, et al.

► **To cite this version:**

Li Qin, Zhuqing Zhou, Qiang Li, Chun Zhai, Lijiang Liu, et al.. Specific Recruitment of Phosphoinositide Species to the Plant-Pathogen. *The Plant cell*, 2020, 32 (5), pp.1665-1688. 10.1105/tpc.19.00970 . hal-02568171

**HAL Id: hal-02568171**

**<https://hal.science/hal-02568171v1>**

Submitted on 8 May 2020

**HAL** is a multi-disciplinary open access archive for the deposit and dissemination of scientific research documents, whether they are published or not. The documents may come from teaching and research institutions in France or abroad, or from public or private research centers.

L'archive ouverte pluridisciplinaire **HAL**, est destinée au dépôt et à la diffusion de documents scientifiques de niveau recherche, publiés ou non, émanant des établissements d'enseignement et de recherche français ou étrangers, des laboratoires publics ou privés.

1 **RESEARCH ARTICLE**

2  
3 **Specific Recruitment of Phosphoinositide Species to the Plant–Pathogen**  
4 **Interfacial Membrane Underlies Arabidopsis Susceptibility to Fungal**  
5 **Infection**

6  
7 **Li Qin,<sup>a,1</sup> Zhuqing Zhou,<sup>b,1</sup> Qiang Li,<sup>a</sup> Chun Zhai,<sup>c</sup> Lijiang Liu,<sup>a,d</sup> Teagen D. Quilichini,<sup>e</sup> Peng Gao,<sup>f</sup>**  
8 **Sharon A. Kessler,<sup>g</sup> Yvon Jaillais,<sup>h</sup> Raju Datla,<sup>f</sup> Gary Peng,<sup>c</sup> Daoquan Xiang,<sup>e</sup> and Yangdou Wei<sup>a,2</sup>**  
9

10 <sup>a</sup>Department of Biology, University of Saskatchewan, Saskatoon, SK S7N 5E2, Canada

11 <sup>b</sup>Laboratory of Cell Biology, College of Life Science and Technology, Huazhong Agricultural University,  
12 Wuhan, Hubei 430070, China

13 <sup>c</sup>Saskatoon Research and Development Centre, Agriculture and Agri-Food Canada, Saskatoon, SK S7N  
14 0X2, Canada

15 <sup>d</sup>Key Laboratory of Biology and Genetic Improvement of Oil Crops, Ministry of Agriculture, Oil Crops  
16 Research Institute, Chinese Academy of Agricultural Sciences, Wuhan, Hubei 430062, China

17 <sup>e</sup>National Research Council Canada, Saskatoon, SK, S7N 0W9, Canada

18 <sup>f</sup>Global Institute for Food Security, University of Saskatchewan, Saskatoon, SK S7N 0W9, Canada

19 <sup>g</sup>Department of Botany and Plant Pathology, Purdue University, West Lafayette, Indiana 47907, USA

20 <sup>h</sup>Laboratoire Reproduction et Développement des Plantes, Université de Lyon, ENS de Lyon, UCB Lyon  
21 1, CNRS, INRA, Lyon 69342, France

22  
23 **Short title:** PI(4,5)P<sub>2</sub> as a susceptibility factor for plant disease

24  
25 **One-sentence summary:** Plant biotrophic and hemibiotrophic pathogens modulate cellular  
26 distribution of host phosphoinositides and recruit PI(4,5)P<sub>2</sub> to the plant-pathogen interfacial  
27 membrane as a susceptibility factor for disease development.

28  
29 <sup>1</sup>These authors contributed equally to this work.

30 <sup>2</sup>Address correspondence to [yangdou.wei@usask.ca](mailto:yangdou.wei@usask.ca).

31  
32 The author responsible for distribution of materials integral to the findings presented in this  
33 article in accordance with the policy described in the Instructions for Authors ([www.plantcell.org](http://www.plantcell.org))  
34 is: Yangdou Wei ([yangdou.wei@usask.ca](mailto:yangdou.wei@usask.ca)).  
35

36 **ABSTRACT**

37 Different phosphoinositides enriched at the membranes of specific subcellular compartments  
38 within plant cells contribute to organelle identity, ensuring appropriate cellular trafficking and  
39 function. During the infection of plant cells, biotrophic pathogens such as powdery mildews  
40 enter plant cells and differentiate into haustoria. Each haustorium is enveloped by an  
41 extrahaustorial membrane (EHM) derived from the host plasma membrane. Little is known about  
42 the EHM biogenesis and identity. Here, we demonstrate that among the two plasma membrane

43 phosphoinositides in *Arabidopsis thaliana*, PI(4,5)P<sub>2</sub> is dynamically up-regulated at powdery  
44 mildew infection sites and recruited to the EHM, whereas PI4P is absent in the EHM. Lateral  
45 transport of PI(4,5)P<sub>2</sub> into the EHM occurs through a Brefeldin A-insensitive but actin-  
46 dependent trafficking pathway. Furthermore, the lower levels of PI(4,5)P<sub>2</sub> in *pip5k1 pip5k2*  
47 mutants inhibit fungal pathogen development and cause disease resistance, independent of cell  
48 death-associated defenses and involving impaired host susceptibility. Our results reveal that plant  
49 biotrophic and hemibiotrophic pathogens modulate the subcellular distribution of host  
50 phosphoinositides and recruit PI(4,5)P<sub>2</sub> as a susceptibility factor for plant disease.

51

52 **KEY WORDS:** Haustorium, Extrahaustorial membrane, Biotroph, Hemibiotroph, Susceptibility,  
53 Plant immunity, Phosphoinositide, Cellular trafficking, Membrane lipid, Membrane domain

54

## 55 INTRODUCTION

56 Filamentous phytopathogens have evolved numerous strategies to gain nutrients from host plants,  
57 but arguably one of the most specialized among these is that of the biotrophic fungi and  
58 oomycetes, which feed only on living plant cells to support their growth and propagation. These  
59 pathogens consist of a diverse range of species from phylogenetically distinct groups: the fungal  
60 powdery mildews (Ascomycetes) and rusts (Basidiomycetes) and the oomycete downy mildews,  
61 cause substantial economic losses in major agricultural crops and environmental destruction in  
62 natural ecosystems. A distinguishing feature of these obligate biotrophs is the formation of a  
63 feeding structure called a haustorium, which forms inside the host cell after a specialized fungal  
64 hypha penetrates the plant cell wall. The haustorium, however, remains separated from the host  
65 cell cytoplasm, surrounded by a highly modified membrane, the extrahaustorial membrane  
66 (EHM), derived from the invaginated host plasma membrane (PM) (Gil and Gay, 1977; Roberts  
67 et al., 1993). Haustoria appear to play essential roles in plant-fungus recognition, uptake of  
68 nutrients into the pathogen and delivery of secreted effector proteins into host cells for the  
69 establishment of a successful biotrophic relationship (Heath, 1997; Hahn and Mendgen, 2001;  
70 Voegelé and Mendgen, 2003; Catanzariti et al., 2006; Yi and Valent, 2013; Lo Presti et al., 2015).  
71 Similar to haustoria, the biotrophic hyphae of some hemibiotrophic fungi, such as *Colletotrichum*  
72 spp. and *Magnaporthe oryzae*, grow intracellularly in host tissue. The biotrophic hyphae are  
73 surrounded by an extra-invasive hyphal membrane (EIHM) contiguous with the host PM,

74 forming a tight biotrophic interface. The biotrophic stage of hemibiotrophic fungi, without  
75 killing host cells, is a crucial step for the pathogen to initiate infection.

76 Although the EHM is considered by some models to be derived from the host PM,  
77 cytological studies revealed that the two membranes have distinct structure and composition (Gil  
78 and Gay, 1977; Micali et al., 2011). In *Arabidopsis thaliana* - powdery mildew interactions, all  
79 PM-localized proteins tested appear to be absent at the EHM (Koh et al., 2005; Micali et al.,  
80 2011), while several proteins that are associated with the endomembrane system are detected at  
81 the EHM (Inada et al., 2016; Berkey et al., 2017; Kwaaitaal et al., 2017). Thus, uncovering the  
82 proteinaceous nature of the EHM challenges existing models of the origin and constitution of the  
83 EHM, and provides fresh insight into understanding the cellular mechanisms underlying the  
84 biogenesis of the EHM.

85 Membrane identities are acquired by the combined presence of specific proteins and  
86 lipids. Biological membranes are composed of a diverse array of lipids (Van Meer et al., 2008).  
87 Phosphoinositides (also known as phosphatidylinositol phosphates) are a family of anionic  
88 phospholipids that are present in minute amounts in cell membranes. Phosphoinositide species  
89 are distinctly partitioned in membranes by type, and thereby contribute to organelle identity  
90 (Noack and Jaillais, 2017). The principal roles of phosphoinositides are to coordinate the  
91 complex exchange of metabolites and information across membranes, the controlled expansion  
92 or reduction of membrane area, the interaction of membranes with the cytoskeleton and  
93 intracellular organelles, and the polarized distribution of peripheral or membrane-integral  
94 proteins. In plants, five out of seven known phosphoinositides have been detected, with PI4P  
95 constituting approximately 80%, followed in abundance by PI(4,5)P<sub>2</sub>, PI3P and PI(3,5)P<sub>2</sub>  
96 (Heilmann and Heilmann, 2015; Noack and Jaillais, 2017). PI4P and PI(4,5)P<sub>2</sub> are essential lipid  
97 determinants of the PM (Hammond et al., 2012). However, remarkable differences in  
98 phosphoinositide composition can be noted between plants and animals. In plants, the major pool  
99 of PI4P appears at the PM, whereas in animals, PI4P prominently resides in the Golgi/TGN  
100 compartments and to a lesser extent at the PM (Simon et al., 2014; Simon et al., 2016).  
101 Additionally, PI(4,5)P<sub>2</sub> is found in much lower abundance in plant cells than animal cells  
102 (Munnik and Vermeer, 2010; Munnik and Nielsen, 2011). Together with the mystery concerning  
103 the origin of the EHM, little is known about the membrane lipid composition of the EHM.

104 In this study, by using genetically encoded biosensors for each phosphoinositide species  
105 in *Arabidopsis thaliana* challenged by the powdery mildew fungus *Erysiphe cichoracearum*, we  
106 show that among the two phosphoinositides at the PM, PI(4,5)P<sub>2</sub> pools were dynamically up-  
107 regulated at pathogen infection sites and further integrated into the EHM, whereas PI4P  
108 maintained steady levels at the PM and was absent in the EHM. Further pharmacological  
109 intervention revealed that the dynamic movement of PI(4,5)P<sub>2</sub> into the EHM occurred via a  
110 Brefeldin A (BFA)-insensitive but actin-dependent transport pathway. Depletion of the PM  
111 PI(4,5)P<sub>2</sub> pool by knockout mutation of the two major phosphatidylinositol 4-phosphate 5-  
112 kinases genes *PIP5K1* and *PIP5K2*, responsible for PI(4,5)P<sub>2</sub> biosynthesis at the PM in leaf  
113 tissues, prevents susceptible responses and disease development of host plants against biotrophic  
114 and hemibiotrophic fungal pathogens. Together, our results suggest that fungal pathogens  
115 modulate the subcellular distribution of host phosphoinositides during pathogenesis and adopt  
116 PI(4,5)P<sub>2</sub> as an essential susceptibility factor for plant disease development.

117

## 118 RESULTS

### 119 Differential Distribution of Phosphoinositides at the Haustorial Periphery upon Powdery 120 Mildew Infection

121 Phosphoinositides are key components of cellular membrane lipids. Recently, a full set of  
122 genetically encoded biosensors for detecting PI3P, PI4P and PI(4,5)P<sub>2</sub> was developed to probe  
123 the localizations and partitioning of phosphoinositides within the cells and tissues of stable  
124 transgenic *Arabidopsis* lines (Vermeer et al., 2006; van Leeuwen et al., 2007; Vermeer et al.,  
125 2009; Munnik and Nielsen, 2011; Simon et al., 2014; Platre and Jaillais, 2016). We used these  
126 well-defined biosensors to investigate the subcellular distribution of phosphoinositides in  
127 *Arabidopsis* plants in response to the invasion of biotrophic and hemibiotrophic fungal pathogens.

128 Initially, we examined the subcellular localization of PI3P, PI4P and PI(4,5)P<sub>2</sub> in leaves  
129 of transgenic *Arabidopsis* plants expressing mCITRINE (mCIT)-tagged variants of the  
130 biosensors mCIT-2xFYVE<sup>HRS</sup>, mCIT-2xPH<sup>FAPP1</sup>, and mCIT-1xPH<sup>PLCδ1</sup>, respectively (Simon et  
131 al., 2014), upon inoculation with the biotrophic powdery mildew fungus, *Erysiphe*  
132 *cichoracearum* (*Ec*). PI3P was previously shown to localize in late endosomes/prevacuolar  
133 compartments (PVCs) and to a lesser extent to the tonoplast in plant cells (Simon et al., 2014).  
134 Upon infection at 2 days post inoculation (dpi) with *Ec* conidiospores, confocal imaging revealed

135 that signals for the PI3P biosensor mCIT-2xFYVE<sup>HRS</sup> were detected at a distinct membrane  
136 structure surrounding the *Ec* haustorium, as well as at cytosolic punctate particles likely  
137 associated with late endosomes/PVCs (Figure 1A). The signals for mCIT-2xFYVE<sup>HRS</sup>-targeted  
138 membrane formed an outer layer loosely surrounding the callosic encasement (stained by  
139 propidium iodide, PI) of the haustorial complex and was less constricted against the haustorial  
140 peripheral surface, which suggests that PI3P is integrated into the host tonoplast rather than  
141 targeting into EHM.

142 Using biosensors for PI4P and PI(4,5)P<sub>2</sub>, the two most abundant phosphoinositides at the  
143 PM (Simon et al., 2014; Simon et al., 2016), confocal imaging showed that signals for PI4P  
144 sensor mCIT-2xPH<sup>FAPP1</sup> in *Ec*-infected leaf epidermal cells were associated with the PM of *Ec*-  
145 infected host cells. Furthermore, mCIT-2xPH<sup>FAPP1</sup> also appeared at the outer surface of the  
146 encasement, which is covered by host PM. However, the continuous signal stopped at the  
147 haustorial neck region and was completely absent at the haustorial periphery (Figure 1B;  
148 Supplemental Figures 1A and 1B; Supplemental Movie 1). In contrast, the signal for the  
149 PI(4,5)P<sub>2</sub> sensor mCIT-1xPH<sup>PLCδ1</sup> in *Ec*-infected leaf epidermal cells accumulated at the  
150 periphery of *Ec* haustoria likely associated with the EHM in addition to its localization at the  
151 host PM (Figure 1C; Supplemental Figures 1C and 1D; Supplemental Movie 2). Detailed spatial  
152 imaging revealed that PI(4,5)P<sub>2</sub> signals formed the outer and inner layers covering the surface of  
153 haustorial encasement, and occasionally displayed contiguous connections between the  
154 haustorial periphery and host PM (Supplemental Figure 1C).

155 To validate the distinct accumulation patterns of PI4P and PI(4,5)P<sub>2</sub> signals observed  
156 after *Ec*-infection, we simultaneously captured PI4P and PI(4,5)P<sub>2</sub> signals from the same  
157 infection site using Arabidopsis plants expressing 2xCypET-1xPH<sup>FAPP1</sup> and mCIT-1xPH<sup>PLCδ1</sup>  
158 (Figure 1D). Indeed, the PI4P sensor was completely absent on the haustorial periphery, whereas  
159 the signal for the PI(4,5)P<sub>2</sub> sensor formed a peripheral layer surrounding the haustorium. Similar  
160 distribution patterns for each phosphoinositide species were observed in *Ec*-infected epidermal  
161 cells regardless of the sensors' affinity for their cognate lipid (i.e., using one or two repeats of an  
162 identical lipid-binding domain) or the lipid-binding domain used, i.e., mCIT-2xPH<sup>FAPP1</sup>, mCIT-  
163 1xPH<sup>FAPP1</sup> and mCIT-P4M<sup>SiDM</sup> for PI4P, and mCIT-1xPH<sup>PLCδ1</sup>, mCIT-2xPH<sup>PLCδ1</sup> and mCIT-  
164 1xTUBBY-C for PI(4,5)P<sub>2</sub> (Figures 1B and 1C; Supplemental Table 1). These results indicate  
165 that various phosphoinositide biosensors provide specific, reproducible detection of distinct

166 phosphoinositide species' subcellular localization in Arabidopsis leaf epidermal cells in  
167 association with *Ec* infection.

168 To independently validate that PI(4,5)P<sub>2</sub> is specifically recruited to the EHM, we  
169 established a protocol for whole mount immunolocalization of PI(4,5)P<sub>2</sub> or PI4P in *Ec*-infected  
170 leaf epidermal cells using antibodies specifically recognizing PI(4,5)P<sub>2</sub> or PI4P (Hammond et al.,  
171 2006; Hammond et al., 2009). The anti-PI(4,5)P<sub>2</sub> antibody labeled a membrane layer around the  
172 haustorium as well as the cell periphery (Figure 1E). Staining with anti-PI4P antibody produced  
173 the intracellular punctate signals likely corresponding to Golgi in leaf epidermal cells (Figure  
174 1E). As shown in an earlier study using the same anti-PI4P antibody, a punctate signal was also  
175 observed in root epidermal cells (Tejos et al., 2014). This localization pattern was somewhat  
176 unexpected considering that signals for PI4P biosensors localize primarily to both the PM and  
177 Golgi apparatus (Figure 1B) (Vermeer et al., 2009). However, it is known that different  
178 conditions are required for the preservation of PM and Golgi, and the immunofluorescence  
179 protocol for PI4P detection adapted from a previous study likely preserves Golgi staining  
180 opposed to those best for PM staining (Capasso and D'Angelo, 2019). Nevertheless, no distinct  
181 locations of anti-PI4P signals were detected surrounding the haustorial periphery (Figure 1E). No  
182 specific labeling was observed in the negative control processed without the primary antibodies.  
183 Thus, the immunofluorescence data corroborate the localization patterns of PI(4,5)P<sub>2</sub> and PI4P at  
184 the haustorial periphery, as revealed by the biosensors in *Ec*-infected Arabidopsis cells.

185

### 186 **PI(4,5)P<sub>2</sub>, but not PI4P, Is Selectively Targeted to the EHM**

187 The haustorium is typically surrounded by a series of subcellular compartment layers, including,  
188 from innermost to outermost: (i) the extrahaustorial matrix (EHM<sub>x</sub>), (ii) the EHM, (iii) the host  
189 cytosol, and (iv) the host tonoplast. The haustorial encasement often forms around the haustorial  
190 neck region, separating host cytosolic contents and the tonoplast from the haustorial surface.

191 To test whether the PI(4,5)P<sub>2</sub> was selectively targeted to the EHM, we conducted a  
192 comprehensive colocalization analysis with a set of host cellular markers. Both PI3P and  
193 PI(4,5)P<sub>2</sub> were incorporated into distinct membranous layers at the haustorial periphery. To  
194 uncover the nature and identity of these membrane layers, we first co-expressed each of three  
195 phosphoinositide biosensors with a tonoplast marker Tono-CFP (Nelson et al., 2007). At 2 dpi,  
196 the signal for PI3P sensor mCIT-2xFYVE<sup>HRS</sup> surrounding haustoria was tightly co-localized with

197 Tono-CFP (Figures 2A and 2B), indicating that the PI3P is indeed targeted to the tonoplast. In  
198 contrast, the PI(4,5)P<sub>2</sub> biosensor mCIT-1xPH<sup>PLCδ1</sup> did not co-localize with Tono-CFP, but  
199 appeared as a distinct membrane layer between the haustorial body and tonoplast (Figures 2A  
200 and 2B). With regard to PI4P, the signals of mCIT-2xPH<sup>FAPP1</sup> were continuous along the PM and  
201 terminated at the haustorial neck region (Figures 2A and 2B). These data suggest that the  
202 PI(4,5)P<sub>2</sub> is integrated into the EHM, while PI4P appears to be absent from the EHM.

203 A previous study reported that the EHM-specific marker RPW8.2-RFP and its homologs  
204 YFP-HR3 proteins remained attached to the haustorial complex while the cytoplasm was pulled  
205 off the haustorial surface upon plasmolysis of powdery mildew-infected cells (Berkey et al.,  
206 2017). To test the association of PI(4,5)P<sub>2</sub> with the EHM, we subjected *Ec*-inoculated leaves co-  
207 expressing mCIT-1xPH<sup>PLCδ1</sup> and Tono-CFP to the plasmolysis. After incubating with 0.85 M  
208 KCl for ~30 min, the cytoplasm along with the Tono-CFP-labeled tonoplast appeared retracted  
209 from the haustorial complex, whereas the localization of mCIT-1xPH<sup>PLCδ1</sup> signals at the EHM  
210 was unaffected (Figure 2C). These data support PI(4,5)P<sub>2</sub> localization at the EHM.

211 Due to the turgor pressure generated by the central vacuole in leaf epidermal cells, the  
212 cytoplasmic contents of the host cell appear to form a discontinuous layer with variable  
213 thicknesses between the EHM and the tonoplast (Koh et al., 2005). We examined the cellular  
214 distribution of a cytosolic marker (Cyto-YFP) (DeBono et al., 2009) in comparison with the  
215 PI(4,5)P<sub>2</sub> biosensors in *Ec*-infected epidermal cells. Cyto-YFP yielded uneven, occasionally  
216 discontinuous signals, surrounding the haustoria and the outer surface of encasement (Figure 2D;  
217 Supplemental Figure 2). Further, faint signals were detected at the inner side of the encasement.  
218 By contrast, both PI(4,5)P<sub>2</sub> probes mCIT-1xPH<sup>PLCδ1</sup> and mCIT-2xPH<sup>PLCδ1</sup> exhibited an intense  
219 sharp layer with uniform thickness around the haustoria, and the detectable signals also appeared  
220 consistently at the inner side of the encasement (Figure 2D; Supplemental Figures 2). As  
221 revealed previously, the 1xPH<sup>PLCδ1</sup> probe with a single PI(4,5)P<sub>2</sub> binding motif displayed a  
222 cytosolic proportion of the signals (van Leeuwen et al., 2007; Munnik and Nielsen, 2011; Simon  
223 et al., 2014), although the fluorescence intensity in the cytosol was weaker than at the PM and  
224 EHM. Notably, the probe mCIT-2xPH<sup>PLCδ1</sup> with two PI(4,5)P<sub>2</sub> binding motifs that was  
225 demonstrated to be exclusively localized to the PM (Simon et al., 2014) showed a sharp  
226 accumulation at the EHM as well as at the PM in *Ec*-infected cells.



227 During the infection process, the host nucleus often moves towards the infection site of  
228 haustorium-containing cells (Inada et al., 2016; Scheler et al., 2016). We observed mCIT-  
229 1xPH<sup>PLC $\delta$ 1</sup> and mCIT-2xPH<sup>PLC $\delta$ 1</sup> signals as a distinct layer surrounding the haustorium,  
230 separating the haustorium from the nucleus, whereas no clear boundary appeared between the  
231 haustorium and its neighbouring nucleus by either the Cyto-YFP-labeled cytosol or the Tono-  
232 YFP-labeled tonoplast (Figure 2D). Notably, the EHM marker RPW8.2-YFP (Wang et al., 2007;  
233 Wang et al., 2009) also displayed a sharp boundary layer between the haustorium and the  
234 adjacent nucleus, while the Tono-YFP-labeled tonoplast surrounded the haustorium and the  
235 nucleus (Figure 2D).

236 To further examine the localization of phosphoinositides in association with the EHM,  
237 we co-expressed mCIT-tagged biosensors with the EHM-specific marker RPW8.2-RFP (Wang et  
238 al., 2007). At 2 dpi, a continuous layer of both mCIT-1xPH<sup>PLC $\delta$ 1</sup> and mCIT-2xPH<sup>PLC $\delta$ 1</sup>  
239 encompassing the haustoria was tightly colocalized with the RPW8.2-RFP (Figure 2E). Signals  
240 for both PI(4,5)P<sub>2</sub> biosensors (mCIT-1xPH<sup>PLC $\delta$ 1</sup> and mCIT-2xPH<sup>PLC $\delta$ 1</sup>) as well as for RPW8.2-  
241 RFP were evident at the haustorial neck region. Further colocalization studies revealed that the  
242 PI4P biosensor mCIT-2xPH<sup>FAPP1</sup> covered the encasement surface, but was not detected from the  
243 RPW8.2-RFP-labelled EHM (Figure 2E). The PI3P biosensor mCIT-2xFYVE<sup>HRS</sup> formed an  
244 additional layer outside the RPW8.2-RFP-labelled EHM, targeting to the tonoplast (Figure 2E).  
245 Taken together, these results reveal that PI4P and PI(4,5)P<sub>2</sub>, two of the most abundant  
246 phosphoinositides at the PM in plant cells (Vermeer et al., 2009; Simon et al., 2014; Simon et al.,  
247 2016), are likely associated with independent lipid determinants of membrane identity, and only  
248 PI(4,5)P<sub>2</sub> is selectively integrated into EHM during haustorial biogenesis (Figure 2F).

249 To investigate whether the distribution of phosphoinositides at the EHM was a common  
250 characteristic of the interactions between host plants and haustorium-forming pathogens, we  
251 examined the localizations of PI3P, PI4P and PI(4,5)P<sub>2</sub> in leaves of Arabidopsis plants  
252 expressing corresponding biosensors upon infection with the white rust oomycete, *Albugo*  
253 *candida*. At 2 days post inoculation with zoospores, confocal imaging revealed that the PI3P  
254 biosensor mCIT-2xFYVE<sup>HRS</sup> formed a membrane layer enveloping the *A. candida* haustorium,  
255 likely targeting it to the host tonoplast (Supplemental Figures 3A). Similar to infection by the  
256 powdery mildew, the signals for PI4P biosensor mCIT-2xPH<sup>FAPP1</sup> discontinued at the haustorial  
257 neck region and were absent from the peripheral surface of *A. candida* haustoria (Supplemental

258 Figures 3B). Both PI(4,5)P<sub>2</sub> biosensors mCIT-1xPH<sup>PLCδ1</sup> and mCIT-2xPH<sup>PLCδ1</sup> were recruited to  
259 the EHM of white rust (Supplemental Figures 3C). These data indicate that haustorium-forming  
260 pathogens promote the redistribution of host phosphoinositides during the infection processes,  
261 and the EHM from different host-pathogen systems has similar, but unique phosphoinositide  
262 compositions.

263

### 264 **Cellular Trafficking Pathways Responsible for the Recruitment of PI(4,5)P<sub>2</sub> into the EHM**

265 To investigate the potential role of cellular trafficking pathways in the redistribution and  
266 recruitment of PI(4,5)P<sub>2</sub> to the EHM, we evaluated the impact of pharmacological inhibitors on  
267 the dynamic accumulation of PI(4,5)P<sub>2</sub> at the EHM. This involved quantification of the PI(4,5)P<sub>2</sub>  
268 signals at the EHM in the presence or absence of latrunculin A, oryzalin, brefeldin A (BFA),  
269 methyl-β-cyclodextrin (MβCD), or wortmannin. Interestingly, treatment with latrunculin A,  
270 which sequesters G-actin and prevents F-actin assembly (Spector et al., 1983), led to a  
271 significant depletion of PI(4,5)P<sub>2</sub> from the EHM. Treatments with oryzalin, which depolymerizes  
272 microtubules (Morejohn, 1991), had no effect on PI(4,5)P<sub>2</sub> accumulation at the EHM (Figures  
273 3A and 3B). Strikingly, inhibition of vesicle-mediated trafficking by BFA, which inactivates  
274 ARF-GEF GNOM activity (Geldner et al., 2003; Nielsen et al., 2012), had no significant effect  
275 on the targeting of PI(4,5)P<sub>2</sub> to the EHM. Treatment with MβCD, which depletes the PM sterols  
276 (Ohtani et al., 1989), resulted in significant inhibition of PI(4,5)P<sub>2</sub> accumulation at the EHM. We  
277 then investigated the effects of wortmannin, a well-characterized inhibitor of both PI 3-Kinases  
278 and type III PI 4-Kinases (Matsuoka et al., 1995; Nakanishi et al., 1995; Cutler et al., 1997;  
279 Krinke et al., 2007; Jha et al., 2018). Treatment with a high concentration of wortmannin (30 μM)  
280 caused a significant depletion of PI(4,5)P<sub>2</sub> at the EHM (Figures 3A and 3B). At this high  
281 concentration (30 μM), wortmannin has been shown to inhibit the function of type III PI 4-  
282 kinases, thus depleting cellular PI4P contents, although we cannot rule out that the PI3P-  
283 dependent process could contribute to the observed effect. These results indicate that the  
284 accumulation of PI(4,5)P<sub>2</sub> at the EHM is dependent on the formation of the actin cytoskeleton  
285 and sterols, and less sensitive to GNOM-mediated vesicular transport, and the PI(4,5)P<sub>2</sub> pool at  
286 the EHM is likely derived from *de novo* synthesis from the precursor PI4P via the type III PI 4-  
287 kinases.

288

289 **Spatial and Temporal Distribution of PI(4,5)P<sub>2</sub> Biosensors in Host Cells in Response to**  
290 **Infection by Powdery Mildew Fungus**

291 To uncover PI(4,5)P<sub>2</sub> dynamics in host cells in response to powdery mildew attack, we examined  
292 the PI(4,5)P<sub>2</sub> signals in leaf epidermal cells at *Ec* invasion sites, over an infection time course.  
293 Confocal imaging revealed that at an early infection stage, ~11 hours post inoculation (hpi), the  
294 PI(4,5)P<sub>2</sub> signals aggregated near *Ec* penetration sites (Figure 4A). After successful penetration,  
295 PI(4,5)P<sub>2</sub> signals appeared in the EHM in the zone surrounding haustorial primordia and around  
296 fully developed haustoria.

297 Strong induction of PI(4,5)P<sub>2</sub> signals was observed in leaf epidermal cells that hosted a  
298 fully developed *Ec*-haustorium, and was not detected in neighboring non-infected cells (Figure  
299 4B). High resolution analyses revealed that induced PI(4,5)P<sub>2</sub> signals intensified on the  
300 peripheral surface of infected epidermal cells in association with the PM, and strong signals also  
301 sharply labeled the EHM. Both infected and non-infected epidermal cells maintained a similar  
302 level of PI(4,5)P<sub>2</sub> signals in the cytosol (Figure 4B). No induction of free YFP expression was  
303 detected in *Ec*-colonized cells compared with neighboring non-infected cells of transgenic plants  
304 expressing pUBQ10:YFP with the same promoter driving the expression of the PI(4,5)P<sub>2</sub>  
305 biosensor mCIT-1xPH<sup>PLC $\delta$ 1</sup> (Supplemental Figure 4), suggesting that the powdery mildew  
306 infection has no significant effects on *pUBQ10* promoter activity.

307 To examine the dynamic details of enhanced production of PI(4,5)P<sub>2</sub> signals in PM, we  
308 treated *Ec*-infected leaves with FM4-64, a lipophilic styryl dye widely used as a fluorescent  
309 probe for detection of PM internalization during the endocytosis and membrane trafficking  
310 (Jelinkova et al., 2010). After 15-min of stain uptake, FM4-64-labeled PM appeared as intensive  
311 aggregates in both *Ec*-infected and non-infected epidermal cells (Figures 4C and 4D). In the  
312 epidermal cells hosting haustoria, enhanced PI(4,5)P<sub>2</sub> signals formed amorphous accumulations  
313 that co-localized with the FM4-64-labeled aggregates, whereas the FM4-64-labeled aggregates in  
314 non-infected cells were coupled with less or no PI(4,5)P<sub>2</sub> signals. These results suggest that  
315 induced PI(4,5)P<sub>2</sub> pools in haustorium-forming cells are likely associated with enhanced PM  
316 trafficking.

317

318 **PI(4,5)P<sub>2</sub> Production via PI4P 5-kinases Is an Essential Susceptibility Factor in Plant-**  
319 **Pathogen Interactions**

320 PI4P 5-kinase (PIP5K) converts PI4P to PI(4,5)P<sub>2</sub> in eukaryotes (Toker, 1998; Choi et al., 2015).  
321 The *Arabidopsis thaliana* genome contains genes encoding eleven isoforms of PIP5Ks that are  
322 classified into two distinct subfamilies: type A includes PIP5K10 and PIP5K11 with domain  
323 structures similar to PI4P 5-kinases in mammals and yeasts, while type B includes isoforms  
324 PIP5K1-PIP5K9 with additional N-terminal Lin and MORN domains (Mueller-Roeber and Pical,  
325 2002; Heilmann and Heilmann, 2015). The Affymetrix microarray data from Genevestigator  
326 (<https://www.genevestigator.com>) (Hruz et al., 2008) revealed that *PIP5K1*, -2, -3, -7, -8, -9 and  
327 -11 expressed at varying but substantial levels in rosette leaves, especially in mature leaves  
328 (Supplemental Figure 5A). To validate the microarray data and to identify which isoform(s) of  
329 PIP5K contributes to PI(4,5)P<sub>2</sub> production upon powdery mildew attack, we employed RT-PCR  
330 analysis for expression profiling of *PIP5K* isoforms in *Arabidopsis* leaves with or without *Ec*  
331 inoculation (Supplemental Figure 5B). RT-PCR results showed detectable expression of *PIP5K1*,  
332 -2, -5, -7, -8, and -9 in mature *Arabidopsis* leaves. Among those, *PIP5K1* and *PIP5K2* were  
333 constitutively expressed at high levels. The expression of *PIP5K8* was slightly induced by *Ec*-  
334 infection compared with non-inoculated leaves.

335 To elucidate the function of the kinases encoded by expressed *PIP5K* genes in  
336 *Arabidopsis*-powdery mildew interactions, we undertook a reverse genetic approach employing  
337 T-DNA insertion mutants for pathogenicity tests. We obtained and confirmed homozygous T-  
338 DNA mutant lines for *PIP5K1* (SALK\_146728), *PIP5K2* (SALK\_012487), *PIP5K5*  
339 (SALK\_147475), *PIP5K7* (SALK\_151429), *PIP5K8* (SAIL\_561\_F09) and *PIP5K9*  
340 (WiscDsLox434B6) (Supplemental Figure 5C). Since both *PIP5K1* and *PIP5K2* showed high  
341 levels of expression in *Arabidopsis* mature leaves, and recombinant PIP5K1 and PIP5K2  
342 displayed the highest catalytic activities *in vitro* among ubiquitously expressed PIP5Ks from  
343 *Arabidopsis* (Supplemental Figures 5A and 5B) (Stenzel et al., 2008; Ischebeck et al., 2013), we  
344 generated a double mutant *pip5k1 pip5k2* by crossing the respective single insertion lines. As  
345 described previously, the *pip5k1 pip5k2* double mutant exhibited reduced growth in the seedling  
346 and rosette stages, characterized by reduced leaf expansion and slow growth (Supplemental  
347 Figure 6) (Ischebeck et al., 2013; Tejos et al., 2014). The triple (*pip5k1 pip5k2 pip5k5*; *pip5k1*  
348 *pip5k2 pip5k8*) and quadruple (*pip5k1 pip5k2 pip5k5 pip5k8*) mutants were generated by  
349 crossing the single (*pip5k5* or *pip5k8*) with the double mutant (*pip5k1<sup>-/-</sup> pip5k2<sup>-/+</sup>*). The triple and  
350 quadruple mutants showed similar phenotypes to the double mutant, but the triple (*pip5k1 pip5k2*

351 *pip5k8*) and quadruple (*pip5k1 pip5k2 pip5k5 pip5k8*) mutants displayed enhanced growth  
352 defects (Supplemental Figure 6). The results indicate that the expressed *PIP5K* genes exhibit  
353 partially redundant and additive roles in Arabidopsis vegetative growth and development with  
354 *PIP5K1* and *PIP5K2* playing the most predominant functions.

355 When challenged with *Ec*, all single mutants supported wild type levels of hyphal growth,  
356 and *Ec* was able to sporulate at 7 dpi (Figures 5A and 5B; Supplemental Figure 5D). In contrast,  
357 *Ec* growth and development were severely impaired on the *pip5k1 pip5k2* double mutant  
358 (Figures 5A and 5B; Supplemental Figure 5D). On the mature leaves of *pip5k1 pip5k2*, *Ec*  
359 displayed a remarkably lower penetration rate, and formed smaller colonies with statistically  
360 significant reduction in second hypha length and branches, total haustorial numbers per colony  
361 and total conidiophores per colony (Figures 5C to 5I). The triple (*pip5k1 pip5k2 pip5k5*; *pip5k1*  
362 *pip5k2 pip5k8*) and quadruple (*pip5k1 pip5k2 pip5k5 pip5k8*) mutants exhibited similar levels of  
363 disease severity after *Ec* infection as the double mutant (Figure 5A and 5B). Thus, among the  
364 highly expressed *PIP5K* genes in leaf tissues, *PIP5K1* and *PIP5K2* play predominant functions  
365 in powdery mildew susceptibility, and disruption of both genes renders knockout mutants highly  
366 resistant to the compatible powdery mildew fungus.

367 We further examined plant susceptibility to a second biotrophic phytopathogen, white  
368 rust oomycete, *Albugo candida* (isolate Acem1), and pathogenicity assays were conducted on the  
369 double, triple and quadruple *pip5k* mutants. After inoculation with zoospores, abundant white  
370 blisters surrounding the inoculation sites were observed on the abaxial surface of wild type  
371 leaves at 10-15 dpi (Supplemental Figure 7). At the same inoculation stages, no visible  
372 symptoms appeared on leaves of the double, triple and quadruple mutants (Supplemental Figure  
373 7), indicating that these mutants gained strong resistance to *Albugo candida*.

374 The impact of disruption of *PIP5K1* and *PIP5K2* genes on cellular dynamics of PI(4,5)P<sub>2</sub>  
375 was further investigated in leaf epidermal cells of the mutant with or without *Ec*-inoculation. We  
376 introduced the PI(4,5)P<sub>2</sub> biosensor mCIT-1xPH<sup>PLCδ1</sup> into the *pip5k1 pip5k2* mutant, and  
377 examined the fluorescence intensity at the PM. Quantitative imaging revealed that the mCIT-  
378 1xPH<sup>PLCδ1</sup> signal intensity at the PM was significantly reduced in the mutant compared to wild  
379 type plants (Supplemental Figures 8A and 8B). RT-PCR revealed that wild type and *pip5k1*  
380 *pip5k2* mutant expressed comparable levels of the *mCIT-1xPH<sup>PLCδ1</sup>* transcripts (Supplemental  
381 Figure 8C), indicating that reduced levels of mCIT-1xPH<sup>PLCδ1</sup> signal intensity in the *pip5k1*

382 *pip5k2* mutant were not due to transgene silencing. At the PM of wild type leaf epidermal cells,  
383 the clustered signals from PI(4,5)P<sub>2</sub> biosensors coalesced, forming distinct microdomains.  
384 However, this characteristic distribution of PI(4,5)P<sub>2</sub> was substantially diminished in the PM of  
385 *pip5k1 pip5k2* mutant (Supplemental Figure 8A). Together, these data indicate that isoforms  
386 PIP5K1 and PIP5K2 are key members of the Arabidopsis PI4P 5-kinase family and are required  
387 to maintain the PM pool of PI(4,5)P<sub>2</sub> in leaf epidermal cells.

388 Furthermore, when challenged with *Ec*, the relative fluorescence intensity of mCIT-  
389 1xPH<sup>PLC $\delta$ 1</sup> at the EHM was dramatically reduced in *Ec*-infected epidermal cells of *pip5k1 pip5k2*  
390 compared with wild type (Supplemental Figure 8D), suggesting that targeting of PI(4,5)P<sub>2</sub> to the  
391 EHM was impaired in the mutant. Interestingly, although the PI(4,5)P<sub>2</sub> signals were significantly  
392 reduced at the PM and EHM in epidermal cells of *pip5k1 pip5k2*, the epidermal cell hosting *Ec*-  
393 haustoria still displayed stronger PI(4,5)P<sub>2</sub> signals than that of adjacent non-infected epidermal  
394 cells (Supplemental Figure 8E). This observation suggests that other isoform(s) of PI4P 5-kinase  
395 family rather than PIP5K1 and PIP5K2 are likely involved in the induction of PI(4,5)P<sub>2</sub> pools in  
396 the *Ec*-infected epidermal cells although we could not exclude the possible prevention of  
397 PI(4,5)P<sub>2</sub> degradation that may occur in the *Ec*-infected epidermis.

398 Since PIP5K1 and PIP5K2 are predominantly responsible for replenishing the PI(4,5)P<sub>2</sub>  
399 pools in the PM of epidermal cells and at the EHM, we next tested whether the *in situ*  
400 localization of PIP5K1 and PIP5K2 directly contributes to the biosynthesis of PI(4,5)P<sub>2</sub> at the  
401 location. We generated transgenic Arabidopsis plants expressing *PIP5K1:PIP5K1-YFP* and  
402 *PIP5K2:PIP5K2-YFP* to enable cellular visualization of the kinase enzymes. After introducing  
403 the *PIP5K1:PIP5K1-YFP* and *PIP5K2:PIP5K2-YFP* transgenes into *pip5k1 pip5k2*, we found  
404 that ectopic expression of either construct could rescue the retarded growth phenotype of the  
405 *pip5k1 pip5k2* mutant (Supplemental Figure 6). These data indicate that the stable transgenic  
406 expression of *PIP5K1-YFP* and *PIP5K2-YFP* produced fully functional kinases. In leaf  
407 epidermal cells, both PIP5K1-YFP and PIP5K2-YFP localized predominantly at the PM  
408 (Supplemental Figures 9A and 9B), resembling the localization patterns found in root cells  
409 (Ischebeck et al., 2013; Tejos et al., 2014). Upon *Ec* attack, PIP5K1-YFP and PIP5K2-YFP  
410 accumulated at *Ec*-penetration sites around the haustorial neck region. Noticeably, no detectable  
411 signals of PIP5K1-YFP or PIP5K2-YFP could be observed at the EHM (Supplemental Figures  
412 9C and 9D). These results suggest that the PIP5K1 and PIP5K2 kinases generate PI(4,5)P<sub>2</sub> at the

413 PM, whereas the PI(4,5)P<sub>2</sub> at the EHM results from the lateral transport of pre-existing PM pools  
414 to the EHM.

415

#### 416 **Mechanisms Underlying Powdery Mildew Resistance in *pip5k1 pip5k2* Mutant**

417 The enhanced resistance to biotrophic pathogen infection observed in the *pip5k1 pip5k2* double  
418 mutant suggests underlying mechanisms may support disease resistance. To elucidate the  
419 potential mechanism(s) contributing to powdery mildew resistance in *pip5k1 pip5k2*, we  
420 examined the expression of defense-associated genes in response to powdery mildew infection  
421 by whole transcriptome shotgun sequencing (RNA-seq). Analysis of the differentially expressed  
422 genes revealed that some of the genes involved in jasmonic acid (JA) biosynthesis, signaling and  
423 response, e.g., *12-OXOPHYTODIENOATE REDUCTASE 3 (OPR3)*, *CYP82C2*, *CYP94C1*,  
424 *ALLENE OXIDE SYNTHASE (AOS)*, *MYC4* and *ETHYLENE RESPONSE FACTOR 1 (ERF1)*,  
425 displayed constitutively higher expression in the *pip5k1 pip5k2* mutant than in wild type under  
426 the non-inoculated condition. However, upon *Ec*-inoculation, the majority of these genes in  
427 *pip5k1 pip5k2* showed down-regulation in comparison to wild type expression levels (Figure 6A;  
428 Supplemental Data Set 1). Thus, the JA-signaling and defense pathway's role in mediating the  
429 enhanced resistance of *pip5k1 pip5k2* plants to the powdery mildew infection appears negligible.

430 In contrast, the expression of salicylic acid (SA) associated defense responsive genes,  
431 such as *PR1* and *PR2*, was significantly higher in the *pip5k1 pip5k2* mutant than in the wild type  
432 under the *Ec*-inoculated condition (Figure 6A; Supplemental Figure 10; Supplemental Data Set  
433 1). However, a full set of genes known to be involved in SA biosynthesis and signaling were  
434 coordinately down-regulated in the *pip5k1 pip5k2* mutant compared to wild type (Figure 6A).  
435 Measurement of SA and JA contents in leaf tissues without pathogen inoculation revealed no  
436 significant differences between wild type and *pip5k1 pip5k2*. Upon powdery mildew infection at  
437 5 dpi, SA levels increased in infected leaves of wild type and *pip5k1 pip5k2*, but were much  
438 lower in *pip5k1 pip5k2* (Figures 6B and 6C). Collectively, these results suggest that the SA-  
439 independent defense reactions with induction of a set of *PR* genes underlie the enhanced  
440 resistance of the *pip5k1 pip5k2* mutant against powdery mildew infection.

441 The microbe- or pathogen-associated molecular patterns (MAMPs or PAMPs) have been  
442 shown to activate early-defense signaling and responses, and induce expression of MAMP-  
443 specific marker genes (Asai et al., 2002; He et al., 2006; Boudsocq et al., 2010). Our RNA-seq

444 data revealed that although the expression of MAMP-specific marker genes, such as *FLG22-*  
445 *INDUCED RECEPTOR-LIKE KINASE 1 (FRK1)*, *NDR1/HIN1-LIKE 10 (NHL10)*, *CYP81F2*,  
446 *WALL-ASSOCIATED KINASE 2 (WAK2)* and *FAD-LINKED OXIDOREDUCTASE (FOX)*, was  
447 coordinately induced in the *pip5k1 pip5k2* mutant upon powdery mildew attack, the expression  
448 levels of these genes remained lower than in *Ec*-attacked wild type (Figure 6A; Supplemental  
449 Figure 10; Supplemental Data Set 1). These findings suggest that MAMP-triggered immunity is  
450 unlikely to contribute to the increased resistance of *pip5k1 pip5k2* plants.

451 On mature *pip5k1 pip5k2* mutant leaves, successfully penetrated *Ec* displayed remarkably  
452 retarded growth, producing significantly smaller colonies than those on wild type leaves (Figure  
453 5). We determined whether the resistance in *pip5k1 pip5k2* is mediated by basal defense  
454 responses by staining infected leaves with aniline blue to highlight callose deposition, a sensitive  
455 cellular marker for basal defense responses (Hauck et al., 2003). In wild type and *pip5k1 pip5k2*  
456 plants, callose deposition was detected only at *Ec*-penetration sites at 2 dpi, whereas the *edr1*, a  
457 mutant that is constitutively primed for SA-inducible defenses and associated with cell death at  
458 powdery mildew infection sites (Frye and Innes, 1998), displayed enhanced callose depositions  
459 in *Ec*-infected epidermal cells that underwent accelerated cell death during infection (Figure 6D).  
460 Resistance triggered in *edr1* mutants was also associated with enhanced H<sub>2</sub>O<sub>2</sub> accumulation and  
461 autofluorescence at *Ec*-infected epidermal cells (Figures 6E and 6F). In contrast, wild type and  
462 *pip5k1 pip5k2* plants showed similar patterns of H<sub>2</sub>O<sub>2</sub> production and autofluorescence on *Ec*-  
463 colonized leaves. No apparent cell death accompanied by enhanced callose deposition, H<sub>2</sub>O<sub>2</sub>  
464 accumulation and autofluorescence was observed in infected epidermal cells underneath fungal  
465 colonies on *pip5k1 pip5k2* or wild type plants (Figures 6D to 6F). Thus, we conclude that the  
466 resistance in *pip5k1 pip5k2* to the powdery mildew fungus is not due to pathogen-triggered cell  
467 death-associated responses; rather it may depend on reduced host susceptibility.

468 MLO (Mildew Locus O), a protein with seven transmembrane domains reminiscent of a  
469 G-protein coupled receptor, is a conserved susceptibility factor to various powdery mildew  
470 species present on dicot and monocot plants (Consonni et al., 2006). It has been shown that the  
471 MLO proteins in barley (*Hordeum vulgare*) leaves focally accumulate beneath powdery mildew  
472 penetration sites coincident with the initiation of pathogen entry into host cells (Bhat et al., 2005).  
473 In Arabidopsis, the three co-orthologs (*AtMLO2*, *AtMLO6* and *AtMLO12*) of barley *MLO* are  
474 partially functionally redundant, with a predominant role for *AtMLO2* in the establishment of



475 compatibility with the powdery mildew fungus (Consonni et al., 2006). We used transgenic lines  
476 expressing MLO2-GFP (Jones et al., 2017) to investigate spatial and temporal dynamics of  
477 MLO2 proteins at *Ec*-penetration sites. In leaf epidermal cells without *Ec*-challenge, most of the  
478 MLO2-GFP fusion proteins localized at the cellular periphery as well as at cytoplasmic punctate  
479 structures that have previously been shown to co-localize with the Golgi marker Man49-mCherry  
480 (Jones et al., 2017) (Supplemental Figure 11A). Upon challenge with *Ec*, a striking focal  
481 accumulation of the fusion protein appeared beneath fungal penetration sites at ~11 hpi (Figure  
482 7A). Polarized MLO2-GFP accumulation at the *Ec*-penetration site appeared to be independent  
483 of actin cytoskeleton function since disruption of actin cytoskeleton by latrunculin A had a  
484 negligible impact on the MLO2-GFP accumulation (Figures 7B and 7C), consistent with  
485 previous findings (Bhat et al., 2005). Remarkably, at 12-13 hpi coincident with host cell  
486 penetration, most MLO2-GFP proteins aggregated to *Ec*-penetration sites, resulting in dramatic  
487 signal quenching specifically within infected cells (Figures 7A; Supplemental Figure 11A).  
488 However, after successful penetration of *Ec* at ~14 hpi, distribution of cytoplasmic MLO2-GFP  
489 in *Ec*-infected cells resumed similar patterns as the surrounding non-infected cells (Supplemental  
490 Figure 11A), and at the *Ec*-penetration sites, MLO2-GFP proteins were incorporated into  
491 extracellular encasements surrounding the neck region of haustoria (Supplemental Figure 11B).

492 To examine whether the dynamic response and function of MLO2 is involved in  
493 modulating *Ec*-penetration in the *pip5k1 pip5k2* mutant, we introduced the MLO2-GFP  
494 transgene into *pip5k1 pip5k2* plants. At 11-14 hpi when the *Ec*-attempted penetration failed to  
495 develop haustoria in *pip5k1 pip5k2* epidermal cells, focal accumulation of MLO2-GFP was  
496 greatly reduced or abolished beneath the *Ec* penetration sites (Figures 7A; Supplemental Figure  
497 11C), whereas where the fungus occasionally penetrated into epidermal cells, strong focal  
498 accumulation of MLO2-GFP proteins was detected surrounding the penetration sites, despite the  
499 similar levels of the *MLO2-GFP* transcripts in wild type and *pip5k1 pip5k2* mutant plants  
500 (Supplemental Figure 11D). Taken together, these findings demonstrate that a rapid, transient  
501 recruitment of MLO2 proteins into the fungal invasion site correlates with successful fungal  
502 penetration, and in the *pip5k1 pip5k2* mutant, an absence of focal accumulation of MLO2-GFP at  
503 the fungal penetration site correlates with the penetration failure of the powdery mildew fungus.

504 In eukaryotic cells, PI(4,5)P<sub>2</sub> is critical for the assembly and organization of actin  
505 filaments (AFs) (Moseley and Goode, 2006; Pollard, 2007). We next examined the potential

506 impact of altered PI(4,5)P<sub>2</sub> levels in the *pip5k1 pip5k2* mutant on AF organization and dynamics  
507 upon *Ec* invasion. In non-inoculated wild type plants expressing GFP-ABD2-GFP, which  
508 permits acquisition of highly resolved AF images (Wang et al., 2008), cortical AFs labelled by  
509 GFP-ABD2-GFP appeared to be branched and randomly oriented, forming a dense meshwork  
510 along the surface of the outer periclinal and anticlinal cell walls of leaf pavement cells  
511 (Supplemental Figure 11E). In contrast, cortical AFs in *pip5k1 pip5k2* cells were remarkably  
512 thinner and showed less branching than those in wild type, and tended to form disorganized  
513 bundles. The results demonstrate that depletion of PM PI(4,5)P<sub>2</sub> leads to diminished AF  
514 assembly and defects in AF organization. Upon powdery mildew attack at 12 hpi, fine AFs in  
515 wild type epidermal cells formed an intense network surrounding the pathogen-attempted  
516 penetration site, whereas in *pip5k1 pip5k2* cells, no distinct AF network appeared underneath  
517 fungal penetration sites, and AFs were preferentially organized into thick parallel bundles  
518 radiating across epidermal cells toward the infection site (Figure 7D). After the fungus  
519 successfully penetrated into epidermal cells, static and dense AFs, but not microtubules, closely  
520 surrounded developing haustoria in wild type epidermal cells at 20 hpi (Figures 7E and 7F).

521 At the same infection stage in *pip5k1 pip5k2* mutants, GFP-ABD2-GFP exhibited  
522 relatively high levels of diffuse cytoplasmic fluorescence compared with that of wild type, and  
523 AFs were barely visible on the surface of developing haustoria (Figure 7E). At 7 dpi, powdery  
524 mildew infection resulted in rapid colony development and fungal sporulation on the surface of  
525 wild type leaves, and within the epidermal cells hosting mature haustoria, abundant thick AF  
526 bundles were highly dynamic and frequently arrayed from the surface of mature haustorium  
527 towards cortical region of the cells (Figure 7G; Supplemental Movie 3). In the *pip5k1 pip5k2*  
528 mutant, AF bundles in *Ec*-infected cells dispersed in connection with the *Ec*-infection site,  
529 showing reduced cohesive attachment to the haustorial surface (Figure 7G; Supplemental Movie  
530 4). The impaired AF network at the fungal penetration site as well as on the haustorial surface  
531 suggests that *pip5k1 pip5k2* mutants displayed reduced actin-dependent cellular processes  
532 underlying the Arabidopsis-powdery mildew interaction.

533

534 **PI(4,5)P<sub>2</sub> Acts as a Susceptibility Factor for the Non-haustorium-forming Hemibiotroph**  
535 ***Colletotrichum higginsianum***

536 The crucifer anthracnose fungal pathogen *Colletotrichum higginsianum* (*Ch*) displays a  
537 multistage hemibiotrophic infection strategy on host *Arabidopsis* (Liu et al., 2007b). The  
538 pathogen invades *Arabidopsis* plants through direct penetration of host cell walls, forming  
539 invasive primary hyphae in epidermal cells. Following a brief biotrophic phase, the large primary  
540 hyphae switch to thin necrotrophic secondary hyphae that are associated with necrotic lesion  
541 development (Liu et al., 2007b). Similar to haustoria, the biotrophic hyphae of *Colletotrichum*  
542 spp. are completely encased by a specialized membrane structure, known as the extra-invasive  
543 hyphal membrane (EIHM). The specialized EIHM has been suggested to resemble the  
544 functionality of the EHM in haustorium-forming biotrophs (Lo Presti et al., 2015).

545 To determine the distribution of PI4P and PI(4,5)P<sub>2</sub> in association with the EIHM, plants  
546 expressing respective biosensors, mCIT-2xPH<sup>FAPP1</sup> and mCIT-1xPH<sup>PLCδ1</sup>, were inoculated with  
547 *Ch* and examined by confocal microscopy. Remarkably, signals for both PI4P biosensor mCIT-  
548 2xPH<sup>FAPP1</sup> and PI(4,5)P<sub>2</sub> biosensors mCIT-1xPH<sup>PLCδ1</sup> and mCIT-2xPH<sup>PLCδ1</sup> were located around  
549 the infection vesicles and primary hyphae where the enrichment of PI(4,5)P<sub>2</sub> biosensor mCIT-  
550 2xPH<sup>PLCδ1</sup> was occasionally observed (Figures 8A and 8B), as indicated by a previous study  
551 (Shimada et al., 2019). This result is in contrast to the absence of mCIT-2xPH<sup>FAPP1</sup> at the EHM  
552 surrounding the powdery mildew and white rust haustoria (Figure 1; Supplementary Figure 3),  
553 suggesting that the EHM encompassing haustoria and the EIHM surrounding *Ch* primary hyphae  
554 are not one homogenous entity, but instead are composed of distinct phosphoinositide pools.  
555 Nevertheless, PI(4,5)P<sub>2</sub> appears as a conserved and predominant phosphoinositide of both  
556 membrane compartments.

557 To evaluate the susceptibility of *pip5k1 pip5k2* mutant to *Ch*, intact plants of wild type  
558 and *pip5k1 pip5k2* mutant were sprayed with conidia of *Ch*. At 3 dpi, wild type leaves showed  
559 water-soaking lesions, and infected plants subsequently became withered and eventually died at  
560 4 dpi. In contrast, *pip5k1 pip5k2* plants barely produced visible anthracnose symptoms (Figure  
561 8C). Likewise, droplet inoculation on detached leaves further revealed that necrotic water-soaked  
562 lesions surrounded by chlorotic halos developed at the inoculation sites of wild type leaves 3 dpi,  
563 and water-soaked lesion expansion and tissue maceration rapidly spread over the inoculated leaf.  
564 The infection on leaves of *pip5k1 pip5k2* plants was strictly restricted at the inoculated site and  
565 did not spread beyond the inoculated area at extended incubation time until 6 dpi (Supplemental  
566 Figure 12). Thus, PI(4,5)P<sub>2</sub>, the resulting product of PIP5K1 and PIP5k2, is an important

567 determinant factor of host susceptibility to the hemibiotrophic *Colletotrichum* fungus as well as  
568 to the haustorium-forming biotrophic powdery mildew and white rust pathogens.

569 To investigate which stage of fungal development was impaired in the *pip5k1 pip5k2*  
570 mutant, we collected leaf tissues of wild type and *pip5k1 pip5k2* plants inoculated with *Ch* for  
571 microscopic examination. At 2 dpi, large primary hyphae colonized leaf epidermal cells of wild  
572 type and *pip5k1 pip5k2* plants (Figure 8D). In infected cells of wild type plants at 3 dpi,  
573 abundant thin secondary hyphae arose from primary hyphae and spread into several adjacent  
574 cells in leaf tissues showing water-soaking lesions. At 4 dpi, leaf tissues of wild type completely  
575 collapsed with systemic colonization by fungal secondary hyphae (Figure 8D). In contrast, in  
576 epidermal cells of *pip5k1 pip5k2* plants until 4 dpi, most infection sites were associated with  
577 extensive growth of primary hyphae, resulting in the first infected cells becoming filled with  
578 fungal hyphae.

579 To test whether extensive growth of primary hyphae within infected leaf epidermal cells  
580 of *pip5k1 pip5k2* plants at 4 dpi was still associated with the biotrophic phase of the interaction,  
581 infected leaf tissues were submitted for plasmolysis to assess the viability of host cells.  
582 Epidermal cells of *pip5k1 pip5k2* plants with extensive colonization of primary hyphae as well as  
583 adjacent non-infected cells displayed plasmolysis, and intact tonoplast membrane was clearly  
584 visible within the plasmolyzed cytoplasm of the infected cell (Figures 8E and 8F; Supplemental  
585 Movie 5). These results suggest that PI(4,5)P<sub>2</sub> is presented at the biotrophic interface in the *Ch*-  
586 *Arabidopsis* interaction, and mutation of both *PIP5K1* and *PIP5K2* genes inhibits the transition  
587 from the biotrophic to the necrotrophic stage, thus preventing the development of visible necrotic  
588 symptoms.

589

## 590 **DISCUSSION**

591 The structural singularity of the EHM has been well documented for the haustoria formed by  
592 powdery mildew and rust fungi. This membrane is continuous with the plant PM (Littlefield and  
593 Bracker, 1970), but the properties and molecular composition of the EHM are distinct. Electron  
594 micrographs reveal that an electron-dense haustorial neckband appears at the junction of the host  
595 PM, and the EHM exhibits a thick and convoluted appearance, which is distinct from the thin,  
596 smooth host PM (Gil and Gay, 1977; Celio et al., 2004; Micali et al., 2011). Furthermore, the  
597 EHM appears to lack several common plant PM proteins (Spencer-Phillips and Gay, 1981; Koh

598 et al., 2005; Micali et al., 2011), instead possessing a unique set of membrane proteins of the  
599 endomembrane system (Inada et al., 2016; Berkey et al., 2017; Kwaaitaal et al., 2017). In this  
600 study, we show that the host PM and EHM differ in their constituent lipids: both PI4P and  
601 PI(4,5)P<sub>2</sub> localize at the PM although PI(4,5)P<sub>2</sub> is found in relatively low abundance in plant  
602 cells (van Leeuwen et al., 2007; Vermeer et al., 2009; Munnik and Vermeer, 2010; Munnik and  
603 Nielsen, 2011; Simon et al., 2014; Simon et al., 2016), whereas only PI(4,5)P<sub>2</sub>, but not PI4P, is  
604 integrated into the EHM of powdery mildew (Figure 1). This distinct distribution pattern also  
605 appears on the EHM among other haustorium-forming biotrophs, such as the white rust *Albugo*  
606 *candida* (Supplemental Figure 3) and the downy mildew *Hyaloperonospora arabidopsidis*  
607 (Shimada et al., 2019). In contrast, both PI(4,5)P<sub>2</sub> and PI4P are present at the extra-invasive  
608 hyphal membrane (EIHM) enclosing the invasive hyphae of hemibiotroph *Colletotrichum*  
609 *higginsianum* (Figure 8) (Shimada et al., 2019) and at the periarbuscular membrane (PAM)  
610 formed during arbuscular mycorrhizal symbiosis (Ivanov and Harrison, 2019). The distinct  
611 nature of the EHM from the EIHM and PAM led us to explore the impact of PI4P absence on the  
612 characteristics of the EHM and the potential role of PI(4,5)P<sub>2</sub> on the functionality of haustoria.

613 In mammalian cells, PI4P is generated in many cellular membranes, including a major  
614 pool in the Golgi/TGN, and two relatively minor pools at the PM and late endosomes/lysosomes  
615 (Hammond et al., 2014). PI4P enriched at the cytosolic face of the *trans*-Golgi in mammalian  
616 cells recruits cytosolic proteins that bind to PI4P, and functions in Golgi-to-PM trafficking  
617 (Lenoir and Overduin, 2013; Makowski et al., 2017). In contrast, PI4P in plant cells  
618 predominantly accumulates at the PM, establishing it as a hallmark of this membrane (Simon et  
619 al., 2014; Simon et al., 2016). Critical roles of PI4P at the PM in animal and plant cells were only  
620 recently recognized as PI4P generates a high electrostatic field that contributes to the PM  
621 localization and function of proteins with polybasic motifs, including proteins involved in  
622 cytoskeleton dynamics, hormone transport and receptor-like kinase signaling (Hammond et al.,  
623 2012; Simon et al., 2014; Simon et al., 2016). Additionally, recent data indicate multiple PI4P  
624 binding proteins function as non-vesicular lipid transporters and drive lipid export from the  
625 endoplasmic reticulum to other organelles through the reciprocal transfer of PI4P at membrane  
626 contact sites (Cockcroft and Raghu, 2018). Thus, PI4P together with its effector proteins play  
627 essential roles in membrane biogenesis, cell signaling and cellular trafficking. The lack of PI4P

628 at the EHM likely contributes to the inability to anchor effector proteins at the EHM and further  
629 neglects the impact of PI4P-driven physical membrane property at the EHM.

630 Using PI4P as the precursor, PI4P 5-kinases participate in the biosynthesis of PI(4,5)P<sub>2</sub>,  
631 which primarily takes place at the PM (Simon et al., 2014). Notably, both PIP5K1 and PIP5K2  
632 are ubiquitously expressed in *Arabidopsis* and locate at the PM (Ischebeck et al., 2013), but are  
633 absent from the EHM (Supplemental Figure 9). The absence of PI4P 5-kinases and its precursor  
634 PI4P at the EHM suggests that PIP5K1 and PIP5K2 are not directly involved in the *in situ*  
635 synthesis of PI(4,5)P<sub>2</sub> at the EHM, and the PI(4,5)P<sub>2</sub> pool at the EHM is likely derived from the  
636 PM. We observed PI(4,5)P<sub>2</sub> signals likely bundled to the cytoskeleton between the host PM and  
637 the EHM (Supplemental Figure 1C). Disruption of actin filaments by latrunculin A prevents the  
638 trafficking of PI(4,5)P<sub>2</sub>, resulting in a weak signal intensity of PI(4,5)P<sub>2</sub> on the EHM (Figures 3A  
639 and 3B), indicating that the transport of PI(4,5)P<sub>2</sub> to the surface of the EHM is mediated by the  
640 actin cytoskeleton. Intriguingly, targeting of PI(4,5)P<sub>2</sub> signals to the EHM is not inhibited by  
641 brefeldin A (BFA), a fungal toxin that inhibits the activity of ARF-GEF GNOM-mediated  
642 vesicular trafficking in both endocytic and secretory pathways. The result supports targeting of  
643 PI(4,5)P<sub>2</sub> to the EHM independent from the GNOM-mediated vesicular transport. Whether other  
644 BFA-insensitive ARF-GEFs, such as BIG3 and/or BIG5/MIN7 (Geldner et al., 2003; Nomura et  
645 al., 2011; Richter et al., 2014), mediate the transport of PI(4,5)P<sub>2</sub> to the EHM remains to be  
646 determined. In eukaryotic cells, PI(4,5)P<sub>2</sub> is concentrated in sterol-rich domains at the PM (Pike  
647 and Miller, 1998; Graber et al., 2014; Stanislas et al., 2015). Upon depletion of phytosterols in  
648 *Arabidopsis* leaves by MβCD treatment, PI(4,5)P<sub>2</sub> signals are significantly reduced at the EHM  
649 as well as at the PM (Figures 3A and 3B), suggesting that the steady level of cellular sterols is  
650 required to maintain PI(4,5)P<sub>2</sub> pools at the PM and the EHM. Taken together, our data suggest  
651 that during establishment of powdery mildew haustoria, PI(4,5)P<sub>2</sub> at the EHM is likely derived  
652 from the PI(4,5)P<sub>2</sub> pool synthesized from PI4P at the PM, and the lateral transport of PI(4,5)P<sub>2</sub>  
653 from the PM to the EHM is actin-dependent.

654 Cellular imaging of PI(4,5)P<sub>2</sub> biosensors provides an indirect way to localize this  
655 phospholipid. The biosensor PH<sup>PLCδ1</sup> has a high selectivity for PI(4,5)P<sub>2</sub> and has been robustly  
656 expressed in many different organisms including yeast, mammalian and plant cells where the  
657 PH<sup>PLCδ1</sup> biosensor is recruited to the membranes that accumulate this lipid (Platre and Jaillais,  
658 2016). Notably, under low levels or in the absence of target lipid, the biosensor PH<sup>PLCδ1</sup> remains

659 unbound in the cytosol, making it unsuitable to quantitatively measure PI(4,5)P<sub>2</sub> contents with  
660 spatial resolution (van Leeuwen et al., 2007; Platre and Jaillais, 2016). Nonetheless, increased  
661 signal intensity of the PH<sup>PLCδ1</sup> biosensor was observed at the PM under conditions known to  
662 induce PI(4,5)P<sub>2</sub> synthesis or prevent its hydrolysis, such as high NaCl concentration or  
663 inhibition of phosphoinositide-specific PLC activity (van Leeuwen et al., 2007; Lee et al., 2019).  
664 Thus, a positive correlation exists between the signal intensity of the PH<sup>PLCδ1</sup> biosensor and the  
665 PI(4,5)P<sub>2</sub> contents, under conditions where this lipid becomes concentrated in membranes (van  
666 Leeuwen et al., 2007; Lee et al., 2019; Colin and Jaillais, 2020). Upon powdery mildew infection,  
667 the fluorescence intensity of the PI(4,5)P<sub>2</sub> biosensor mCIT-1xPH<sup>PLCδ1</sup> is specifically elevated in  
668 the infected cells, suggesting increased PI(4,5)P<sub>2</sub> levels in host cells during the infection process.  
669 Increased PI(4,5)P<sub>2</sub> content appears to be tightly associated with the host PM dynamics, and is  
670 focally aggregated around the pathogen penetration site and integrates into the EHM. Active  
671 recruitment of PI(4,5)P<sub>2</sub> into interaction sites suggests that pathogen infection alters the  
672 distribution of PI(4,5)P<sub>2</sub> to modulate the cellular activities of host cells. Although PI(4,5)P<sub>2</sub> is a  
673 minor component of the PM, its functions are broad (Tan et al., 2015). PI(4,5)P<sub>2</sub> is able to  
674 directly recruit and/or activate integral and peripheral membrane proteins that function in several  
675 essential cellular processes including the regulation of cellular trafficking, actin polymerization,  
676 focal adhesion assembly, and polarity establishment (Tan et al., 2015; Noack and Jaillais, 2017).  
677 Over the last decade, PI(4,5)P<sub>2</sub> has been shown to play physiological roles in plants in the  
678 regulation of auxin transport (Mei et al., 2012; Ischebeck et al., 2013), stomatal opening (Lee et  
679 al., 2007), root hair development (Kusano et al., 2008; Stenzel et al., 2008), pollen tube growth  
680 (Ischebeck et al., 2008; Sousa et al., 2008; Ischebeck et al., 2010; Ischebeck et al., 2011; Gillaspay,  
681 2013), and biotic and abiotic stress responses (Williams et al., 2005; Munnik and Vermeer, 2010;  
682 Shimada et al., 2019). Many of these processes occur in a strict spatially and temporally  
683 regulated fashion, requiring precise PI(4,5)P<sub>2</sub> targeting and concentrations (Krishnamoorthy et  
684 al., 2014; Noack and Jaillais, 2017). In this study, we showed that inactivation of Arabidopsis  
685 PI4P 5-kinase activity, caused by *PIP5K1* and *PIP5K2* gene knockouts, results in depletion of  
686 PM PI(4,5)P<sub>2</sub>, and diminishes the assembly and organization of cortical AFs. In support of these  
687 findings, PI(4,5)P<sub>2</sub> is the best-characterized regulator of actin cytoskeleton in yeast and  
688 mammalian cells amongst the functionally characterized phosphoinositides. PI(4,5)P<sub>2</sub> interacts  
689 directly with several central actin-binding proteins such as profilin, cofilin/ADF, formins, N-

690 WASP, and capping proteins, as well as many signaling and scaffolding proteins, which interact  
691 with actin-binding proteins to control their activities and/or subcellular localization. As a  
692 consequence, PI(4,5)P<sub>2</sub> promotes the formation of AF structures adjacent to the inner leaflet of  
693 the PM (Saarikangas et al., 2010; Senju and Lappalainen, 2019). Although the actin cytoskeleton  
694 and its accessory elements are highly conserved across eukaryotic species, the regulation of  
695 actin-binding proteins and associated proteins by PI(4,5)P<sub>2</sub> has yet to be validated in plants.

696       Upon powdery mildew infection of the *pip5k1 pip5k2* mutant, PI(4,5)P<sub>2</sub> depletion results  
697 in a concomitant reduction in the organization and dynamics of AFs under the pathogen  
698 penetration site and surrounding the haustorial surface. The actin cytoskeleton of host cells is  
699 commonly harnessed by intracellular pathogens to promote their own survival, replication, and  
700 cell-to-cell spread in various animal systems (Galán and Collmer, 1999; Galán and Zhou, 2000;  
701 Gouin et al., 2005). The diminished AF assembly and dynamics observed in the *pip5k1 pip5k2*  
702 mutant at powdery mildew fungus interaction sites is likely to facilitate actin-dependent cellular  
703 processes required for the powdery mildew disease development. For instance, AF arrangement  
704 on the haustorial surface was observed in the barley-powdery mildew system (Opalski et al.,  
705 2005) and was suggested to guide the spatial shaping of haustoria and/or deliver the molecules  
706 needed by the pathogen to feeding structures (Schmidt and Panstruga, 2007). The *pip5k1 pip5k2*  
707 mutant is also defective for focal accumulation of MLO2-GFP at the pathogen-attempted  
708 penetration sites and displays an enhanced penetration resistance against powdery mildew. The  
709 role of *MLO* genes as a major susceptibility factor to powdery mildews has been demonstrated in  
710 a wide range of monocot and dicot species (Kusch and Panstruga, 2017). Polarized MLO  
711 accumulation at pathogen penetration sites appears to be independent of actin cytoskeleton  
712 functions (Figures 7) (Bhat et al., 2005; Feechan et al., 2013), and potentially modulates focal  
713 actin reorganization at the penetration site (Opalski et al., 2005). However, the function of *mlo* in  
714 penetration resistance at the cell periphery requires both actin-dependent and actin-independent  
715 pathways (Opalski et al., 2005; Miklis et al., 2007). Therefore, PM PI(4,5)P<sub>2</sub> may also regulate  
716 the actin cytoskeleton-independent cellular trafficking that is required for MLO localization  
717 during powdery mildew infection. While the effects of cellular PI(4,5)P<sub>2</sub> depletion in the *pip5k1*  
718 *pip5k2* mutant on AF dynamics and focal MLO accumulation during powdery mildew infection  
719 are clear, the underlying mechanisms remain unknown. Targeted depletion of PI(4,5)P<sub>2</sub>  
720 specifically at the EHM could provide a specific strategy to evaluate the impact of PI(4,5)P<sub>2</sub> on



721 haustorial formation and function. Given that PI(4,5)P<sub>2</sub> has pleiotropic effects in regulating  
722 cellular functions, future work should address whether PI(4,5)P<sub>2</sub> depletion contributes to  
723 enhanced disease resistance in *pip5k* mutants through other cellular processes.

724 The depletion of PI(4,5)P<sub>2</sub> in the *pip5k1 pip5k2* mutant results in reduced disease  
725 incidence by inhibiting multiple stages of pathogen development of biotrophic powdery mildew,  
726 white rust and the hemibiotrophic *Colletotrichum* pathogens. On *pip5k1 pip5k2* leaves, powdery  
727 mildew establishment displays a low penetration rate, decreased haustorial development, and  
728 poor hypha growth. Likewise, restricted symptom development in *pip5k1 pip5k2* mutants is  
729 associated with the prevention of the switch from a biotrophic to a necrotrophic lifestyle of  
730 hemibiotrophic *C. higginsianum*. Evidently, no cell death was detected at either powdery mildew  
731 or *C. higginsianum* infection sites on *pip5k1 pip5k2* plants. Moreover, upon powdery mildew  
732 inoculation *pip5k1 pip5k2* mutants show similar levels of accumulation of autofluorescent  
733 compounds, callose deposition, and H<sub>2</sub>O<sub>2</sub> production at infection sites as compared to wild type.  
734 These results indicate that these cellular defense activities have a negligible contribution to  
735 enhanced disease resistance in the *pip5k1 pip5k2* mutant. However, the expression of several  
736 defense-responsive genes, including *PR1*, *PR2*, *BG3* and *PR4*, is significantly greater in the  
737 *pip5k1 pip5k2* mutant as compared to wild type upon powdery mildew infection. Intriguingly,  
738 the expression of these defense associated genes is induced in a salicylic acid (SA)-independent  
739 manner, since many genes involved in SA-synthesis and signaling are down-regulated in the  
740 mutant compared to wild type (Figure 5A). In addition, we found the SA level in the *pip5k1*  
741 *pip5k2* mutant is reduced to 55% of the wild type levels. A previous study indicated that  
742 sustained activation of two mitogen-activated protein kinases, MPK3 and MPK6, could be  
743 sufficient to confer SA-independent regulation of most SA-responsive genes in Arabidopsis  
744 (Tsuda et al., 2013). Recent work showed that phosphorylation by MPK6 inhibits PIP5K6  
745 activity and controls PI(4,5)P<sub>2</sub> production in the apical PM domain for tip growth of pollen tubes  
746 (Hempel et al., 2017). It would be interesting to examine whether MAPK activation is similarly  
747 involved in regulating SA-responsive genes in the *pip5k1 pip5k2* mutant.

748 In conclusion, our results demonstrate that the inhibition of multiple stages of disease  
749 progression in *pip5k1 pip5k2* mutant does not involve the enhanced activation of cellular  
750 defenses and cell death associated with cell wall lignification, callose deposition, and ROS

751 accumulation. We further show that reduced disease incidence of powdery mildew and  
752 *Colletotrichum* anthracnose appears to be the result of impaired susceptibility of the mutant.

753

## 754 **METHODS**

### 755 **Plant Materials and Growth Conditions**

756 *Arabidopsis thaliana* plants were grown at 21 °C with a 16-h photoperiod of ~125  $\mu\text{E m}^{-2}\text{s}^{-1}$ . All  
757 single T-DNA insertion mutants *pip5k1* (SALK\_146728, At1g21980), *pip5k2* (SALK\_012487,  
758 At1g77740) (Ischebeck et al., 2013), *pip5k5* (SALK\_147475, At2g41210), *pip5k7-1*  
759 (SALK\_151429, At1g10900), *pip5k8* (SAIL\_561\_F09, At1g60890), *pip5k9* (WiscDsLox434B6,  
760 At3g09920) were acquired from the Arabidopsis Biological Resource Center. The double mutant  
761 *pip5k1 pip5k2* was generated by crossing single mutants and propagated from the offspring of  
762 self-crossed plants *pip5k1*<sup>(+/-)</sup>/*pip5k2*<sup>(-/-)</sup>, since the homozygous double mutant did not produce  
763 flowers. The homozygosity of all T-DNA mutants was genotyped by PCR with both gene-  
764 specific and T-DNA border primers listed in Supplemental Table 2.

765 *Arabidopsis* transgenic lines tagged with fluorescent proteins used in this study include:  
766 35S:GFP-LTI6b (Cutler et al., 2000), 35S:PMA-GFP (Lefebvre et al., 2004), 35S:GFP-ABD2-  
767 GFP (Wang et al., 2008), mCherry-MAP4 (El Zawily et al., 2014), ER-GFP (CS16251), Tono-  
768 CFP (CS16256) and Tono-GFP (CS16257) (Nelson et al., 2007), Cyto-YFP (CS68117) (DeBono  
769 et al., 2009), pUBQ10:YFP (CS781646) (Geldner et al., 2009), RPW8.2:RPW8.2-YFP and  
770 RPW8.2:RPW8.2-RFP (Wang et al., 2007), MLO2:MLO2-YFP (Jones et al., 2017), PIPs  
771 biosensors pUBQ10:mCIT-1xPH<sup>PLC $\delta$ 1</sup> (P14Y), pUBQ10:mCIT-2xPH<sup>PLC $\delta$ 1</sup> (P24Y),  
772 pUBQ10:mCIT-1xTUBBY-C (P15Y), pUBQ10:mCIT-2xPH<sup>FAPP1</sup> (P21Y), pUBQ10:mCIT-  
773 1xPH<sup>FAPP1</sup> (P5Y), pUBQ10:2xCyPet-1xPH<sup>FAPP1</sup> (P5C), pUBQ10:mCIT-P4M<sup>SiDM</sup> (P4M) and  
774 pUBQ10:mCIT-2xFYVE<sup>HRS</sup> (P18Y) (Simon et al., 2014; Simon et al., 2016).

775

### 776 **Constructs and Plant Transformation**

777 To create a construct expressing PIP5K1-YFP, a DNA fragment containing ~3.5 kb ORF of  
778 *PIP5K1* gene and a ~2.1 kb promoter region was amplified from the *A. thaliana* genomic DNA  
779 with primers *SpeI*-PIP5K1-FP and *KpnI*-PIP5K1-RP (Supplemental Table 2). After digestion  
780 with enzymes *SpeI* and *KpnI*, the fragment was ligated into binary backbone vector pCNYHB  
781 (Yang et al., 2018), generating pPIP5K1:PIP5K1-YFP. To produce a construct expressing

782 PIP5K2-YFP, a DNA fragment containing a ~3.3 kb ORF of *PIP5K2* gene and a ~2.2 kb  
783 promoter region was amplified from the genomic DNA with primers *Xba*I-PIP5K2-FP and *Sma*I-  
784 PIP5K2-RP (Supplemental Table 2). After digestion with enzymes *Xba*I and *Sma*I, the fragment  
785 was ligated into pCNYHB, generating pPIP5K2:PIP5K2-YFP. The plasmids were introduced  
786 into *Agrobacterium tumefaciens* strain EHA105 and then transformed into Col-0 plants using  
787 floral dipping (Zhang et al., 2006). T<sub>1</sub> seeds were selected on MS medium with kanamycin.

788

### 789 **Pathogen Inoculation**

790 The Arabidopsis-adapted powdery mildew fungus *Erysiphe cichoracearum* (*Ec*) (Liu et al., 2010)  
791 was maintained and propagated on host cucumber (*Cucumis sativus*, variety Sweet Slice,  
792 McKenzie, Canada) plants. Three- to four-week-old Arabidopsis plants were inoculated with  
793 conidiospores at the density of 5-10 conidia mm<sup>-2</sup>. Inoculated leaves at the indicated time points  
794 post inoculation were detached, fixed, and stained as previously described (Yang et al., 2014).

795 The adapted anthracnose pathogen *Colletotrichum higginsianum* (*Ch*) on Arabidopsis  
796 was propagated and handled as described previously (Liu et al., 2007b). For disease assays, 3- to  
797 4-week-old Arabidopsis plants were sprayed with conidial suspensions or spotted with droplets  
798 ( $1 \times 10^6$  conidiospores mL<sup>-1</sup> in distilled water) and immediately the inoculated plants were  
799 placed into a 100% humidity chamber. Inoculated plants were photographed following the  
800 infection time course and infected leaves, at different time points post inoculation, were detached,  
801 fixed, and stained in trypan blue (Liu et al., 2007b).

802 Maintenance and inoculation of white rust *Albugo candida* isolate Acem1 on host  
803 Arabidopsis were performed using the described methods (Borhan et al., 2001). Briefly, *A.*  
804 *candida* was maintained on the Arabidopsis *NahG* plants. Zoosporangia were scratched off *A.*  
805 *candida* colonized leaf surface, resuspended in water (10<sup>5</sup> mL<sup>-1</sup>), and incubated on ice for 30  
806 min for zoospore release. The plants were inoculated by placing a drop of inoculum (10 µL) on  
807 each leaf and grown under a closed incubation chamber to retain humidity. The inoculated plants  
808 were placed in a cold incubator (14-16 °C) in the dark overnight and then kept under 10-h light  
809 and 14-h dark cycles for disease development.

810

### 811 **Chemical Treatments**

812 The following stock solutions in DMSO were used: 1 mM latrunculin A (Sigma), 50 mM  
813 brefeldin A (Sigma), 100 mM oryzalin (Sigma), 20 mM wortmannin (Sigma), 10 mM FM4-64  
814 (Thermo Fisher Scientific). Stocks were stored at -20 °C and subsequently diluted in H<sub>2</sub>O to the  
815 specified concentrations for experiments. The following working concentrations were used: 5  
816 μM latrunculin A, 1 mM oryzalin, 300 μM brefeldin A, 1 mM MβCD, 30 μM wortmannin, 50  
817 μM FM4-64. Leaves of Arabidopsis were pre-infiltrated with latrunculin A, oryzalin, brefeldin A,  
818 MβCD or wortmannin working solutions. After 1 h incubation, infiltrated leaves were inoculated  
819 with *Ec* conidiospores. At 24 hpi, inoculated leaves were examined under a confocal microscope.  
820 For plasmolysis experiments, leaves were mounted in 0.85 M KCl and incubated 15 min before  
821 imaging.

822

### 823 **Microscopy and Imaging**

824 Inoculated and non-inoculated leaves were harvested at varying time points, and fresh or fixed  
825 leaf tissues were examined by microscopy. The leaves were fixed in fixing buffer (60% methanol,  
826 30% chloroform, and 10% acetic acid; v/v). After rehydration through an ethanol gradient, leaves  
827 were stained with 0.05% trypan blue, 0.05% aniline blue and/or 10 μM Alexa Fluor<sup>®</sup>488  
828 conjugate of wheat germ agglutinin (WGA) (Life Technologies) as the experiment required,  
829 followed by light microscopy (AxioPlan, Zeiss) or confocal laser scanning microscopy (ZEISS  
830 LSM 510 Meta). Aniline blue was used to detect callose in 150 mM K<sub>2</sub>HPO<sub>4</sub> (pH 9.5) or to stain  
831 fungal hyphae in acidic water. Macroscopic detection of H<sub>2</sub>O<sub>2</sub> accumulation by DAB staining  
832 was performed as described earlier (Liu et al., 2007a). Fresh leaves were incubated in either  
833 distilled water or 10 μM propidium iodide (PI, Life Technologies), followed by confocal  
834 microscopy. The fluorescence was detected under confocal microscope with the following  
835 setting of excitation/emission wavelengths: CFP and callose (405/420-480 nm), GFP (488/505-  
836 530 nm), RFP (543/581-635 nm), YFP (514/530-560 nm), PI (488/>560 nm), FM4-64 (488/>650  
837 nm). Images were analyzed and performed with software LSM Image Browser, Adobe  
838 Photoshop, or ImageJ.

839 Quantification of YFP signal intensity was performed by confocal microscopy acquired  
840 under strictly identical acquisition parameters (laser power, pinhole, detector gains, speed, zoom  
841 factor, resolution and so on). Intensity quantification was performed using ImageJ. Average

842 intensity was measured and corrected to the average background signal. Quantification was  
843 performed over three plants per each genotype (n = 30).

844

### 845 **Immunofluorescence**

846 Fully expanded rosette leaves were excised from four-week-old Arabidopsis plants, and abaxial  
847 surface was inoculated with *Ec* conidiospores at the density of 5-10 conidia mm<sup>-2</sup>. Inoculated  
848 leaves were incubated in humid Petri dishes at 21 °C for 36 hpi. The adaxial epidermal leaf  
849 surface was affixed to a Scotch transparent adhesive tape with the abaxial side facing upwards.  
850 Subsequently, another strip of the tape was firmly topped on the abaxial surface of the affixed  
851 leaf. The upper tape was then gently pulled away from the lower tape, peeling away the abaxial  
852 epidermal cell layer attached to the lower tape. Epidermal peels attached on the transparent tapes  
853 were cut to ~3×5 mm, and fixed with 4% methanol-free formaldehyde, 0.2% glutaraldehyde in  
854 0.1 M Phosphate-buffered saline (PBS, pH 7.0) at 4 °C overnight.

855 Monoclonal anti-PI(4,5)P<sub>2</sub> antibody (clone 2C11, Z-P045) and anti-PI4P antibody (Z-  
856 P004) were purchased from Echelon Biosciences. Immunofluorescence studies were performed  
857 following the protocol described by Hammond et al. (2009) with some modifications. All steps  
858 from fixation to antibody incubation were performed on ice or 4°C. After fixation, the epidermal  
859 peels were rinsed three times with PBS and digested by incubation with cell wall-degrading  
860 enzyme mix (0.05% cellulase, 0.1% pectinase in PBS, pH 5.0) for 30 min. Then epidermal peels  
861 were blocked and permeabilized for 40 min incubation with a solution containing 5% (w/v) skim  
862 milk and 0.5% saponin (Quillaja bark; Sigma). The epidermal peels were incubated with primary  
863 anti-PI(4,5)P<sub>2</sub> (1:200) or anti-PI4P antibodies (1:200) at 4 °C overnight, followed by the  
864 incubation with the secondary antibody Alexa Fluor® 488 goat anti-mouse IgG (1:200; Abcam)  
865 for 4 h. The epidermal peels were mounted in ProLong® Gold antifade reagent (Invitrogen) and  
866 examined under a Zeiss 880 confocal microscope.

867

### 868 **RNA-Seq and RT-PCR Analysis**

869 Three- to four-week-old Arabidopsis Col-0 wild type and *pip5k1 pip5k2* plants were inoculated  
870 with *Ec* conidiospores. The leaves without or with *Ec*-inoculation at 2, 5 and 7 dpi were collected,  
871 flash frozen in liquid nitrogen, and stored at -80 °C until required. Three biological replicates

872 were obtained for each sample. RNA samples were prepared using the Plant RNA Isolation Mini  
873 Kit (Agilent Technologies) according to the manufacturer's protocol. The yield and purity of  
874 RNA were determined with Nanodrop 1100 (Thermo Fisher Scientific), and the quality was  
875 verified using an Agilent 2100 Bioanalyzer (Agilent Technologies). Purified total RNA was  
876 precipitated and resuspended in RNase-free H<sub>2</sub>O to a final concentration of 100 ng  $\mu\text{L}^{-1}$ . A total  
877 of 36 cDNA libraries were constructed using the TruSeq™ RNA Sample Preparation Kit  
878 (Illumina). Paired-end sequencing was conducted on the Illumina HiSeq2500 Sequencing  
879 System, generating 101-nucleotide reads at the National Research Council, Aquatic and Crop  
880 Resource Development, Saskatoon, Canada. Sequencing adapters were removed, and low-quality  
881 reads were trimmed using Trimmomatic with default settings (Bolger et al., 2014). Reads were  
882 mapped to the annotated *A. thaliana* genomes (TAIR10) using STAR (Dobin et al., 2013).  
883 Transcripts were identified using StringTie (Pertea et al., 2015) followed by Cuffmerge tool  
884 (Trapnell et al., 2012). HTseq-count (Anders et al., 2015) was used to count the reads spread  
885 across the exonic regions of each gene. Differential expression analysis was performed with  
886 DESeq2 between mutants and wild type (Love et al., 2014). Normalized read counts from  
887 DESeq2 were expressed as gene expression levels. Genes with less than 10 reads across all  
888 samples were excluded to eliminate the extremely low expressed transcripts. Differential gene  
889 expression analysis was performed with DESeq2 between mutants and WT at 2, 5 and 7 dpi,  
890 respectively. To identify genes with significant expression differences, a cut-off of  $\text{FDR} < 0.01$   
891 and  $|\log_2\text{FC}| \geq 1$  was applied. The heatmap was generated with the R pheatmap package.

892 For RT-PCR analysis, cDNA was synthesized from 1  $\mu\text{g}$  total RNA using the QuantiTect  
893 Reverse Transcription kit (Qiagen). Gene expression levels were evaluated by RT-PCR for 25 or  
894 28 cycles. The gene *elf4A1* was used as an internal control to normalize amount of cDNA  
895 template. Primers used in this study are listed in Supplemental Table 2.

896

### 897 **Hormone Measurement.**

898 Four-week-old *Arabidopsis* Col-0 and *pip5k1 pip5k2* plants were inoculated with *Ec*  
899 conidiospores at the density of 5-10 conidia  $\text{mm}^{-2}$  or with mock. The leaves at 5 dpi were  
900 harvested and immediately frozen in liquid nitrogen for SA and JA analyses. Three biological  
901 replicates were obtained for each sample. The extraction and quantification of SA and JA was  
902 performed according to the method described previously (Liu et al., 2010).

903

## 904 **Statistical Analysis**

905 Two-tailed Student *t*-test was used for paired comparison of the fluorescence intensities or fungal  
906 development between treatments vs mock or wild type vs mutant (\**P* < 0.05, \*\**P* < 0.01, \*\*\**P* <  
907 0.001). One-way ANOVA with Tukey's HSD (honestly significant difference) test was carried  
908 out for multiple comparison. Samples with statistically significant differences are marked with  
909 different letters (*p* < 0.05, lowercase letters; *p* < 0.01, capital letters). Error bars in all figures  
910 represent standard deviations. Number of replicates is reported in figure legends. All statistical  
911 analyses with ANOVA and/or *t*-test are included in Supplemental Data Set 2.

912

## 913 **Accession Numbers**

914 Sequence data from this article can be found in the Arabidopsis Genome Initiative or  
915 GenBank/EMBL databases under the following accession numbers: PIP5K1 (At1g21980),  
916 PIP5K2 (At1g77740), PIP5K5 (At2g41210), PIP5K7 (At1g10900), PIP5K8 (At1g60890),  
917 PIP5K9 (At3g09920), MLO2 (At1g11310), RPW8.2 (AF273059), PR1 (At2g14610), PDF1.2a  
918 (AT5G44420), FRK1 (AT2G19190) and eIF4A1 (At3g13920). The RNA-seq data used in this  
919 study are available in the Gene Expression Omnibus database under accession number  
920 GSE127919.

921

922

## 923 **Supplemental Data**

924 **Supplemental Figure 1.** Spatial Distribution of PI4P and PI(4,5)P<sub>2</sub> at Penetration Sites of the  
925 Powdery Mildew *E. cichoracearum*.

926 **Supplemental Figure 2.** Differential Distribution of Host Cellular Membrane Compartments in  
927 Association with the Haustorium of the Powdery Mildew *E. cichoracearum*.

928 **Supplemental Figure 3.** Differential Distribution of Phosphoinositides to the Haustorial  
929 Periphery of *Albugo candida*.

930 **Supplemental Figure 4.** Increased Production of PI(4,5)P<sub>2</sub> in *Ec*-colonized Leaf Epidermal  
931 Cells.

932 **Supplemental Figure 5.** Expression Profiling of *Arabidopsis* PI4P 5-kinase Genes and  
933 Characterization of T-DNA Insertion Mutants.

934 **Supplemental Figure 6.** Growth Phenotypes of the *Arabidopsis* Knockout Mutants and  
935 Complemented Mutant Plants of PI4P 5-kinase Genes.

936 **Supplemental Figure 7.** Pathogenicity Assays on Col-0 and *pip5k* Double, Triple and  
937 Quadruple Mutant Plants against the White Rust *Albugo candida*.

938 **Supplemental Figure 8.** Impaired Cellular Levels of PI(4,5)P<sub>2</sub> in *pip5k1 pip5k2* Mutants.

939 **Supplemental Figure 9.** Cellular Localization of PIP5K1-YFP and PIP5K2-YFP in *Arabidopsis*.

940 **Supplemental Figure 10.** Expression Levels of *PR1*, *PDF1.2a*, and *FRK1* Genes in Col-0 Wild  
941 Type and *pip5k1 pip5k2* at 2, 5 and 7 Days after Inoculation with *E. cichoracearum*.

942 **Supplemental Figure 11.** Cellular Dynamics of MLO2 and Reorganization of Actin Filaments  
943 in *pip5k1 pip5k2* Mutant.

944 **Supplemental Figure 12.** Loss of PIP5K1 and PIP5K2 Functions Prevented Disease  
945 Development of *C. higginsianum* Infection on Detached *Arabidopsis* Leaves.

946 **Supplementary Table 1.** Frequency of Phosphoinositide Biosensor Accumulation at the  
947 Extrahaustorial Membrane of Powdery Mildew.

948 **Supplemental Table 2.** Oligonucleotide Sequences of Primers Used in This Study.

949 **Supplemental Data Set 1.** Differentially Expressed Genes in Col-0 Wild Type and *pip5k1*  
950 *pip5k2* at 2, 5 and 7 Days after Inoculation with *E. cichoracearum*.

951 **Supplemental Data Set 2. Statistical Analyses Performed in This Study.**

952 **Supplemental Movie 1.** Z-stack Images Showing the Spatial Distribution of PI4P at the  
953 Penetration Site of Powdery Mildew *E. cichoracearum*.

954 **Supplemental Movie 2.** Z-stack Images Showing the Spatial Distribution of PI(4,5)P<sub>2</sub> at the  
955 Penetration Site of Powdery Mildew *E. cichoracearum*.

956 **Supplemental Movie 3.** Z-stack Images Showing the Actin Filaments in Epidermal Cells of Col-  
957 0 Leaves Hosting a Mature Haustorium of Powdery Mildew *E. cichoracearum*.

958 **Supplemental Movie 4.** Z-stack Images Showing the Actin Filaments in Epidermal Cells of  
959 *pip5k1 pip5k2* Mutant Leaves Hosting a Mature Haustorium of Powdery Mildew *E.*  
960 *cichoracearum*.

961 **Supplemental Movie 5.** Z-stack Images of Epidermal Cells of *pip5k1 pip5k2* Mutant Leaves  
962 Inoculated with *C. higginsianum*.

963

964 **ACKNOWLEDGMENTS**



965 We thank Vipen Sawhney for critically reading the manuscript, Shunyan Xiao and Mohammad  
966 H. Borhan for providing materials. We thank the Arabidopsis Biological Resource Center (Ohio  
967 State University) for providing seeds for T-DNA insertion lines and transgenic marker lines. This  
968 work was supported by grants from the Natural Sciences and Engineering Research Council of  
969 Canada (Discovery Grant) and the Canadian Foundation for Innovation to Y.W., and National  
970 Natural Science Foundation of China (grant no. 31471428) to Z. Z..

971

#### 972 **AUTHOR CONTRIBUTIONS**

973 L.Q., Z.Z. and Y.W. initiated the project. L.Q., Z.Z., L.L. and Y.W. performed microscopic  
974 analyses. L.Q. and Y.W. conducted pathogenicity tests. C.Z., G.P. and L.Q. generated transgenic  
975 plants. P.G., R.D. and D.X. measured hormones. Q.L. and D.X. conducted gene expression  
976 profiling. L.Q. and T.D.Q. performed immunofluorescence. S.A.K. and Y.J. provided  
977 experimental materials. L.Q., Z.Z. and Y.W. wrote the paper with input from Y.J., S.A.K., R.D.,  
978 G.P. and D.X.

979

#### 980 **DECLARATION OF INTERESTS**

981 The authors declare no competing interests.

982

#### 983 **REFERENCES**

- 984 **Anders, S., Pyl, P.T., and Huber, W.** (2015). HTSeq-a Python framework to work with high-  
985 throughput sequencing data. *Bioinformatics* **31**, 166-169.
- 986 **Asai, T., Tena, G., Plotnikova, J., Willmann, M.R., Chiu, W.-L., Gomez-Gomez, L., Boller,**  
987 **T., Ausubel, F.M., and Sheen, J.** (2002). MAP kinase signalling cascade in *Arabidopsis*  
988 innate immunity. *Nature* **415**, 977-983.
- 989 **Berkey, R., Zhang, Y., Ma, X., King, H., Zhang, Q., Wang, W., and Xiao, S.** (2017).  
990 Homologues of the RPW8 resistance protein are localized to the extrahaustorial membrane  
991 that is likely synthesized de novo. *Plant Physiol.* **173**, 600-613.
- 992 **Bhat, R.A., Miklis, M., Schmelzer, E., Schulze-Lefert, P., and Panstruga, R.** (2005).  
993 Recruitment and interaction dynamics of plant penetration resistance components in a plasma  
994 membrane microdomain. *Proc. Natl. Acad. Sci. USA* **102**, 3135-3140.
- 995 **Bolger, A.M., Lohse, M., and Usadel, B.** (2014). Trimmomatic: a flexible trimmer for Illumina  
996 sequence data. *Bioinformatics* **30**, 2114-2120.
- 997 **Borhan, M.H., Brose, E., Beynon, J.L., and Holub, E.B.** (2001). White rust (*Albugo candida*)  
998 resistance loci on three Arabidopsis chromosomes are closely linked to downy mildew  
999 (*Peronospora parasitica*) resistance loci. *Mol. Plant Pathol.* **2**, 87-95.
- 1000 **Boudsocq, M., Willmann, M.R., McCormack, M., Lee, H., Shan, L., He, P., Bush, J., Cheng,**  
1001 **S.H., and Sheen, J.** (2010). Differential innate immune signalling via Ca<sup>2+</sup> sensor protein  
1002 kinases. *Nature* **464**, 418-422.
- 1003 **Capasso, S., and D'Angelo, G.** (2019). Imaging lipid metabolism at the Golgi complex. In  
1004 *Intracellular Lipid Transport: Methods and Protocols*, G. Drin, ed (New York, NY: Springer  
1005 New York), pp. 47-56.

1006 **Catanzariti, A.-M., Dodds, P.N., Lawrence, G.J., Ayliffe, M.A., and Ellis, J.G.** (2006).  
1007 Haustorially expressed secreted proteins from flax rust are highly enriched for avirulence  
1008 elicitors. *Plant Cell* **18**, 243-256.

1009 **Celio, G., Mims, C., and Richardson, E.** (2004). Ultrastructure and immunocytochemistry of  
1010 the host pathogen interface in poinsettia leaves infected with powdery mildew. *Can. J. Bot.* **82**,  
1011 421-429.

1012 **Choi, S., Thapa, N., Tan, X., Hedman, A.C., and Anderson, R.A.** (2015). PIP kinases define  
1013 PI4,5P<sub>2</sub> signaling specificity by association with effectors. *BBA-Mol. Cell Biol. L.* **1851**, 711-  
1014 723.

1015 **Cockcroft, S., and Raghun, P.** (2018). Phospholipid transport protein function at organelle  
1016 contact sites. *Curr. Opin. Cell Biol.* **53**, 52-60.

1017 **Colin, L.A., and Jaillais, Y.** (2020). Phospholipids across scales: lipid patterns and plant  
1018 development. *Curr. Opin. Plant Biol.* **53**, 1-9.

1019 **Consonni, C., Humphry, M.E., Hartmann, H.A., Livaja, M., Durner, J., Westphal, L.,  
1020 Vogel, J., Lipka, V., Kemmerling, B., Schulze-Lefert, P., et al.** (2006). Conserved  
1021 requirement for a plant host cell protein in powdery mildew pathogenesis. *Nature Genet.* **38**,  
1022 716-720.

1023 **Cutler, N.S., Heitman, J., and Cardenas, M.E.** (1997). STT4 is an essential  
1024 phosphatidylinositol 4-kinase that is a target of wortmannin in *Saccharomyces cerevisiae*. *J.*  
1025 *Biol. Chem.* **272**, 27671-27677.

1026 **Cutler, S.R., Ehrhardt, D.W., Griffiths, J.S., and Somerville, C.R.** (2000). Random  
1027 GFP::cDNA fusions enable visualization of subcellular structures in cells of *Arabidopsis* at a  
1028 high frequency. *Proc. Natl. Acad. Sci. USA* **97**, 3718-3723.

1029 **DeBono, A., Yeats, T.H., Rose, J.K., Bird, D., Jetter, R., Kunst, L., and Samuels, L.** (2009).  
1030 *Arabidopsis* LTPG is a glycosylphosphatidylinositol-anchored lipid transfer protein required  
1031 for export of lipids to the plant surface. *Plant Cell* **21**, 1230-1238.

1032 **Dobin, A., Davis, C.A., Schlesinger, F., Drenkow, J., Zaleski, C., Jha, S., Batut, P., Chaisson,  
1033 M., and Gingeras, T.R.** (2013). STAR: ultrafast universal RNA-seq aligner. *Bioinformatics*  
1034 **29**, 15-21.

1035 **El Zawily, A.M., Schwarzlander, M., Finkemeier, I., Johnston, I.G., Benamar, A., Cao, Y.,  
1036 Gissot, C., Meyer, A.J., Wilson, K., Datla, R., et al.** (2014). *FRIENDLY* regulates  
1037 mitochondrial distribution, fusion, and quality control in *Arabidopsis*. *Plant Physiol.* **166**, 808-  
1038 828.

1039 **Feechan, A., Jermakow, A.M., Ivancevic, A., Godfrey, D., Pak, H., Panstruga, R., and Dry,  
1040 I.B.** (2013). Host cell entry of powdery mildew is correlated with endosomal transport of  
1041 antagonistically acting VvPEN1 and VvMLO to the papilla. *Mol. Plant-Microbe Interact.* **26**,  
1042 1138-1150.

1043 **Frye, C.A., and Innes, R.W.** (1998). An *Arabidopsis* mutant with enhanced resistance to  
1044 powdery mildew. *Plant Cell* **10**, 947-956.

1045 **Galán, J.E., and Collmer, A.** (1999). Type III secretion machines: bacterial devices for protein  
1046 delivery into host cells. *Science* **284**, 1322-1328.

1047 **Galán, J.E., and Zhou, D.** (2000). Striking a balance: modulation of the actin cytoskeleton by  
1048 *Salmonella*. *Proc. Natl. Acad. Sci. USA* **97**, 8754-8761.

1049 **Geldner, N., Denervaud-Tendon, V., Hyman, D.L., Mayer, U., Stierhof, Y.D., and Chory, J.**  
1050 (2009). Rapid, combinatorial analysis of membrane compartments in intact plants with a  
1051 multicolor marker set. *Plant J.* **59**, 169-178.

1052 **Geldner, N., Anders, N., Wolters, H., Keicher, J., Kornberger, W., Muller, P., Delbarre, A.,**  
1053 **Ueda, T., Nakano, A., and Jürgens, G.** (2003). The *Arabidopsis* GNOM ARF-GEF mediates  
1054 endosomal recycling, auxin transport, and auxin-dependent plant growth. *Cell* **112**, 219-230.  
1055 **Gil, F., and Gay, J.L.** (1977). Ultrastructural and physiological properties of the host interfacial  
1056 components of haustoria of *Erysiphe pisi* *in vivo* and *in vitro*. *Physiol. Plant Pathol.* **10**, 1-12.  
1057 **Gillaspy, G.E.** (2013). The role of phosphoinositides and inositol phosphates in plant cell  
1058 signaling. *Adv. Exp. Med. Biol.* **991**, 141-157.  
1059 **Gouin, E., Welch, M.D., and Cossart, P.** (2005). Actin-based motility of intracellular  
1060 pathogens. *Curr. Opin. Microbiol.* **8**, 35-45.  
1061 **Graber, Z.T., Gericke, A., and Kooijman, E.E.** (2014). Phosphatidylinositol-4,5-bisphosphate  
1062 ionization in the presence of cholesterol, calcium or magnesium ions. *Chem. Phys. Lipids* **182**,  
1063 62-72.  
1064 **Hahn, M., and Mendgen, K.** (2001). Signal and nutrient exchange at biotrophic plant–fungus  
1065 interfaces. *Curr. Opin. Plant Biol.* **4**, 322-327.  
1066 **Hammond, G.R., Schiavo, G., and Irvine, R.F.** (2009). Immunocytochemical techniques  
1067 reveal multiple, distinct cellular pools of PtdIns4P and PtdIns(4,5)P<sub>2</sub>. *Biochem. J.* **422**, 23-35.  
1068 **Hammond, G.R., Machner, M.P., and Balla, T.** (2014). A novel probe for phosphatidylinositol  
1069 4-phosphate reveals multiple pools beyond the Golgi. *J. Cell Biol.* **205**, 113-126.  
1070 **Hammond, G.R., Fischer, M.J., Anderson, K.E., Holdich, J., Koteci, A., Balla, T., and**  
1071 **Irvine, R.F.** (2012). PI4P and PI(4,5)P<sub>2</sub> are essential but independent lipid determinants of  
1072 membrane identity. *Science* **337**, 727-730.  
1073 **Hammond, G.R.V., Dove, S.K., Nicol, A., Pinxteren, J.A., Zicha, D., and Schiavo, G.** (2006).  
1074 Elimination of plasma membrane phosphatidylinositol (4,5)-bisphosphate is required for  
1075 exocytosis from mast cells. *J. Cell Sci.* **119**, 2084-2094.  
1076 **Hauck, P., Thilmony, R., and He, S.Y.** (2003). A *Pseudomonas syringae* type III effector  
1077 suppresses cell wall-based extracellular defense in susceptible *Arabidopsis* plants. *Proc. Natl.*  
1078 *Acad. Sci. USA* **100**, 8577-8582.  
1079 **He, P., Shan, L., Lin, N.C., Martin, G.B., Kemmerling, B., Nurnberger, T., and Sheen, J.**  
1080 (2006). Specific bacterial suppressors of MAMP signaling upstream of MAPKKK in  
1081 *Arabidopsis* innate immunity. *Cell* **125**, 563-575.  
1082 **Heath, M.C.** (1997). Signalling between pathogenic rust fungi and resistant or susceptible host  
1083 plants. *Ann. Bot.* **80**, 713-720.  
1084 **Heilmann, M., and Heilmann, I.** (2015). Plant phosphoinositides-complex networks controlling  
1085 growth and adaptation. *BBA-Mol. Cell Biol. L.* **1851**, 759-769.  
1086 **Hempel, F., Stenzel, I., Heilmann, M., Krishnamoorthy, P., Menzel, W., Golbik, R., Helm,**  
1087 **S., Dobritzsch, D., Baginsky, S., Lee, J., et al.** (2017). MAPKs influence pollen tube growth  
1088 by controlling the formation of phosphatidylinositol 4,5-bisphosphate in an apical plasma  
1089 membrane domain. *Plant Cell* **29**, 3030-3050.  
1090 **Hruz, T., Laule, O., Szabo, G., Wessendorp, F., Bleuler, S., Oertle, L., Widmayer, P.,**  
1091 **Gruissem, W., and Zimmermann, P.** (2008). Genevestigator v3: a reference expression  
1092 database for the meta-analysis of transcriptomes. *Adv. Bioinf.* **2008**, 420747.  
1093 **Inada, N., Betsuyaku, S., Shimada, T.L., Ebine, K., Ito, E., Kutsuna, N., Hasezawa, S.,**  
1094 **Takano, Y., Fukuda, H., Nakano, A., et al.** (2016). Modulation of plant RAB GTPase-  
1095 mediated membrane trafficking pathway at the interface between plants and obligate  
1096 biotrophic pathogens. *Plant Cell Physiol.* **57**, 1854-1864.

1097 **Ischebeck, T., Stenzel, I., and Heilmann, I.** (2008). Type B phosphatidylinositol-4-phosphate  
1098 5-kinases mediate *Arabidopsis* and *Nicotiana tabacum* pollen tube growth by regulating  
1099 apical pectin secretion. *Plant Cell* **20**, 3312-3330.

1100 **Ischebeck, T., Vu, L.H., Jin, X., Stenzel, I., Löffke, C., and Heilmann, I.** (2010). Functional  
1101 cooperativity of enzymes of phosphoinositide conversion according to synergistic effects on  
1102 pectin secretion in tobacco pollen tubes. *Molecular Plant* **3**, 870-881.

1103 **Ischebeck, T., Stenzel, I., Hempel, F., Jin, X., Mosblech, A., and Heilmann, I.** (2011).  
1104 Phosphatidylinositol-4,5-bisphosphate influences Nt-Rac5-mediated cell expansion in pollen  
1105 tubes of *Nicotiana tabacum*. *Plant J.* **65**, 453-468.

1106 **Ischebeck, T., Werner, S., Krishnamoorthy, P., Lerche, J., Meijón, M., Stenzel, I., Löffke, C.,  
1107 Wiessner, T., Im, Y.J., Perera, I.Y., et al.** (2013). Phosphatidylinositol 4,5-bisphosphate  
1108 influences PIN polarization by controlling clathrin-mediated membrane trafficking in  
1109 *Arabidopsis*. *Plant Cell* **25**, 4894-4911.

1110 **Ivanov, S., and Harrison, M.J.** (2019). Accumulation of phosphoinositides in distinct regions  
1111 of the periarbuscular membrane. *New Phytol.* **221**, 2213-2227.

1112 **Jelinkova, A., Malinska, K., Simon, S., Kleine-Vehn, J., Parezova, M., Pejchar, P., Kubes,  
1113 M., Martinec, J., Friml, J., Zazimalova, E., et al.** (2010). Probing plant membranes with  
1114 FM dyes: tracking, dragging or blocking? *Plant J.* **61**, 883-892.

1115 **Jha, S.G., Larson, E.R., Humble, J., Domozych, D.S., Barrington, D.S., and Tierney, M.L.**  
1116 (2018). *Vacuolar Protein Sorting 26C* encodes an evolutionarily conserved large retromer  
1117 subunit in eukaryotes that is important for root hair growth in *Arabidopsis thaliana*. *Plant J.*  
1118 **94**, 595-611.

1119 **Jones, D.S., Yuan, J., Smith, B.E., Willoughby, A.C., Kumimoto, E.L., and Kessler, S.A.**  
1120 (2017). MILDEW RESISTANCE LOCUS O function in pollen tube reception is linked to its  
1121 oligomerization and subcellular distribution. *Plant Physiol.* **175**, 172-185.

1122 **Koh, S., Andre, A., Edwards, H., Ehrhardt, D., and Somerville, S.** (2005). *Arabidopsis*  
1123 *thaliana* subcellular responses to compatible *Erysiphe cichoracearum* infections. *Plant J.* **44**,  
1124 516-529.

1125 **Krinke, O., Ruelland, E., Valentová, O., Vergnolle, C., Renou, J.-P., Taconnat, L., Flemr,  
1126 M., Burketová, L., and Zachowski, A.** (2007). Phosphatidylinositol 4-kinase activation is an  
1127 early response to salicylic acid in *Arabidopsis* suspension cells. *Plant Physiol.* **144**, 1347-1359.

1128 **Krishnamoorthy, P., Sanchez-Rodriguez, C., Heilmann, I., and Persson, S.** (2014).  
1129 Regulatory roles of phosphoinositides in membrane trafficking and their potential impact on  
1130 cell-wall synthesis and re-modelling. *Ann. Bot.* **114**, 1049-1057.

1131 **Kusano, H., Testerink, C., Vermeer, J.E., Tsuge, T., Shimada, H., Oka, A., Munnik, T., and  
1132 Aoyama, T.** (2008). The *Arabidopsis* phosphatidylinositol phosphate 5-kinase PIP5K3 is a  
1133 key regulator of root hair tip growth. *Plant Cell* **20**, 367-380.

1134 **Kusch, S., and Panstruga, R.** (2017). *mlo*-based resistance: an apparently universal “weapon”  
1135 to defeat powdery mildew disease. *Mol. Plant-Microbe Interact.* **30**, 179-189.

1136 **Kwaaitaal, M., Nielsen, M.E., Böhlenius, H., and Thordal-Christensen, H.** (2017). The plant  
1137 membrane surrounding powdery mildew haustoria shares properties with the endoplasmic  
1138 reticulum membrane. *J. Exp. Bot.* **68**, 5731-5743.

1139 **Lee, E., Vanneste, S., Pérez-Sancho, J., Benítez-Fuente, F., Strelau, M., Macho, A.P.,  
1140 Botella, M.A., Friml, J., and Rosado, A.** (2019). Ionic stress enhances ER-PM connectivity  
1141 via phosphoinositide-associated SYT1 contact site expansion in *Arabidopsis*. *Proceedings of*  
1142 *the National Academy of Sciences* **116**, 1420-1429.

1143 **Lee, Y., Kim, Y.W., Jeon, B.W., Park, K.Y., Suh, S.J., Seo, J., Kwak, J.M., Martinoia, E.,**  
1144 **Hwang, I., and Lee, Y.** (2007). Phosphatidylinositol 4,5-bisphosphate is important for  
1145 stomatal opening. *Plant J.* **52**, 803-816.

1146 **Lefebvre, B., Batoko, H., Duby, G., and Boutry, M.** (2004). Targeting of a *Nicotiana*  
1147 *plumbaginifolia* H<sup>+</sup>-ATPase to the plasma membrane is not by default and requires cytosolic  
1148 structural determinants. *Plant Cell* **16**, 1772-1789.

1149 **Lenoir, M., and Overduin, M.** (2013). PtdIns(4)P signalling and recognition systems. *Adv. Exp.*  
1150 *Med. Biol.* **991**, 59-83.

1151 **Littlefield, L.J., and Bracker, C.E.** (1970). Continuity of host plasma membrane around  
1152 haustoria of *Melampsora lini*. *Mycologia* **62**, 609-614.

1153 **Liu, G., Greenshields, D.L., Sammynaiken, R., Hirji, R.N., Selvaraj, G., and Wei, Y.**  
1154 (2007a). Targeted alterations in iron homeostasis underlie plant defense responses. *J. Cell Sci.*  
1155 **120**, 596-605.

1156 **Liu, G., Kennedy, R., Greenshields, D.L., Peng, G., Forseille, L., Selvaraj, G., and Wei, Y.**  
1157 (2007b). Detached and attached *Arabidopsis* leaf assays reveal distinctive defense responses  
1158 against hemibiotrophic *Colletotrichum* spp. *Mol. Plant-Microbe Interact.* **20**, 1308-1319.

1159 **Liu, G., Ji, Y., Bhuiyan, N.H., Pilot, G., Selvaraj, G., Zou, J., and Wei, Y.** (2010). Amino  
1160 acid homeostasis modulates salicylic acid-associated redox status and defense responses in  
1161 *Arabidopsis*. *Plant Cell* **22**, 3845-3863.

1162 **Lo Presti, L., Lanver, D., Schweizer, G., Tanaka, S., Liang, L., Tollot, M., Zuccaro, A.,**  
1163 **Reissmann, S., and Kahmann, R.** (2015). Fungal effectors and plant susceptibility. *Annu.*  
1164 *Rev. Plant Biol.* **66**, 513-545.

1165 **Love, M.I., Huber, W., and Anders, S.** (2014). Moderated estimation of fold change and  
1166 dispersion for RNA-seq data with DESeq2. *Genome Biol.* **15**, 1.

1167 **Makowski, S.L., Tran, T.T., and Field, S.J.** (2017). Emerging themes of regulation at the  
1168 Golgi. *Curr. Opin. Cell Biol.* **45**, 17-23.

1169 **Matsuoka, K., Bassham, D.C., Raikhel, N.V., and Nakamura, K.** (1995). Different sensitivity  
1170 to wortmannin of two vacuolar sorting signals indicates the presence of distinct sorting  
1171 machineries in tobacco cells. *J. Cell Biol.* **130**, 1307-1318.

1172 **Mei, Y., Jia, W.-J., Chu, Y.-J., and Xue, H.-W.** (2012). *Arabidopsis* phosphatidylinositol  
1173 monophosphate 5-kinase 2 is involved in root gravitropism through regulation of polar auxin  
1174 transport by affecting the cycling of PIN proteins. *Cell Res.* **22**, 581-597.

1175 **Micali, C.O., Neumann, U., Grunewald, D., Panstruga, R., and O'Connell, R.** (2011).  
1176 Biogenesis of a specialized plant-fungal interface during host cell internalization of  
1177 *Golovinomyces orontii* haustoria. *Cell Microbiol.* **13**, 210-226.

1178 **Miklis, M., Consonni, C., Bhat, R.A., Lipka, V., Schulze-Lefert, P., and Panstruga, R.**  
1179 (2007). Barley MLO modulates actin-dependent and actin-independent antifungal defense  
1180 pathways at the cell periphery. *Plant Physiol.* **144**, 1132-1143.

1181 **Morejohn, L.C.** (1991). The molecular pharmacology of plant tubulin and microtubules. In *The*  
1182 *Cytoskeletal Basis of Plant Growth and Form*, C.W. Loyd, ed (London: Academic), pp. 29-43.

1183 **Moseley, J.B., and Goode, B.L.** (2006). The yeast actin cytoskeleton: from cellular function to  
1184 biochemical mechanism. *Microbiol. Mol. Biol. Rev.* **70**, 605-645.

1185 **Mueller-Roeber, B., and Pical, C.** (2002). Inositol phospholipid metabolism in *Arabidopsis*.  
1186 Characterized and putative isoforms of inositol phospholipid kinase and phosphoinositide-  
1187 specific phospholipase C. *Plant Physiol.* **130**, 22-46.

1188 **Munnik, T., and Vermeer, J.E.** (2010). Osmotic stress-induced phosphoinositide and inositol  
1189 phosphate signalling in plants. *Plant Cell Environ.* **33**, 655-669.

1190 **Munnik, T., and Nielsen, E.** (2011). Green light for polyphosphoinositide signals in plants.  
1191 *Curr. Opin. Plant Biol.* **14**, 489-497.

1192 **Nakanishi, S., Catt, K.J., and Balla, T.** (1995). A wortmannin-sensitive phosphatidylinositol 4-  
1193 kinase that regulates hormone-sensitive pools of inositolphospholipids. *Proc. Natl. Acad. Sci.*  
1194 *USA* **92**, 5317-5321.

1195 **Nelson, B.K., Cai, X., and Nebenführ, A.** (2007). A multicolored set of *in vivo* organelle  
1196 markers for co-localization studies in Arabidopsis and other plants. *Plant J.* **51**, 1126-1136.

1197 **Nielsen, M.E., Feechan, A., Bohlenius, H., Ueda, T., and Thordal-Christensen, H.** (2012).  
1198 *Arabidopsis* ARF-GTP exchange factor, GNOM, mediates transport required for innate  
1199 immunity and focal accumulation of syntaxin PEN1. *Proc. Natl. Acad. Sci. USA* **109**, 11443-  
1200 11448.

1201 **Noack, L.C., and Jaillais, Y.** (2017). Precision targeting by phosphoinositides: how PIs direct  
1202 endomembrane trafficking in plants. *Curr. Opin. Plant Biol.* **40**, 22-33.

1203 **Nomura, K., Mecey, C., Lee, Y.-N., Imboden, L.A., Chang, J.H., and He, S.Y.** (2011).  
1204 Effector-triggered immunity blocks pathogen degradation of an immunity-associated vesicle  
1205 traffic regulator in *Arabidopsis*. *Proc. Natl. Acad. Sci. USA* **108**, 10774-10779.

1206 **Ohtani, Y., Irie, T., Uekama, K., Fukunaga, K., and Pitha, J.** (1989). Differential effects of  $\alpha$ -  
1207  $\beta$ -and  $\gamma$ -cyclodextrins on human erythrocytes. *Eur. J. Biochem.* **186**, 17-22.

1208 **Opalski, K.S., Schultheiss, H., Kogel, K.H., and Hükelhoven, R.** (2005). The receptor-like  
1209 MLO protein and the RAC/ROP family G-protein RACB modulate actin reorganization in  
1210 barley attacked by the biotrophic powdery mildew fungus *Blumeria graminis* f.sp. *hordei*.  
1211 *Plant J.* **41**, 291-303.

1212 **Perte, M., Perte, G.M., Antonescu, C.M., Chang, T.-C., Mendell, J.T., and Salzberg, S.L.**  
1213 (2015). StringTie enables improved reconstruction of a transcriptome from RNA-seq reads.  
1214 *Nature Biotechnol.* **33**, 290.

1215 **Pike, L.J., and Miller, J.M.** (1998). Cholesterol depletion delocalizes phosphatidylinositol  
1216 bisphosphate and inhibits hormone-stimulated phosphatidylinositol turnover. *J. Biol. Chem.*  
1217 **273**, 22298-22304.

1218 **Platre, M.P., and Jaillais, Y.** (2016). Guidelines for the use of protein domains in acidic  
1219 phospholipid imaging. *Methods Mol. Biol.* **1376**, 175-194.

1220 **Pollard, T.D.** (2007). Regulation of actin filament assembly by Arp2/3 complex and formins.  
1221 *Annu. Rev. Biophys. Biomol. Struct.* **36**, 451-477.

1222 **Richter, S., Kientz, M., Brumm, S., Nielsen, M.E., Park, M., Gavidia, R., Krause, C., Voss,  
1223 U., Beckmann, H., Mayer, U., et al.** (2014). Delivery of endocytosed proteins to the cell-  
1224 division plane requires change of pathway from recycling to secretion. *eLife* **3**, e02131.

1225 **Roberts, A.M., Mackie, A.J., Hathaway, V., Callow, J.A., and Green, J.R.** (1993). Molecular  
1226 differentiation in the extrahaustorial membrane of pea powdery mildew haustoria at early and  
1227 late stages of development. *Physiol. Mol. Plant Pathol.* **43**, 147-160.

1228 **Saarikangas, J., Zhao, H., and Lappalainen, P.** (2010). Regulation of the actin cytoskeleton-  
1229 plasma membrane interplay by phosphoinositides. *Physiol. Rev.* **90**, 259-289.

1230 **Scheler, B., Schnepf, V., Galgenmüller, C., Ranf, S., and Hükelhoven, R.** (2016). Barley  
1231 disease susceptibility factor RACB acts in epidermal cell polarity and positioning of the  
1232 nucleus. *J. Exp. Bot.* **67**, 3263-3275.

1233 **Schmidt, S.M., and Panstruga, R.** (2007). Cytoskeleton functions in plant-microbe interactions.  
1234 *Physiol. Mol. Plant Pathol.* **71**, 135-148.

1235 **Senju, Y., and Lappalainen, P.** (2019). Regulation of actin dynamics by PI(4,5)P<sub>2</sub> in cell  
1236 migration and endocytosis. *Curr. Opin. Cell Biol.* **56**, 7-13.

1237 **Shimada, T.L., Betsuyaku, S., Inada, N., Ebine, K., Fujimoto, M., Uemura, T., Takano, Y.,**  
1238 **Fukuda, H., Nakano, A., and Ueda, T.** (2019). Enrichment of phosphatidylinositol 4,5-  
1239 bisphosphate in the extra-invasive hyphal membrane promotes *Colletotrichum* infection of  
1240 *Arabidopsis thaliana*. *Plant Cell Physiol.* **60**, 1514-1524.

1241 **Simon, M.L., Platre, M.P., Marquès-Bueno, M.M., Armengot, L., Stanislas, T., Bayle, V.,**  
1242 **Caillaud, M.-C., and Jaillais, Y.** (2016). A PI4P-driven electrostatic field controls cell  
1243 membrane identity and signaling in plants. *Nature plants* **2**, 16089.

1244 **Simon, M.L., Platre, M.P., Assil, S., van Wijk, R., Chen, W.Y., Chory, J., Dreux, M.,**  
1245 **Munnik, T., and Jaillais, Y.** (2014). A multi-colour/multi-affinity marker set to visualize  
1246 phosphoinositide dynamics in *Arabidopsis*. *Plant J.* **77**, 322-337.

1247 **Sousa, E., Kost, B., and Malhó, R.** (2008). *Arabidopsis* phosphatidylinositol-4-monophosphate  
1248 5-kinase 4 regulates pollen tube growth and polarity by modulating membrane recycling.  
1249 *Plant Cell* **20**, 3050-3064.

1250 **Spector, I., Shochet, N.R., Kashman, Y., and Groweiss, A.** (1983). Latrunculins: novel marine  
1251 toxins that disrupt microfilament organization in cultured cells. *Science* **219**, 493-495.

1252 **Spencer-Phillips, P., and Gay, J.** (1981). Domains of ATPase in plasma membranes and  
1253 transport through infected plant cells. *New Phytol.* **89**, 393-400.

1254 **Stanislas, T., Hüser, A., Barbosa, I.C., Kiefer, C.S., Brackmann, K., Pietra, S., Gustavsson,**  
1255 **A., Zourelidou, M., Schwechheimer, C., and Grebe, M.** (2015). *Arabidopsis* D6PK is a  
1256 lipid domain-dependent mediator of root epidermal planar polarity. *Nature plants* **1**, 15162.

1257 **Stenzel, I., Ischebeck, T., König, S., Holubowska, A., Sporysz, M., Hause, B., and Heilmann,**  
1258 **I.** (2008). The type B phosphatidylinositol-4-phosphate 5-kinase 3 is essential for root hair  
1259 formation in *Arabidopsis thaliana*. *Plant Cell* **20**, 124-141.

1260 **Tan, X., Thapa, N., Choi, S., and Anderson, R.A.** (2015). Emerging roles of PtdIns(4,5)P<sub>2</sub> -  
1261 beyond the plasma membrane. *J. Cell Sci.* **128**, 4047-4056.

1262 **Tejos, R., Sauer, M., Vanneste, S., Palacios-Gomez, M., Li, H., Heilmann, M., van Wijk, R.,**  
1263 **Vermeer, J.E., Heilmann, I., Munnik, T., et al.** (2014). Bipolar plasma membrane  
1264 distribution of phosphoinositides and their requirement for auxin-mediated cell polarity and  
1265 patterning in *Arabidopsis*. *Plant Cell* **26**, 2114-2128.

1266 **Toker, A.** (1998). The synthesis and cellular roles of phosphatidylinositol 4,5-bisphosphate. *Curr.*  
1267 *Opin. Cell Biol.* **10**, 254-261.

1268 **Trapnell, C., Roberts, A., Goff, L., Pertea, G., Kim, D., Kelley, D.R., Pimentel, H., Salzberg,**  
1269 **S.L., Rinn, J.L., and Pachter, L.** (2012). Differential gene and transcript expression analysis  
1270 of RNA-seq experiments with TopHat and Cufflinks. *Nature Protoc.* **7**, 562.

1271 **Tsuda, K., Mine, A., Bethke, G., Igarashi, D., Botanga, C.J., Tsuda, Y., Glazebrook, J.,**  
1272 **Sato, M., and Katagiri, F.** (2013). Dual regulation of gene expression mediated by extended  
1273 MAPK activation and salicylic acid contributes to robust innate immunity in *Arabidopsis*  
1274 *thaliana*. *PLoS Genet.* **9**, e1004015.

1275 **van Leeuwen, W., Vermeer, J.E., Gadella, T.W., and Munnik, T.** (2007). Visualization of  
1276 phosphatidylinositol 4,5-bisphosphate in the plasma membrane of suspension-cultured  
1277 tobacco BY-2 cells and whole *Arabidopsis* seedlings. *Plant J.* **52**, 1014-1026.

- 1278 **Van Meer, G., Voelker, D.R., and Feigenson, G.W.** (2008). Membrane lipids: where they are  
 1279 and how they behave. *Nature Rev. Mol. Cell Biol.* **9**, 112-124.
- 1280 **Vermeer, J.E., Thole, J.M., Goedhart, J., Nielsen, E., Munnik, T., and Gadella, T.W.** (2009).  
 1281 Imaging phosphatidylinositol 4-phosphate dynamics in living plant cells. *Plant J.* **57**, 356-372.
- 1282 **Vermeer, J.E., van Leeuwen, W., Tobena-Santamaria, R., Laxalt, A.M., Jones, D.R.,**  
 1283 **Divecha, N., Gadella, T.W., Jr., and Munnik, T.** (2006). Visualization of PtdIns3P  
 1284 dynamics in living plant cells. *Plant J.* **47**, 687-700.
- 1285 **Voegelé, R.T., and Mendgen, K.** (2003). Rust haustoria: nutrient uptake and beyond. *New*  
 1286 *Phytol.* **159**, 93-100.
- 1287 **Wang, W., Devoto, A., Turner, J.G., and Xiao, S.** (2007). Expression of the membrane-  
 1288 associated resistance protein RPW8 enhances basal defense against biotrophic pathogens. *Mol.*  
 1289 *Plant-Microbe Interact.* **20**, 966-976.
- 1290 **Wang, W., Wen, Y., Berkey, R., and Xiao, S.** (2009). Specific targeting of the *Arabidopsis*  
 1291 resistance protein RPW8.2 to the interfacial membrane encasing the fungal Haustorium  
 1292 renders broad-spectrum resistance to powdery mildew. *Plant Cell* **21**, 2898-2913.
- 1293 **Wang, Y.S., Yoo, C.M., and Blancaflor, E.B.** (2008). Improved imaging of actin filaments in  
 1294 transgenic *Arabidopsis* plants expressing a green fluorescent protein fusion to the C- and N-  
 1295 termini of the fimbrin actin-binding domain 2. *New Phytol.* **177**, 525-536.
- 1296 **Williams, M.E., Torabinejad, J., Cohick, E., Parker, K., Drake, E.J., Thompson, J.E.,**  
 1297 **Hortter, M., and DeWald, D.B.** (2005). Mutations in the *Arabidopsis* phosphoinositide  
 1298 phosphatase gene *SAC9* lead to overaccumulation of PtdIns(4,5)P<sub>2</sub> and constitutive expression  
 1299 of the stress-response pathway. *Plant Physiol.* **138**, 686-700.
- 1300 **Yang, G., Tang, L., Gong, Y., Xie, J., Fu, Y., Jiang, D., Li, G., Collinge, D.B., Chen, W., and**  
 1301 **Cheng, J.** (2018). A cerato-platanin protein SsCP1 targets plant PR1 and contributes to  
 1302 virulence of *Sclerotinia sclerotiorum*. *New Phytol.* **217**, 739-755.
- 1303 **Yang, L., Qin, L., Liu, G., Peremyslov, V.V., Dolja, V.V., and Wei, Y.** (2014). Myosins XI  
 1304 modulate host cellular responses and penetration resistance to fungal pathogens. *Proc. Natl.*  
 1305 *Acad. Sci. USA* **111**, 13996-14001.
- 1306 **Yi, M., and Valent, B.** (2013). Communication between filamentous pathogens and plants at the  
 1307 biotrophic interface. *Annu. Rev. Phytopathol.* **51**, 587-611.
- 1308 **Zhang, X., Henriques, R., Lin, S.-S., Niu, Q.-W., and Chua, N.-H.** (2006). *Agrobacterium*-  
 1309 mediated transformation of *Arabidopsis thaliana* using the floral dip method. *Nature Protoc.* **1**,  
 1310 641-646.

1311

1312

### 1313 **Figure Legends**

1314 **Figure 1.** Differential Targeting of Phosphoinositides to the Haustorial Periphery of the Powdery  
 1315 Mildew *E. cichoracearum*.

1316 **(A) to (C)** Leaves of *Arabidopsis* plants expressing biosensors were inoculated with *Ec* and  
 1317 viewed under the confocal microscope at 2 dpi. Fungal structures and plant cell walls were  
 1318 stained with propidium iodide (PI). ha, haustorium; en, encasement; EHM, extrahaustorial  
 1319 membrane. Scale bars, 10 μm.



1320 (A) Representative image of PI3P biosensor mCIT-2xFYVE<sup>HRS</sup>.

1321 (B) Representative images of PI4P biosensors: mCIT-1xPH<sup>FAPP1</sup>, mCIT-2xPH<sup>FAPP1</sup> and mCIT-  
1322 P4M<sup>SiDM</sup>.

1323 (C) Representative images of PI(4,5)P<sub>2</sub> biosensors: mCIT-1xPH<sup>PLCδ1</sup>, mCIT-2xPH<sup>PLCδ1</sup> and  
1324 mCIT-1xTUBBY-C.

1325 (D) Simultaneous labelling of PI(4,5)P<sub>2</sub> (mCIT-1xPH<sup>PLCδ1</sup>) and PI4P (2xCyPet-1xPH<sup>FAPP1</sup>)  
1326 during haustorium formation at 2 dpi. Scale bars, 10 μm.

1327 (E) Immunofluorescence of *Ec*-infected leaf epidermal cells with the antibodies to PI(4,5)P<sub>2</sub>  
1328 [anti-PI(4,5)P<sub>2</sub>] and PI4P (anti-PI4P). Distribution of PI(4,5)P<sub>2</sub> and PI4P in *Ec*-infected cells was  
1329 revealed by whole mount immunolocalization of leaf epidermal tissues of Arabidopsis plants at 2  
1330 dpi. Images of mock were taken in the absence of primary antibody. Asterisks indicate *Ec*  
1331 penetration sites in epidermal cells. Scale bars, 10 μm.

1332

1333 **Figure 2.** PI(4,5)P<sub>2</sub>, but not PI4P, Is Selectively Targeted to the Extrahaustorial Membrane of  
1334 Powdery Mildew.

1335 (A) Representative images of *Ec*-infected Arabidopsis epidermal cells co-expressing tonoplast  
1336 marker Tono-CFP and PIP biosensors: mCIT-2xFYVE<sup>HRS</sup> for PI3P, mCIT-2xPH<sup>FAPP1</sup> for PI4P,  
1337 or mCIT-1xPH<sup>PLCδ1</sup> for PI(4,5)P<sub>2</sub> at 2 dpi.

1338 (B) Plots show relative fluorescence intensity along the paths of dotted arrows in left panels  
1339 corresponding to (A).

1340 (C) Arabidopsis leaves co-expressing PI(4,5)P<sub>2</sub> biosensor mCIT-1xPH<sup>PLCδ1</sup> and Tono-CFP were  
1341 inoculated with *Ec* and subjected to plasmolysis at 2 dpi. Cell walls of an infected epidermal cell  
1342 were marked by dotted line. After plasmolysis, PI(4,5)P<sub>2</sub> signals retained on the haustorial  
1343 peripheral surface were indicated by arrowheads.

1344 (D) Arabidopsis leaves expressing mCIT-1xPH<sup>PLCδ1</sup>, mCIT-2xPH<sup>PLCδ1</sup>, RPW8.2-YFP, Cyto-YFP  
1345 or Tono-GFP were inoculated with *Ec* and stained by PI at 2 dpi. Arrowheads indicate the  
1346 boundary between the haustorium (ha) and the host nucleus (N). Cell wall, encasement (en) and  
1347 nucleus were stained with PI.

1348 (E) Representative images of *Ec*-infected Arabidopsis epidermal cells co-expressing EHM  
1349 marker RPW8.2-RFP and PIP biosensors: mCIT-1xPH<sup>PLCδ1</sup> and mCIT-2xPH<sup>PLCδ1</sup> for PI(4,5)P<sub>2</sub>,  
1350 mCIT-2xPH<sup>FAPP1</sup> for PI4P, or mCIT-2xFYVE<sup>HRS</sup> for PI3P at 2 dpi.

1351 (F) Diagram illustrating the distribution of host phosphoinositide species in different membrane  
1352 compartments associated with an *Ec* haustorium in infected epidermal cell. PM, plasma  
1353 membrane; EHM, extrahaustorial membrane; Tn, tonoplast; N, nucleus; en, encasement. Scale  
1354 bar, 10  $\mu\text{m}$ .

1355

1356 **Figure 3.** Cellular Trafficking Pathways Responsible for Recruiting PI(4,5)P<sub>2</sub> into the EHM.

1357 (A) and (B) Effects of pharmacological inhibitors on the targeting of PI(4,5)P<sub>2</sub> into EHM. (A)  
1358 Representative images showing the targeting of mCIT-1xPH<sup>PLC $\delta$ 1</sup> to EHM at 24 h post *Ec*  
1359 inoculation after indicated treatments. The leaves were infiltrated with Mock (H<sub>2</sub>O), 5  $\mu\text{M}$   
1360 latrunculin A (Lat-A), 1 mM oryzalin, 300  $\mu\text{M}$  BFA, 1 mM M $\beta$ CD, or 30  $\mu\text{M}$  wortmannin one  
1361 hour before inoculation with *Ec*. The haustorial neck regions are indicated by arrowheads. ha,  
1362 haustorium; EHM, extrahaustorial membrane. Scale bar, 10  $\mu\text{m}$ . (B) Quantification of relative  
1363 fluorescence intensity for mCIT-1xPH<sup>PLC $\delta$ 1</sup> at EHM. Data are normalized over the intensity at  
1364 EHM from the mock treatment. Data are means  $\pm$  SD, n = 30. Different letters indicate  
1365 statistically significant differences determined by one-way ANOVA with Tukey's HSD (p <  
1366 0.01).

1367

1368 **Figure 4.** Induced PI(4,5)P<sub>2</sub> Dynamics in Host Cells in Response to Powdery Mildew Infection.

1369 (A) Time course responses of PI(4,5)P<sub>2</sub> dynamics revealed by mCIT-1xPH<sup>PLC $\delta$ 1</sup> probe in *Ec*-  
1370 infected epidermal cells at 9 to 14 hpi. Notably, signals of mCIT-1xPH<sup>PLC $\delta$ 1</sup> were focally  
1371 accumulated underneath the penetration site initially at ~11 hpi and then targeted the EHM  
1372 during haustorial development. Asterisks indicate the penetration sites that are enlarged in insets  
1373 for close views; arrowheads indicate the EHM.

1374 (B) Enhanced production of PI(4,5)P<sub>2</sub> specifically in *Ec*-colonized cells. The lower panel is the  
1375 enlarged view of an *Ec*-colonized cell at 24 hpi, showing enhanced PI(4,5)P<sub>2</sub> signals at the EHM  
1376 as well as along PM of the infected cell. Fungal structures and plant cell walls were stained with  
1377 PI. Induced accumulation was observed in 47 of 79 *Ec*-colonized cells.

1378 (C) and (D) Association of induced PI(4,5)P<sub>2</sub> production with PM and endocytic processes in  
1379 *Ec*-colonized cells. *Ec*-inoculated leaves at 24 hpi were incubated in FM4-64 for 15 min. (C) An  
1380 *Ec*-infected (a) and a neighboring non-infected cell (b) are highlighted in dash-lined boxes. The  
1381 same inoculation sites were viewed on the peripheral surface (upper panel) or inside the cell

1382 (lower panel) of leaf epidermis. **(D)** Enlarged views of *Ec*-infected cell (a) and non-infected cells  
1383 (b). Note that PI(4,5)P<sub>2</sub> signal revealed by mCIT-1xPH<sup>PLCδ1</sup> was induced only in the *Ec*-  
1384 colonized cell, and co-localized with FM4-64-labeled endocytic PM compartments on the  
1385 peripheral surface of the infected cell.  
1386 app, appressorium; c, conidium; ha, haustorium; en, encasement. Scale bars, 10 μm.

1387

1388 **Figure 5.** Loss of PIP5K1 and PIP5K2 Functions Prevented Growth and Development of the  
1389 Compatible Powdery Mildew Fungus.

1390 **(A)** Macroscopic infection phenotypes of double (*pip5k1 pip5k2*), triple (*pip5k1 pip5k2 pip5k5*,  
1391 *pip5k1 pip5k2 pip5k8*) and quadruple (*pip5k1 pip5k2 pip5k5 pip5k8*) mutant plants at 10 dpi with  
1392 *Ec*.

1393 **(B)** Impaired growth and development of *Ec* on indicated genotypes at 7 dpi with *Ec*. Leaf  
1394 tissues were stained with aniline blue and viewed by light microscopy. Scale bars, 100 μm.

1395 **(C)** Time-course showing the development of *Ec* on mature leaves of *pip5k1 pip5k2* mutant.  
1396 Leaf tissues of wild type and *pip5k1 pip5k2* plants at 2, 5, and 7 dpi were stained with aniline  
1397 blue and viewed by light microscopy. Scale bars, 100 μm.

1398 **(D)** Reduced formation of haustoria in mutant *pip5k1 pip5k2*. Fungal structures on the leaf  
1399 surfaces (top panel) and haustoria in epidermal cells (bottom panel) at 7 dpi were stained with  
1400 Alexa Fluor 488 conjugated-WGA, while callose deposition (middle panel) was detected by  
1401 aniline blue. Images were taken under a confocal microscope with maximum projection of Z-  
1402 stacks. Scale bars, 50 μm.

1403 **(E) to (I)** Quantitative analysis of *Ec* growth on leaves of wild type and *pip5k1 pip5k2* plants. **(E)**  
1404 Penetration rate of *Ec*. More than 100 sites for each leaf were scored at 2 dpi. Data are means ±  
1405 SD, n = 4. **(F)** and **(G)** Branch numbers and total lengths of secondary hyphae per colony at 2 dpi.  
1406 Data are means ± SD, n = 75 (wt) or 31 (*pip5k1 pip5k2*). **(H)** Haustorial numbers per colony at 2  
1407 dpi. Data are means ± SD, n = 31 (wt) or 31 (*pip5k1 pip5k2*). \*\*P < 0.01, \*\*\*P < 0.001, student  
1408 *t*-test. **(I)** Number of conidiophores per colony at 7 dpi. Conidiophores were counted from at  
1409 least 30 colonies in five leaves for each genotype, which was repeated three times with similar  
1410 results. Data are means ± SD, n = 30, \*\*\*P < 0.001, student *t*-test.

1411

1412 **Figure 6.** Defense Responses in *pip5k1 pip5k2* Mutants against Powdery Mildew Infection.

1413 (A) Transcriptomic profiling of differentially expressed genes (DEGs) in salicylate and  
1414 jasmonate biosynthesis, signaling and response pathways and MAMP-signaling between *pip5k1*  
1415 *pip5k2* mutant and Col-0 plants without or with *Ec*-inoculation at 2, 5 and 7 dpi. Heatmaps  
1416 display log<sub>2</sub> fold change (log<sub>2</sub>FC) values for pairwise comparison between *pip5k1 pip5k2* mutant  
1417 and Col-0 at each time point.

1418 (B) and (C) Levels of SA and JA in Col-0 and *pip5k1 pip5k2* mutant. Total amounts of SA (B)  
1419 and JA (C) were measured in leaf tissues without or with *Ec*-inoculation at 5 dpi. Data are mean  
1420 ± SD, n = 3 biological replicates. \*P < 0.05; NS, no significant difference, student *t*-test.

1421 (D) to (F) Detection of callose deposition, H<sub>2</sub>O<sub>2</sub> accumulation and autofluorescence material  
1422 production in *Ec*-infected Col-0, *pip5k1 pip5k2* and *edr1* plants at 48 hpi. Arrowheads indicate  
1423 cell death in *edr1* mutant accompanied with callose deposition, H<sub>2</sub>O<sub>2</sub> accumulation, and  
1424 autofluorescence; c, conidia. Scale bars, 20 μm. (D) Callose deposition. *Ec*-inoculated leaves  
1425 were fixed, stained by both aniline blue and Alexa Fluor 488 conjugated-WGA. The images were  
1426 obtained by merging the confocal optical sections (Z stacks). (E) H<sub>2</sub>O<sub>2</sub> production. *Ec*-inoculated  
1427 fresh leaves were stained by DAB, fixed and viewed by compound microscopy. H<sub>2</sub>O<sub>2</sub>  
1428 accumulation was indicated by brownish color. (F) Accumulation of autofluorescence materials.  
1429 *Ec*-inoculated leaves were fixed, and the autofluorescence was directly viewed by fluorescence  
1430 microscopy.

1431

1432 **Figure 7.** Impaired Cellular Responses Associated with Host Susceptibility to Powdery Mildew  
1433 Infection in *pip5k1 pip5k2* Mutant.

1434 (A) Recruitment of MLO2-GFP into *Ec* penetration sites is impaired in *pip5k1 pip5k2*. Leaves of  
1435 Col-0 and *pip5k1 pip5k2* plants expressing MLO2:MLO2-GFP at 13 hpi were examined by  
1436 confocal microscopy. The images were obtained by merging the confocal optical sections (Z-  
1437 stacks).

1438 (B) and (C) Focal aggregation of MLO2-GFP at *Ec* penetration sites is regulated via an actin-  
1439 independent mechanism. Leaves of Col-0 plants expressing MLO2:MLO2-GFP were infiltrated  
1440 with water (Mock) or 5 μM Lat-A and subsequently inoculated with *Ec*. At 13 hpi, the infected  
1441 epidermal cells were examined by confocal microscopy. (B) Representative images obtained by  
1442 merging the confocal optical sections (Z-stacks). (C) Relative fluorescence intensity of MLO2-

1443 GFP around penetration sites. Quantification was performed over 30 sites per treatment. Data are  
1444 means  $\pm$  SD, n = 30. P = 0.665, student *t*-test.

1445 **(D-G)** Dynamics of actin filaments (AFs) at the *Ec*-penetration sites and on the peripheral  
1446 surface of haustoria in leaf tissues of Col-0 and *pip5k1 pip5k2* plants expressing GFP-ABD2-  
1447 GFP. **(D)** Spatial organization of AFs underneath the *Ec*-penetration sites at 12 hpi. **(E)** Spatial  
1448 organization of AFs on the haustorial surface during haustorial development at 20 hpi. **(F)** AFs  
1449 but not microtubules dynamically reorganized on the haustorial surface. Leaves of Col-0 plants  
1450 simultaneously expressing GFP-ABD2-GFP and mCherry-MAP4 at 20 hpi were examined by  
1451 confocal microscopy. The same inoculation sites viewed on the peripheral surface of leaf  
1452 epidermis (upper panel, Z-stacks), on haustorial surface (middle panel, Z-stacks) or on haustorial  
1453 cross-section (lower panel, single section). **(G)** Dynamic responses of AFs associated with  
1454 mature haustoria at 7 dpi.

1455 Arrowheads indicate the *Ec*-penetration site; ha, haustorium; en, encasement; app, appressorium.  
1456 Scale bars, 10  $\mu$ m.

1457

1458 **Figure 8.** Regulation of PI(4,5)P<sub>2</sub> Controls Disease Development in Plants and the Lifestyle of  
1459 the Hemibiotrophic Fungal Pathogen *C. higginsianum*.

1460 **(A)** and **(B)** Association of PI4P biosensor mCIT-2xPH<sup>FAPP1</sup>, PI(4,5)P<sub>2</sub> biosensors mCIT-  
1461 1xPH<sup>PLC $\delta$ 1</sup> and mCIT-2xPH<sup>PLC $\delta$ 1</sup> with the biotrophic stages of *Ch* life cycle. Both PI4P and  
1462 PI(4,5)P<sub>2</sub> signals targeted the surface of infection vesicles (iv) **(A)** and primary hyphae (ph) **(B)**.  
1463 Asterisks indicate the penetration sites.

1464 **(C)** Disease development on Col-0 and *pip5k1 pip5k2* plants. *Ch*-inoculated plants were  
1465 photographed at 3 and 4 dpi.

1466 **(D)** Microscopic images of *Ch*-infected leaf tissues. In *pip5k1 pip5k2* leaves, extensive bulbous  
1467 primary hyphae were restricted within the first infected epidermal cells during the infection time  
1468 course 2-4 dpi, whereas in Col-0 plants thin necrotrophic hyphae developed at 3 dpi and rapidly  
1469 spread into neighboring cells. Infected leaf tissues were stained with trypan blue.

1470 **(E)** and **(F)** Extended biotrophic stages of *Ch* infection in *pip5k1 pip5k2* mutant. **(E)** Viability of  
1471 *Ch*-infected cells at 4 dpi is shown by the host protoplasm contracting from cell wall (CW) after  
1472 plasmolysis. Right panel is the enlarged view of the boxed area in which tonoplast (TN) is

- 1473 clearly distinguishable from the PM. **(F)** Leaf sample showing the same *Ec*-infected site in **(E)**  
1474 was fixed and stained for fungal hyphae with trypan blue.  
1475 Scale bars, 20  $\mu\text{m}$ .

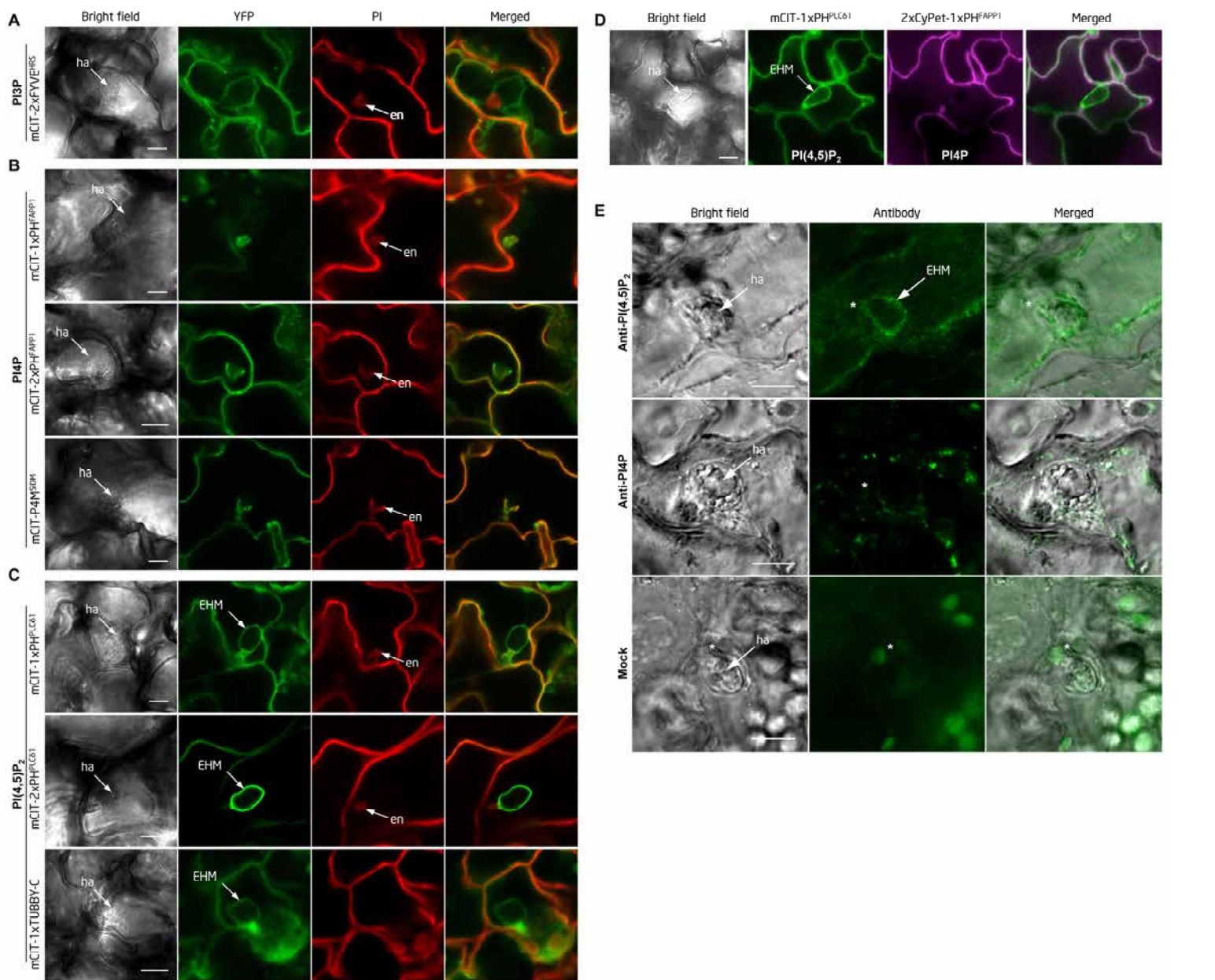


**Figure 1.** Differential Targeting of Phosphoinositides to the Haustorial Periphery of the Powdery Mildew *E. cichoracearum*.

**(A) to (C)** Leaves of *Arabidopsis* plants expressing biosensors were inoculated with *Ec* and viewed under the confocal microscope at 2 dpi. Fungal structures and plant cell walls were stained with propidium iodide (PI). ha, haustorium; en, encasement; EHM, extrahaustorial membrane. Scale bars, 10  $\mu$ m.

**(A)** Representative image of PI3P biosensor mCIT-2xFYVE<sup>HRS</sup>.

**(B)** Representative images of PI4P biosensors: mCIT-1xPH<sup>FAPP1</sup>, mCIT-2xPH<sup>FAPP1</sup> and mCIT-P4M<sup>SiDM</sup>.

**(C)** Representative images of PI(4,5)P<sub>2</sub> biosensors: mCIT-1xPH<sup>PLC $\delta$ 1</sup>, mCIT-2xPH<sup>PLC $\delta$ 1</sup> and mCIT-1xTUBBY-C.

**(D)** Simultaneous labelling of PI(4,5)P<sub>2</sub> (mCIT-1xPH<sup>PLC $\delta$ 1</sup>) and PI4P (2xCyPet-1xPH<sup>FAPP1</sup>) during haustorium formation at 2 dpi. Scale bars, 10  $\mu$ m.

**(E)** Immunofluorescence of *Ec*-infected leaf epidermal cells with the antibodies to PI(4,5)P<sub>2</sub> [anti-PI(4,5)P<sub>2</sub>] and PI4P (anti-PI4P). Distribution of PI(4,5)P<sub>2</sub> and PI4P in *Ec*-infected cells was revealed by whole mount immunolocalization of leaf epidermal tissues of *Arabidopsis* plants at 2 dpi. Images of mock were taken in the absence of primary antibody. Asterisks indicate *Ec* penetration sites in epidermal cells. Scale bars, 10  $\mu$ m.



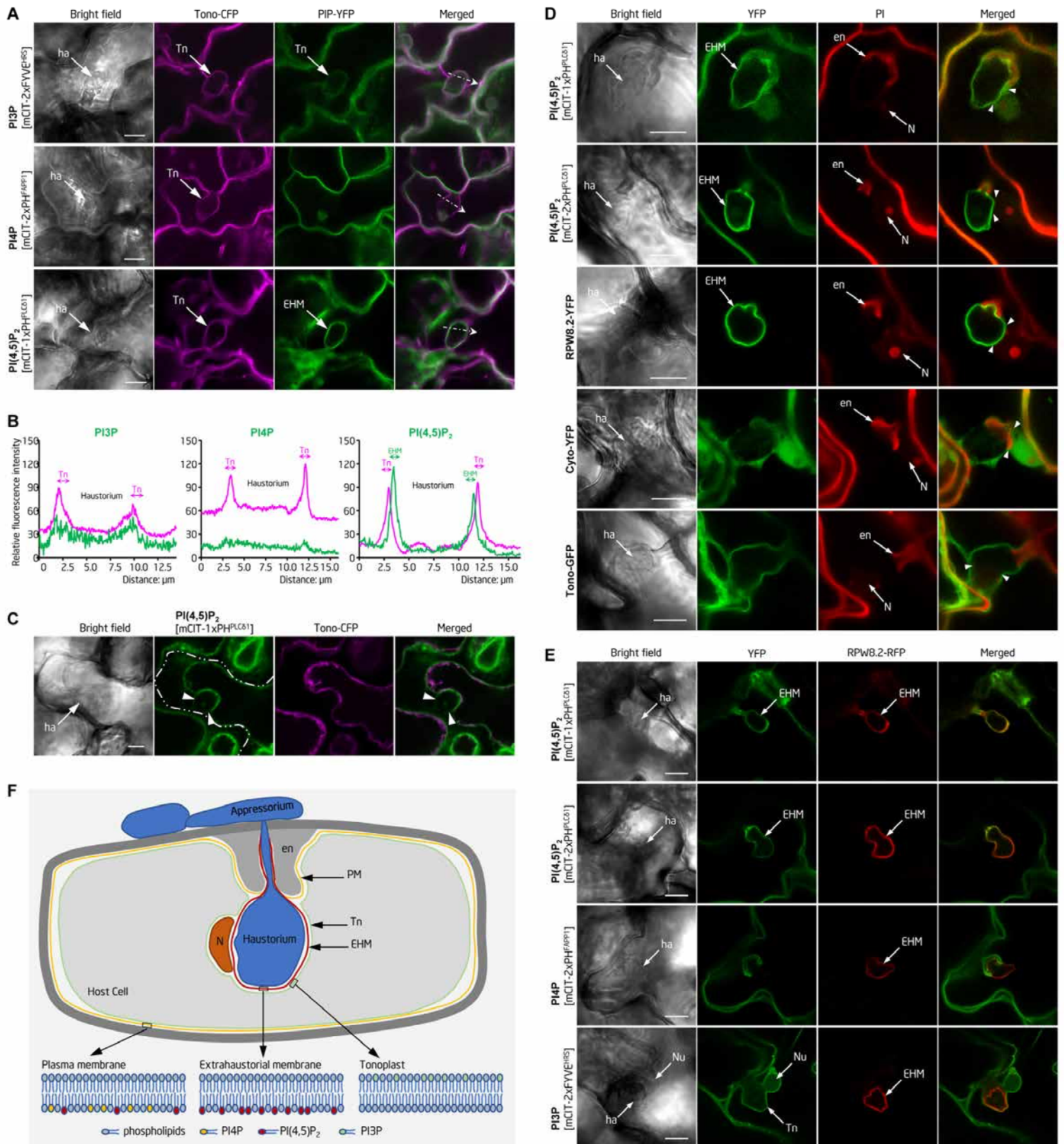


**Figure 2.** PI(4,5)P<sub>2</sub>, but not PI4P, Is Selectively Targeted to the Extrahaustorial Membrane of Powdery Mildew.

**(A)** Representative images of *Ec*-infected Arabidopsis epidermal cells co-expressing tonoplast marker Tono-CFP and PIP biosensors: mCIT-2xYVE<sup>HRS</sup> for PI3P, mCIT-2xPH<sup>FAPP1</sup> for PI4P, or mCIT-1xPH<sup>PLCδ1</sup> for PI(4,5)P<sub>2</sub> at 2 dpi.

**(B)** Plots show relative fluorescence intensity along the paths of dotted arrows in left panels corresponding to **(A)**.

**(C)** Arabidopsis leaves co-expressing PI(4,5)P<sub>2</sub> biosensor mCIT-1xPH<sup>PLCδ1</sup> and Tono-CFP were inoculated with *Ec* and subjected to plasmolysis at 2 dpi. Cell walls of an infected epidermal cell were marked by dotted line. After plasmolysis, PI(4,5)P<sub>2</sub> signals retained on the haustorial peripheral surface were indicated by arrowheads.

**(D)** Arabidopsis leaves expressing mCIT-1xPH<sup>PLCδ1</sup>, mCIT-2xPH<sup>PLCδ1</sup>, RPW8.2-YFP, Cyto-YFP or Tono-GFP were inoculated with *Ec* and stained by PI at 2 dpi. Arrowheads indicate the boundary between the haustorium (ha) and the host nucleus (N). Cell wall, encasement (en) and nucleus were stained with PI.



**(E)** Representative images of *Ec*-infected Arabidopsis epidermal cells co-expressing EHM marker RPW8.2-RFP and PIP biosensors: mCIT-1xPH<sup>PLC $\delta$ 1</sup> and mCIT-2xPH<sup>PLC $\delta$ 1</sup> for PI(4,5)P<sub>2</sub>, mCIT-2xPH<sup>FAPP1</sup> for PI4P, or mCIT-2xFYVE<sup>HRS</sup> for PI3P at 2 dpi.

**(F)** Diagram illustrating the distribution of host phosphoinositide species in different membrane compartments associated with an *Ec* haustorium in infected epidermal cell. PM, plasma membrane; EHM, extrahaustorial membrane; Tn, tonoplast; N, nucleus; en, encasement. Scale bar, 10  $\mu$ m.

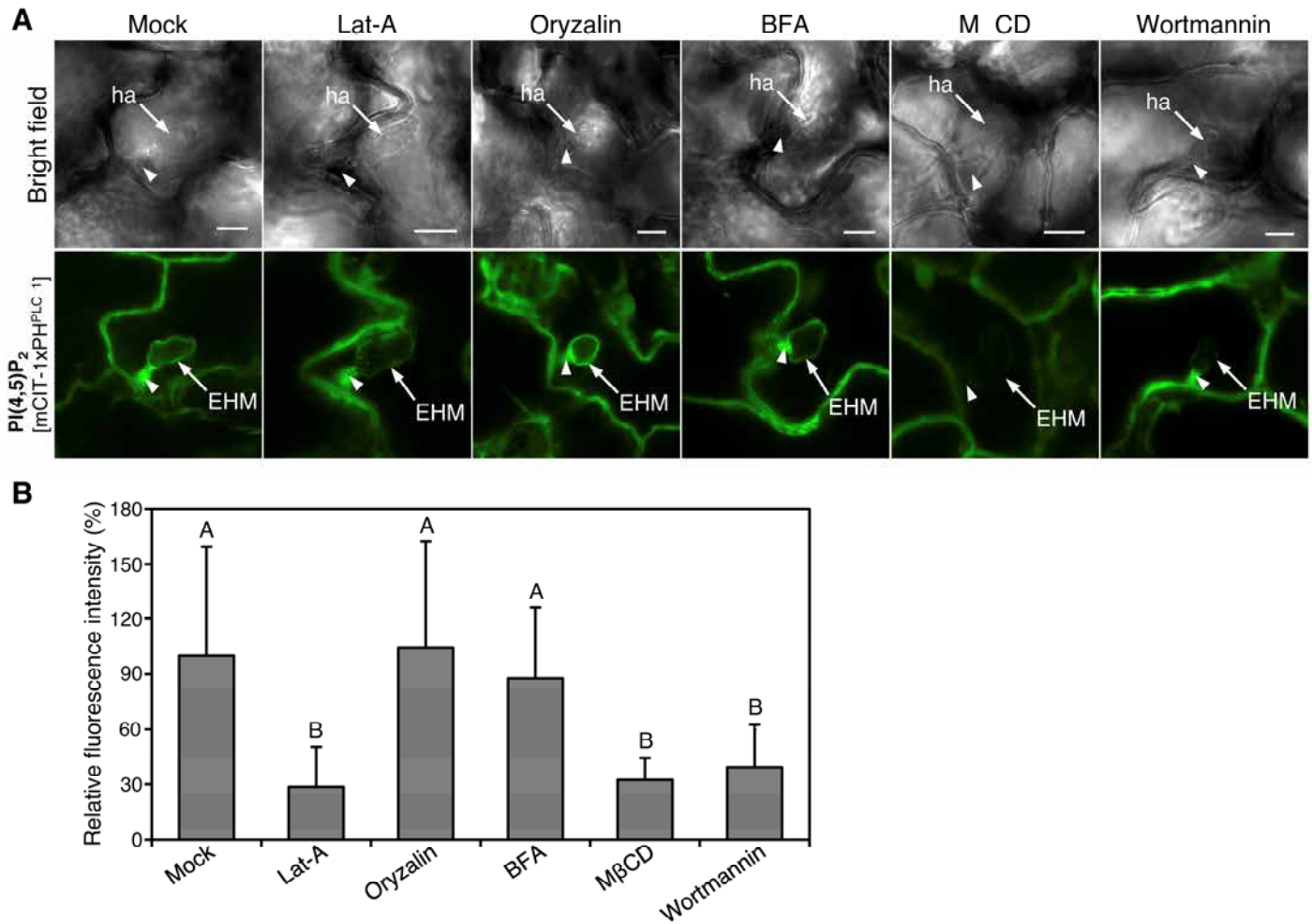


**Figure 3.** Cellular Trafficking Pathways Responsible for Recruiting PI(4,5)P<sub>2</sub> into the EHM.

**(A)** and **(B)** Effects of pharmacological inhibitors on the targeting of PI(4,5)P<sub>2</sub> into EHM. **(A)** Representative images showing the targeting of mCIT-1xPH<sup>PLCδ1</sup> to EHM at 24 h post *Ec* inoculation after indicated treatments. The leaves were infiltrated with Mock (H<sub>2</sub>O), 5 μM latrunculin A (Lat-A), 1 mM oryzalin, 300 μM BFA, 1 mM MβCD, or 30 μM wortmannin one hour before inoculation with *Ec*. The haustorial neck regions are indicated by arrowheads. ha, haustorium; EHM, extra-haustorial membrane. Scale bar, 10 μm. **(B)** Quantification of relative fluorescence intensity for mCIT-1xPH<sup>PLCδ1</sup> at EHM. Data are normalized over the intensity at EHM from the mock treatment. Data are means ± SD (n = 30). Different letters indicate statistically significant differences determined by one-way ANOVA with Tukey's HSD (p < 0.01).

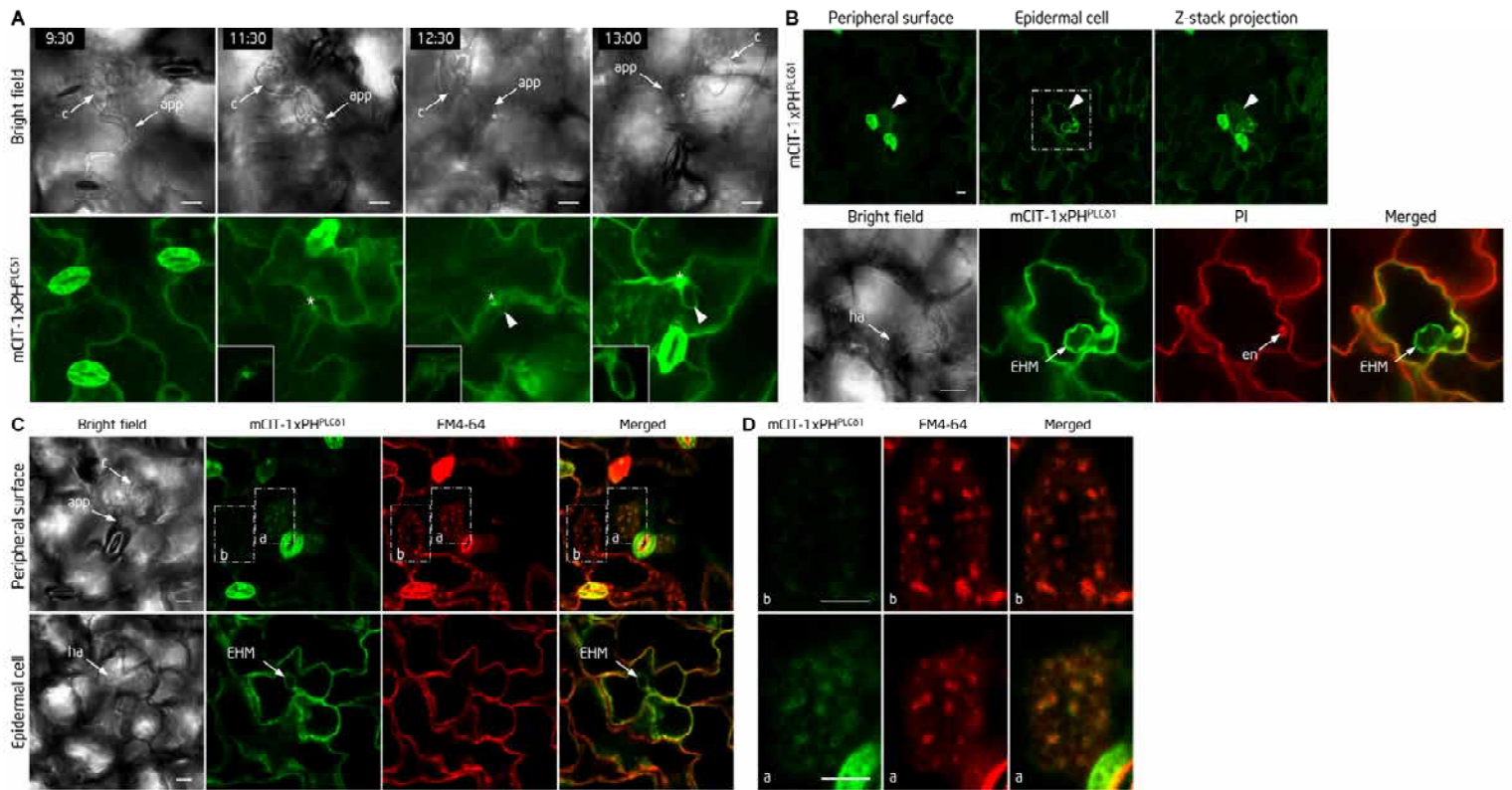


**Figure 4.** Induced PI(4,5)P<sub>2</sub> Dynamics in Host Cells in Response to Powdery Mildew Infection.

**(A)** Time course responses of PI(4,5)P<sub>2</sub> dynamics revealed by mCIT-1xPH<sup>PLCδ1</sup> probe in *Ec*-infected epidermal cells at 9 to 14 hpi. Notably, signals of mCIT-1xPH<sup>PLCδ1</sup> were focally accumulated underneath the penetration site initially at ~11 hpi and then targeted the EHM during haustorial development. Asterisks indicate the penetration sites that are enlarged in insets for close views; arrowheads indicate the EHM.

**(B)** Enhanced production of PI(4,5)P<sub>2</sub> specifically in *Ec*-colonized cells. The lower panel is the enlarged view of an *Ec*-colonized cell at 24 hpi, showing enhanced PI(4,5)P<sub>2</sub> signals at the EHM as well as along PM of the infected cell. Fungal structures and plant cell walls were stained with PI. Induced accumulation was observed in 47 of 79 *Ec*-colonized cells.

**(C)** and **(D)** Association of induced PI(4,5)P<sub>2</sub> production with PM and endocytic processes in *Ec*-colonized cells. *Ec*-inoculated leaves at 24 hpi were incubated in FM4-64 for 15 min. **(C)** An *Ec*-infected (a) and a neighboring non-infected cell (b) are highlighted in dash-lined boxes. The same inoculation sites were viewed on the peripheral surface (upper panel) or inside the cell (lower panel) of leaf epidermis. **(D)** Enlarged views of *Ec*-infected cell (a) and non-infected cells (b). Note that PI(4,5)P<sub>2</sub> signal revealed by mCIT-1xPH<sup>PLCδ1</sup> was induced only in the *Ec*-colonized cell, and co-localized with FM4-64-labeled endocytic PM compartments on the peripheral surface of the infected cell.

app, appressorium; c, conidium; ha, haustorium; en, encasement. Scale bars, 10 μm.

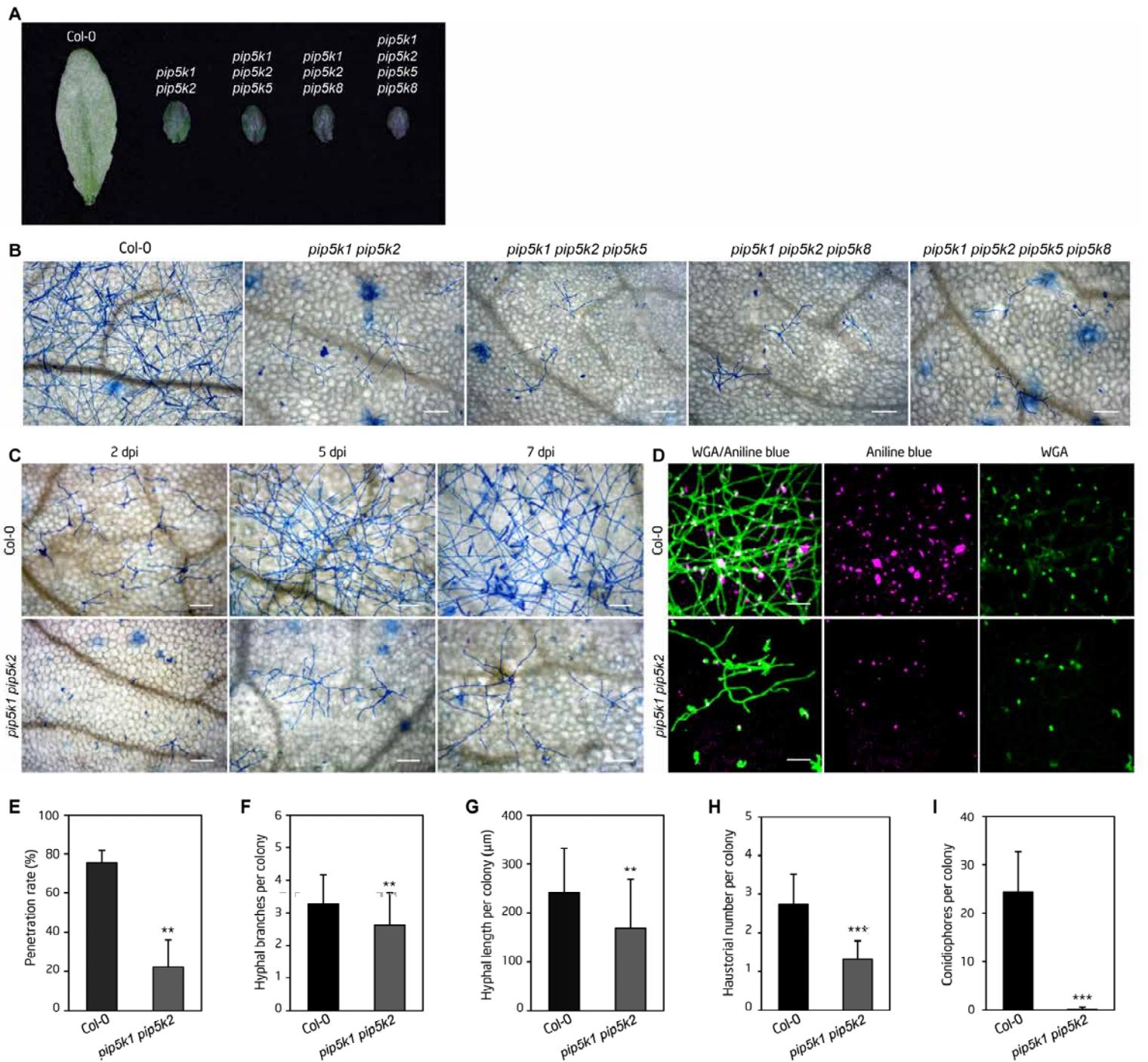


**Figure 5.** Loss of PIP5K1 and PIP5K2 Functions Prevented Growth and Development of the Compatible Powdery Mildew Fungus.

**(A)** Macroscopic infection phenotypes of double (*pip5k1 pip5k2*), triple (*pip5k1 pip5k2 pip5k5*, *pip5k1 pip5k2 pip5k8*) and quadruple (*pip5k1 pip5k2 pip5k5 pip5k8*) mutant plants at 10 dpi with *Ec*.

**(B)** Impaired growth and development of *Ec* on indicated genotypes at 7 dpi with *Ec*. Leaf tissues were stained with aniline blue and viewed by light microscopy. Scale bars, 100 μm.

**(C)** Time-course showing the development of *Ec* on mature leaves of *pip5k1 pip5k2* mutant. Leaf tissues of wild type and *pip5k1 pip5k2* plants at 2, 5, and 7 dpi were stained with aniline blue and viewed by light microscopy. Scale bars, 100 μm.

**(D)** Reduced formation of haustoria in mutant *pip5k1 pip5k2*. Fungal structures on the leaf surfaces (top panel) and haustoria in epidermal cells (bottom panel) at 7 dpi were stained with Alexa Fluor 488 conjugated-WGA, while callose deposition (middle panel) was detected by aniline blue. Images were taken under a confocal microscope with maximum projection of Z-stacks. Scale bars, 50 μm.

**(E) to (I)** Quantitative analysis of *Ec* growth on leaves of wild type and *pip5k1 pip5k2* plants. **(E)** Penetration rate of *Ec*. More than 100 sites for each leaf were scored at 2 dpi. Data are means ± SD, n = 4. **(F)** and **(G)** Branch numbers and total lengths of secondary hyphae per colony at 2 dpi. Data are means ± SD, n = 75 (wt) or 31 (*pip5k1 pip5k2*). **(H)** Haustorial numbers per colony at 2 dpi. Data are means ± SD, n = 31 (wt) or 31 (*pip5k1 pip5k2*). \*\*P < 0.01, \*\*\*P < 0.001, student *t*-test. **(I)** Number of conidiophores per colony at 7 dpi. Conidiophores were counted from at least 30 colonies in five leaves for each genotype, which was repeated three times with similar results. Data are means ± SD, n = 30, \*\*\*P < 0.001, student *t*-test.



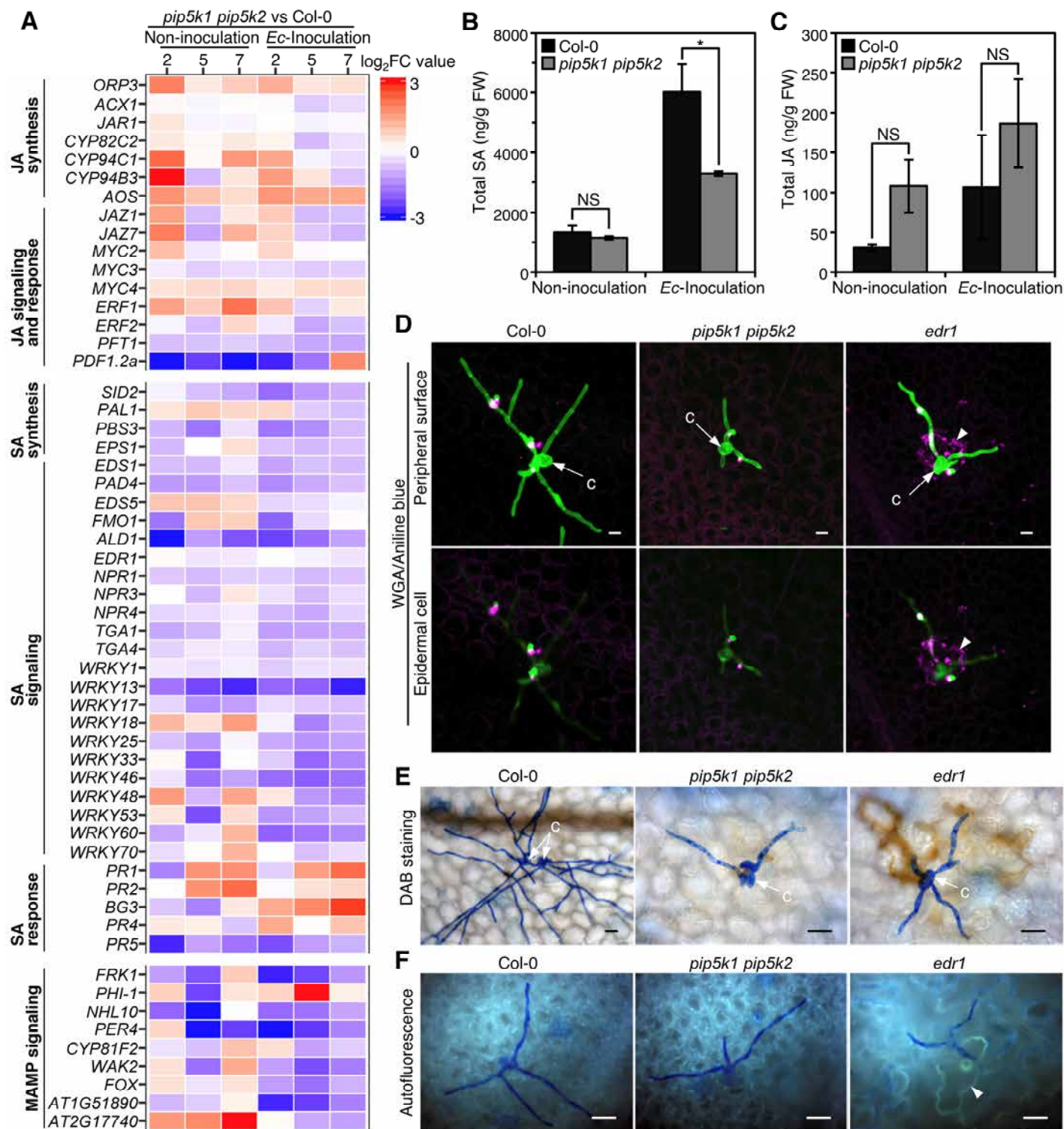


**Figure 6.** Defense Responses in *pip5k1 pip5k2* Mutants against Powdery Mildew Infection.

**(A)** Transcriptomic profiling of differentially expressed genes (DEGs) in salicylate and jasmonate biosynthesis, signaling and response pathways and MAMP-signaling between *pip5k1 pip5k2* mutant and Col-0 plants without or with *Ec*-inoculation at 2, 5 and 7 dpi. Heatmaps display  $\log_2$  fold change ( $\log_2FC$ ) values for pairwise comparison between *pip5k1 pip5k2* mutant and Col-0 at each time point.

**(B)** and **(C)** Levels of SA and JA in Col-0 and *pip5k1 pip5k2* mutant. Total amounts of SA **(B)** and JA **(C)** were measured in leaf tissues without or with *Ec*-inoculation at 5 dpi. Data are mean  $\pm$  SD,  $n = 3$  biological replicates. \* $P < 0.05$ ; NS, no significant difference, student  $t$ -test.

**(D)** to **(F)** Detection of callose deposition,  $H_2O_2$  accumulation and autofluorescence material production in *Ec*-infected Col-0, *pip5k1 pip5k2* and *edr1* plants at 48 hpi. Arrowheads indicate cell death in *edr1* mutant accompanied with callose deposition,  $H_2O_2$  accumulation, and autofluorescence; c, conidia. Scale bars, 20  $\mu m$ . **(D)** Callose deposition. *Ec*-inoculated leaves were fixed, stained by both aniline blue and Alexa Fluor 488 conjugated-WGA. The images were obtained by merging the confocal optical sections (Z stacks). **(E)**  $H_2O_2$  production. *Ec*-inoculated fresh leaves were stained by DAB, fixed and viewed by compound microscopy.  $H_2O_2$  accumulation was indicated by brownish color. **(F)** Accumulation of autofluorescence materials. *Ec*-inoculated leaves were fixed, and the autofluorescence was directly viewed by fluorescence microscopy.

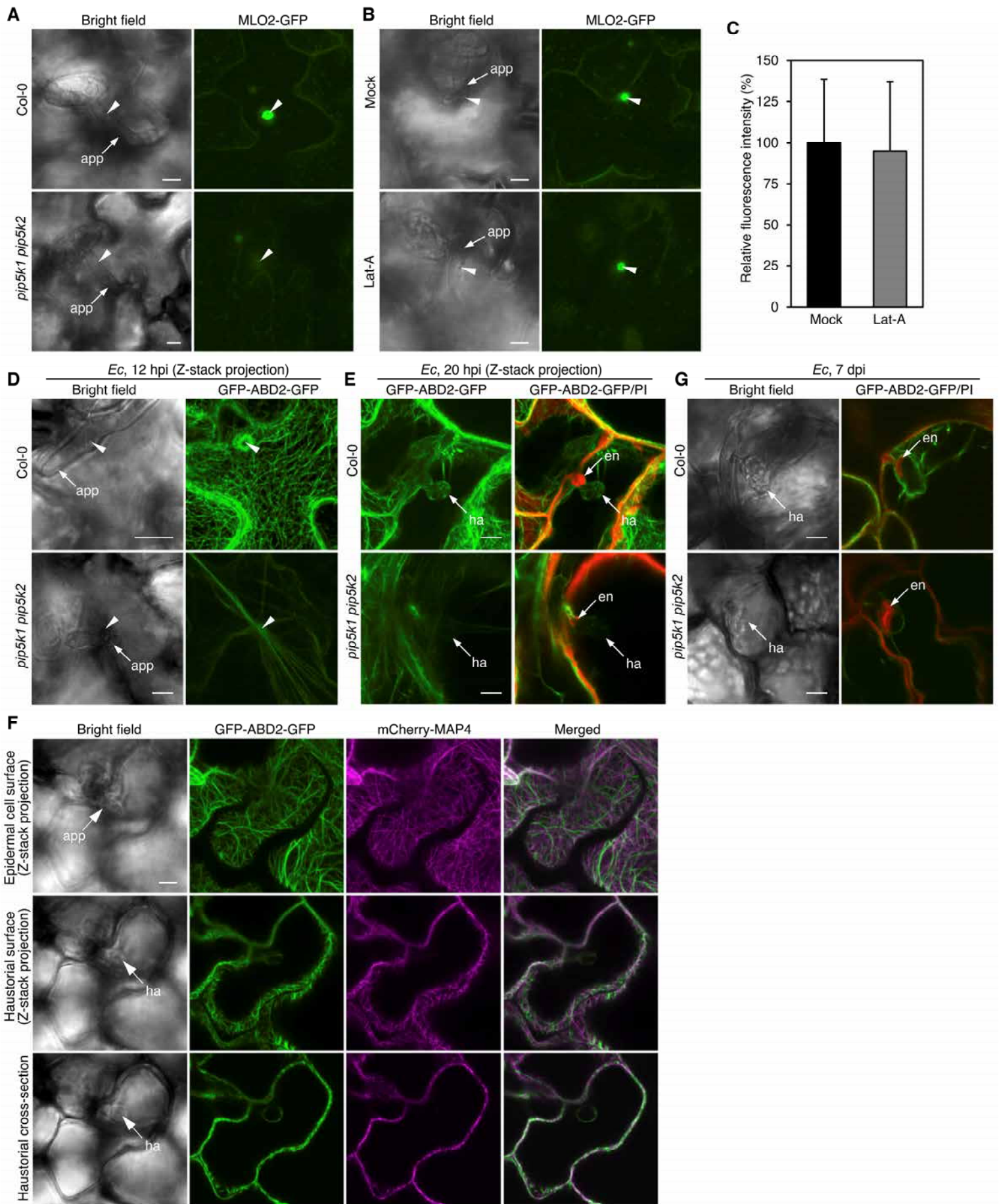


**Figure 7.** Impaired Cellular Responses Associated with Host Susceptibility to Powdery Mildew Infection in *pip5k1 pip5k2* Mutant.

**(A)** Recruitment of MLO2-GFP into *Ec* penetration sites is impaired in *pip5k1 pip5k2*. Leaves of Col-0 and *pip5k1 pip5k2* plants expressing MLO2:MLO2-GFP at 13 hpi were examined by confocal microscopy. The images were obtained by merging the confocal optical sections (Z-stacks).

**(B)** and **(C)** Focal aggregation of MLO2-GFP at *Ec* penetration sites is regulated via an actin-independent mechanism. Leaves of Col-0 plants expressing MLO2:MLO2-GFP were infiltrated with water (Mock) or 5  $\mu$ M Lat-A and subsequently inoculated with *Ec*. At 13 hpi, the infected epidermal cells were examined by confocal microscopy. **(B)** Representative images obtained by merging the confocal optical sections (Z-stacks).

**(C)** Relative fluorescence intensity of MLO2-GFP around penetration sites. Quantification was performed over 30 sites per treatment. Data are means  $\pm$  SD, n = 30. P = 0.665, student *t*-test.

**(D-G)** Dynamics of actin filaments (AFs) at the *Ec*-penetration sites and on the peripheral surface of haustoria in leaf tissues of Col-0 and *pip5k1 pip5k2* plants expressing GFP-ABD2-GFP. **(D)** Spatial organization of AFs underneath the *Ec*-penetration sites at 12 hpi. **(E)** Spatial organization of AFs on the haustorial surface during haustorial development at 20 hpi. **(F)** AFs but not microtubules dynamically reorganized on the haustorial surface. Leaves of Col-0 plants simultaneously expressing GFP-ABD2-GFP and mCherry-MAP4 at 20 hpi were examined by confocal microscopy. The same inoculation sites viewed on the peripheral surface of leaf epidermis (upper panel, Z-stacks), on haustorial surface (middle panel, Z-stacks) or on haustorial cross-section (lower panel, single section). **(G)** Dynamic responses of AFs associated with mature haustoria at 7 dpi. Arrowheads indicate the *Ec*-penetration site; ha, haustorium; en, encasement; app, appressorium. Scale bars, 10  $\mu$ m.



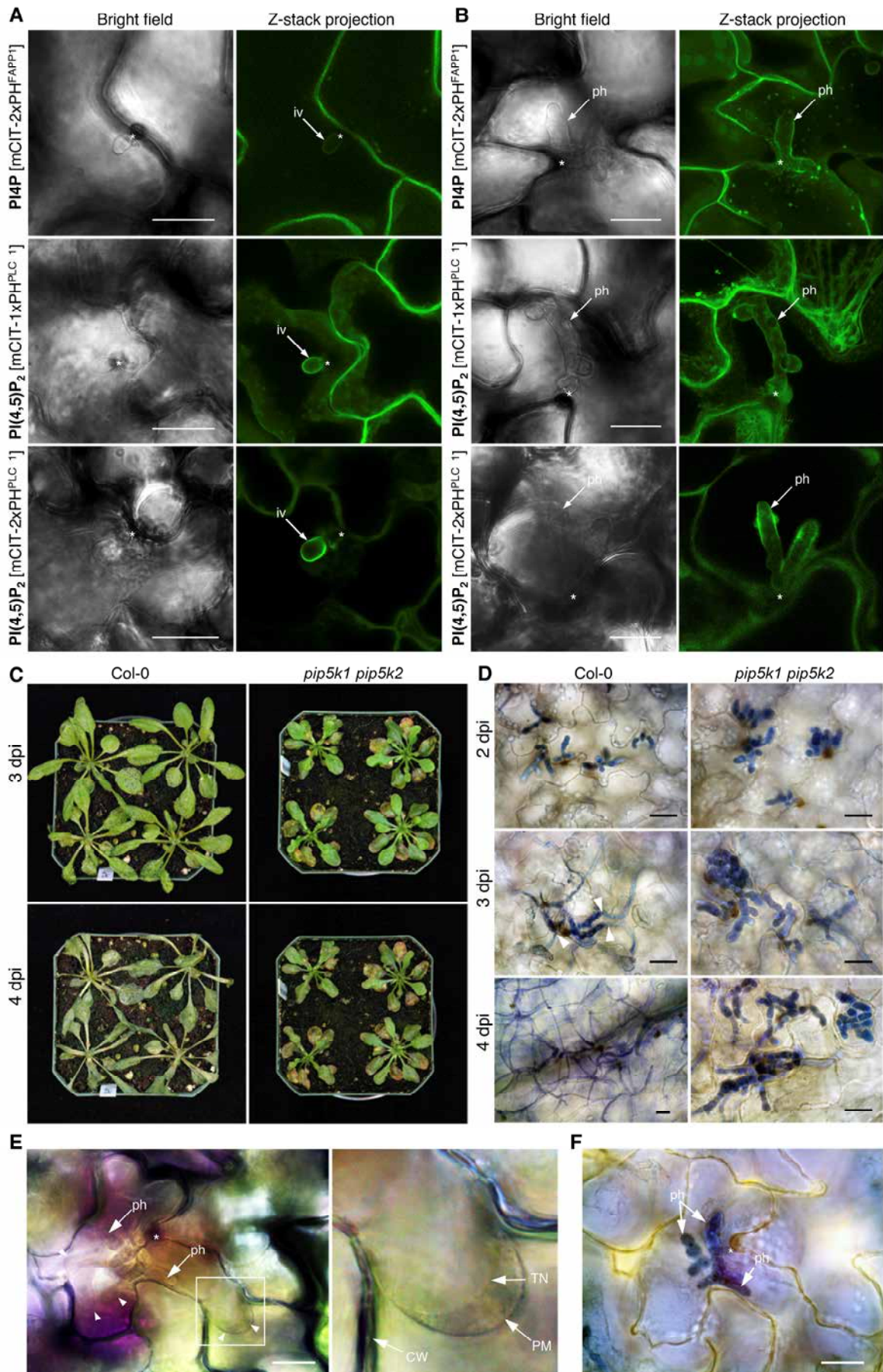


**Figure 8.** Regulation of PI(4,5)P<sub>2</sub> Controls Disease Development in Plants and the Lifestyle of the Hemibiotrophic Fungal Pathogen *C. higginsianum*.



**(A)** and **(B)** Association of PI4P biosensor mCIT-2xPH<sup>FAPP1</sup>, PI(4,5)P<sub>2</sub> biosensors mCIT-1xPH<sup>PLCδ1</sup> and mCIT-2xPH<sup>PLCδ1</sup> with the biotrophic stages of *Ch* life cycle. Both PI4P and PI(4,5)P<sub>2</sub> signals targeted the surface of infection vesicles (iv) **(A)** and primary hyphae (ph) **(B)**. Asterisks indicate the penetration sites.

**(C)** Disease development on Col-0 and *pip5k1 pip5k2* plants. *Ch*-inoculated plants were photographed at 3 and 4 dpi.

**(D)** Microscopic images of *Ch*-infected leaf tissues. In *pip5k1 pip5k2* leaves, extensive bulbous primary hyphae were restricted within the first infected epidermal cells during the infection time course 2-4 dpi, whereas in Col-0 plants thin necrotrophic hyphae developed at 3 dpi and rapidly spread into neighboring cells. Infected leaf tissues were stained with trypan blue.

**(E)** and **(F)** Extended biotrophic stages of *Ch* infection in *pip5k1 pip5k2* mutant. **(E)** Viability of *Ch*-infected cells at 4 dpi is shown by the host protoplasm contracting from cell wall (CW) after plasmolysis. Right panel is the enlarged view of the boxed area in which tonoplast (TN) is clearly distinguishable from the PM. **(F)** Leaf sample showing the same *Ec*-infected site in **(E)** was fixed and stained for fungal hyphae with trypan blue.

Scale bars, 20 μm.

## Parsed Citations

- Anders, S., Pyl, P.T., and Huber, W. (2015). HTSeq-a Python framework to work with high-throughput sequencing data. *Bioinformatics* 31, 166-169.  
Pubmed: [Author and Title](#)  
Google Scholar: [Author Only Title Only Author and Title](#)
- Asai, T., Tena, G., Plotnikova, J., Willmann, M.R., Chiu, W.-L., Gomez-Gomez, L., Boller, T., Ausubel, F.M., and Sheen, J. (2002). MAP kinase signalling cascade in *Arabidopsis* innate immunity. *Nature* 415, 977-983.  
Pubmed: [Author and Title](#)  
Google Scholar: [Author Only Title Only Author and Title](#)
- Berkey, R., Zhang, Y., Ma, X., King, H., Zhang, Q., Wang, W., and Xiao, S. (2017). Homologues of the RPW8 resistance protein are localized to the extrahaustorial membrane that is likely synthesized de novo. *Plant Physiol.* 173, 600-613.  
Pubmed: [Author and Title](#)  
Google Scholar: [Author Only Title Only Author and Title](#)
- Bhat, R.A., Miklis, M., Schmelzer, E., Schulze-Lefert, P., and Panstruga, R. (2005). Recruitment and interaction dynamics of plant penetration resistance components in a plasma membrane microdomain. *Proc. Natl. Acad. Sci. USA* 102, 3135-3140.  
Pubmed: [Author and Title](#)  
Google Scholar: [Author Only Title Only Author and Title](#)
- Bolger, A.M., Lohse, M., and Usadel, B. (2014). Trimmomatic: a flexible trimmer for Illumina sequence data. *Bioinformatics* 30, 2114-2120.  
Pubmed: [Author and Title](#)  
Google Scholar: [Author Only Title Only Author and Title](#)
- Borhan, M.H., Brose, E., Beynon, J.L., and Holub, E.B. (2001). White rust (*Albugo candida*) resistance loci on three *Arabidopsis* chromosomes are closely linked to downy mildew (*Peronospora parasitica*) resistance loci. *Mol. Plant Pathol.* 2, 87-95.  
Pubmed: [Author and Title](#)  
Google Scholar: [Author Only Title Only Author and Title](#)
- Boudsocq, M., Willmann, M.R., McCormack, M., Lee, H., Shan, L., He, P., Bush, J., Cheng, S.H., and Sheen, J. (2010). Differential innate immune signalling via Ca<sup>2+</sup> sensor protein kinases. *Nature* 464, 418-422.  
Pubmed: [Author and Title](#)  
Google Scholar: [Author Only Title Only Author and Title](#)
- Capasso, S., and D'Angelo, G. (2019). Imaging lipid metabolism at the Golgi complex. In *Intracellular Lipid Transport: Methods and Protocols*, G. Drin, ed (New York, NY: Springer New York), pp. 47-56.  
Pubmed: [Author and Title](#)  
Google Scholar: [Author Only Title Only Author and Title](#)
- Catanzariti, A.-M., Dodds, P.N., Lawrence, G.J., Ayliffe, M.A., and Ellis, J.G. (2006). Haustorially expressed secreted proteins from flax rust are highly enriched for avirulence elicitors. *Plant Cell* 18, 243-256.  
Pubmed: [Author and Title](#)  
Google Scholar: [Author Only Title Only Author and Title](#)
- Celio, G., Mims, C., and Richardson, E. (2004). Ultrastructure and immunocytochemistry of the host pathogen interface in poinsettia leaves infected with powdery mildew. *Can. J. Bot.* 82, 421-429.  
Pubmed: [Author and Title](#)  
Google Scholar: [Author Only Title Only Author and Title](#)
- Choi, S., Thapa, N., Tan, X., Hedman, A.C., and Anderson, R.A. (2015). PIP kinases define PI4,5P2 signaling specificity by association with effectors. *BBA-Mol. Cell Biol. L.* 1851, 711-723.  
Pubmed: [Author and Title](#)  
Google Scholar: [Author Only Title Only Author and Title](#)
- Cockcroft, S., and Raghu, P. (2018). Phospholipid transport protein function at organelle contact sites. *Curr. Opin. Cell Biol.* 53, 52-60.  
Pubmed: [Author and Title](#)  
Google Scholar: [Author Only Title Only Author and Title](#)
- Colin, L.A., and Jaillais, Y. (2020). Phospholipids across scales: lipid patterns and plant development. *Curr. Opin. Plant Biol.* 53, 1-9.  
Pubmed: [Author and Title](#)  
Google Scholar: [Author Only Title Only Author and Title](#)
- Consonni, C., Humphry, M.E., Hartmann, H.A., Livaja, M., Durner, J., Westphal, L., Vogel, J., Lipka, V., Kemmerling, B., Schulze-Lefert, P., et al. (2006). Conserved requirement for a plant host cell protein in powdery mildew pathogenesis. *Nature Genet.* 38, 716-720.  
Pubmed: [Author and Title](#)  
Google Scholar: [Author Only Title Only Author and Title](#)
- Cutler, N.S., Heitman, J., and Cardenas, M.E. (1997). STT4 is an essential phosphatidylinositol 4-kinase that is a target of wortmannin in *Saccharomyces cerevisiae*. *J. Biol. Chem.* 272, 27671-27677.  
Pubmed: [Author and Title](#)  
Google Scholar: [Author Only Title Only Author and Title](#)

- Cutler, S.R., Ehrhardt, D.W., Griffiths, J.S., and Somerville, C.R. (2000). Random GFP::cDNA fusions enable visualization of subcellular structures in cells of *Arabidopsis* at a high frequency. *Proc. Natl. Acad. Sci. USA* 97, 3718-3723.  
Pubmed: [Author and Title](#)  
Google Scholar: [Author Only](#) [Title Only](#) [Author and Title](#)
- DeBono, A, Yeats, T.H., Rose, J.K., Bird, D., Jetter, R., Kunst, L., and Samuels, L. (2009). *Arabidopsis* LTPG is a glycosylphosphatidylinositol-anchored lipid transfer protein required for export of lipids to the plant surface. *Plant Cell* 21, 1230-1238.  
Pubmed: [Author and Title](#)  
Google Scholar: [Author Only](#) [Title Only](#) [Author and Title](#)
- Dobin, A, Davis, C.A, Schlesinger, F., Drenkow, J., Zaleski, C., Jha, S., Batut, P., Chaisson, M., and Gingeras, T.R. (2013). STAR: ultrafast universal RNA-seq aligner. *Bioinformatics* 29, 15-21.  
Pubmed: [Author and Title](#)  
Google Scholar: [Author Only](#) [Title Only](#) [Author and Title](#)
- El Zawily, A.M., Schwarzlander, M., Finkemeier, I., Johnston, I.G., Benamar, A, Cao, Y., Gissot, C., Meyer, A.J., Wilson, K., Datla, R., et al. (2014). FRIENDLY regulates mitochondrial distribution, fusion, and quality control in *Arabidopsis*. *Plant Physiol.* 166, 808-828.  
Pubmed: [Author and Title](#)  
Google Scholar: [Author Only](#) [Title Only](#) [Author and Title](#)
- Feechan, A, Jermakow, A.M., Ivancevic, A, Godfrey, D., Pak, H., Panstruga, R., and Dry, I.B. (2013). Host cell entry of powdery mildew is correlated with endosomal transport of antagonistically acting VvPEN1 and VvMLO to the papilla. *Mol. Plant-Microbe Interact.* 26, 1138-1150.  
Pubmed: [Author and Title](#)  
Google Scholar: [Author Only](#) [Title Only](#) [Author and Title](#)
- Frye, C.A, and Innes, R.W. (1998). An *Arabidopsis* mutant with enhanced resistance to powdery mildew. *Plant Cell* 10, 947-956.  
Pubmed: [Author and Title](#)  
Google Scholar: [Author Only](#) [Title Only](#) [Author and Title](#)
- Galán, J.E., and Collmer, A (1999). Type III secretion machines: bacterial devices for protein delivery into host cells. *Science* 284, 1322-1328.  
Pubmed: [Author and Title](#)  
Google Scholar: [Author Only](#) [Title Only](#) [Author and Title](#)
- Galán, J.E., and Zhou, D. (2000). Striking a balance: modulation of the actin cytoskeleton by *Salmonella*. *Proc. Natl. Acad. Sci. USA* 97, 8754-8761.  
Pubmed: [Author and Title](#)  
Google Scholar: [Author Only](#) [Title Only](#) [Author and Title](#)
- Geldner, N., Denervaud-Tendon, V., Hyman, D.L., Mayer, U., Stierhof, Y.D., and Chory, J. (2009). Rapid, combinatorial analysis of membrane compartments in intact plants with a multicolor marker set. *Plant J.* 59, 169-178.  
Pubmed: [Author and Title](#)  
Google Scholar: [Author Only](#) [Title Only](#) [Author and Title](#)
- Geldner, N., Anders, N., Wolters, H., Keicher, J., Kornberger, W., Muller, P., Delbarre, A, Ueda, T., Nakano, A, and Jürgens, G. (2003). The *Arabidopsis* GNOM ARF-GEF mediates endosomal recycling, auxin transport, and auxin-dependent plant growth. *Cell* 112, 219-230.  
Pubmed: [Author and Title](#)  
Google Scholar: [Author Only](#) [Title Only](#) [Author and Title](#)
- Gil, F., and Gay, J.L. (1977). Ultrastructural and physiological properties of the host interfacial components of haustoria of *Erysiphe pisi* in vivo and in vitro. *Physiol. Plant Pathol.* 10, 1-12.  
Pubmed: [Author and Title](#)  
Google Scholar: [Author Only](#) [Title Only](#) [Author and Title](#)
- Gillaspy, G.E. (2013). The role of phosphoinositides and inositol phosphates in plant cell signaling. *Adv. Exp. Med. Biol.* 991, 141-157.  
Pubmed: [Author and Title](#)  
Google Scholar: [Author Only](#) [Title Only](#) [Author and Title](#)
- Gouin, E., Welch, M.D., and Cossart, P. (2005). Actin-based motility of intracellular pathogens. *Curr. Opin. Microbiol.* 8, 35-45.  
Pubmed: [Author and Title](#)  
Google Scholar: [Author Only](#) [Title Only](#) [Author and Title](#)
- Graber, Z.T., Gericke, A, and Kooijman, E.E. (2014). Phosphatidylinositol-4,5-bisphosphate ionization in the presence of cholesterol, calcium or magnesium ions. *Chem. Phys. Lipids* 182, 62-72.  
Pubmed: [Author and Title](#)  
Google Scholar: [Author Only](#) [Title Only](#) [Author and Title](#)
- Hahn, M., and Mendgen, K. (2001). Signal and nutrient exchange at biotrophic plant-fungus interfaces. *Curr. Opin. Plant Biol.* 4, 322-327.  
Pubmed: [Author and Title](#)  
Google Scholar: [Author Only](#) [Title Only](#) [Author and Title](#)
- Hammond, G.R., Schiavo, G., and Irvine, R.F. (2009). Immunocytochemical techniques reveal multiple, distinct cellular pools of PtdIns4P and PtdIns(4,5)P2. *Biochem. J.* 422, 23-35.

- Pubmed: [Author and Title](#)  
Google Scholar: [Author Only Title Only Author and Title](#)
- Hammond, G.R., Machner, M.P., and Balla, T. (2014).** A novel probe for phosphatidylinositol 4-phosphate reveals multiple pools beyond the Golgi. *J. Cell Biol.* 205, 113-126.  
Pubmed: [Author and Title](#)  
Google Scholar: [Author Only Title Only Author and Title](#)
- Hammond, G.R., Fischer, M.J., Anderson, K.E., Holdich, J., Koteci, A., Balla, T., and Irvine, R.F. (2012).** PI4P and PI(4,5)P2 are essential but independent lipid determinants of membrane identity. *Science* 337, 727-730.  
Pubmed: [Author and Title](#)  
Google Scholar: [Author Only Title Only Author and Title](#)
- Hammond, G.R.V., Dove, S.K., Nicol, A., Pinxteren, J.A., Zicha, D., and Schiavo, G. (2006).** Elimination of plasma membrane phosphatidylinositol (4,5)-bisphosphate is required for exocytosis from mast cells. *J. Cell Sci.* 119, 2084-2094.  
Pubmed: [Author and Title](#)  
Google Scholar: [Author Only Title Only Author and Title](#)
- Hauck, P., Thilmony, R., and He, S.Y. (2003).** A *Pseudomonas syringae* type III effector suppresses cell wall-based extracellular defense in susceptible *Arabidopsis* plants. *Proc. Natl. Acad. Sci. USA* 100, 8577-8582.  
Pubmed: [Author and Title](#)  
Google Scholar: [Author Only Title Only Author and Title](#)
- He, P., Shan, L., Lin, N.C., Martin, G.B., Kemmerling, B., Nurnberger, T., and Sheen, J. (2006).** Specific bacterial suppressors of MAMP signaling upstream of MAPKKK in *Arabidopsis* innate immunity. *Cell* 125, 563-575.  
Pubmed: [Author and Title](#)  
Google Scholar: [Author Only Title Only Author and Title](#)
- Heath, M.C. (1997).** Signalling between pathogenic rust fungi and resistant or susceptible host plants. *Ann. Bot.* 80, 713-720.  
Pubmed: [Author and Title](#)  
Google Scholar: [Author Only Title Only Author and Title](#)
- Heilmann, M., and Heilmann, I. (2015).** Plant phosphoinositides-complex networks controlling growth and adaptation. *BBA-Mol. Cell Biol. L.* 1851, 759-769.  
Pubmed: [Author and Title](#)  
Google Scholar: [Author Only Title Only Author and Title](#)
- Hempel, F., Stenzel, I., Heilmann, M., Krishnamoorthy, P., Menzel, W., Golbik, R., Helm, S., Dobritsch, D., Baginsky, S., Lee, J., et al. (2017).** MAPKs influence pollen tube growth by controlling the formation of phosphatidylinositol 4,5-bisphosphate in an apical plasma membrane domain. *Plant Cell* 29, 3030-3050.  
Pubmed: [Author and Title](#)  
Google Scholar: [Author Only Title Only Author and Title](#)
- Hruz, T., Laule, O., Szabo, G., Wessendorp, F., Bleuler, S., Oertle, L., Widmayer, P., Gruissem, W., and Zimmermann, P. (2008).** Genevestigator v3: a reference expression database for the meta-analysis of transcriptomes. *Adv. Bioinf.* 2008, 420747.  
Pubmed: [Author and Title](#)  
Google Scholar: [Author Only Title Only Author and Title](#)
- Inada, N., Betsuyaku, S., Shimada, T.L., Ebine, K., Ito, E., Kutsuna, N., Hasezawa, S., Takano, Y., Fukuda, H., Nakano, A., et al. (2016).** Modulation of plant RAB GTPase-mediated membrane trafficking pathway at the interface between plants and obligate biotrophic pathogens. *Plant Cell Physiol.* 57, 1854-1864.  
Pubmed: [Author and Title](#)  
Google Scholar: [Author Only Title Only Author and Title](#)
- Ischebeck, T., Stenzel, I., and Heilmann, I. (2008).** Type B phosphatidylinositol-4-phosphate 5-kinases mediate *Arabidopsis* and *Nicotiana tabacum* pollen tube growth by regulating apical pectin secretion. *Plant Cell* 20, 3312-3330.  
Pubmed: [Author and Title](#)  
Google Scholar: [Author Only Title Only Author and Title](#)
- Ischebeck, T., Vu, L.H., Jin, X., Stenzel, I., Löffke, C., and Heilmann, I. (2010).** Functional cooperativity of enzymes of phosphoinositide conversion according to synergistic effects on pectin secretion in tobacco pollen tubes. *Molecular Plant* 3, 870-881.  
Pubmed: [Author and Title](#)  
Google Scholar: [Author Only Title Only Author and Title](#)
- Ischebeck, T., Stenzel, I., Hempel, F., Jin, X., Mosblech, A., and Heilmann, I. (2011).** Phosphatidylinositol-4,5-bisphosphate influences Nt-Rac5-mediated cell expansion in pollen tubes of *Nicotiana tabacum*. *Plant J.* 65, 453-468.  
Pubmed: [Author and Title](#)  
Google Scholar: [Author Only Title Only Author and Title](#)
- Ischebeck, T., Werner, S., Krishnamoorthy, P., Lerche, J., Meijón, M., Stenzel, I., Löffke, C., Wiessner, T., Im, Y.J., Perera, I.Y., et al. (2013).** Phosphatidylinositol 4,5-bisphosphate influences PIN polarization by controlling clathrin-mediated membrane trafficking in *Arabidopsis*. *Plant Cell* 25, 4894-4911.  
Pubmed: [Author and Title](#)  
Google Scholar: [Author Only Title Only Author and Title](#)

- Ivanov, S., and Harrison, M.J. (2019). Accumulation of phosphoinositides in distinct regions of the periarbuscular membrane. *New Phytol.* 221, 2213-2227.  
Pubmed: [Author and Title](#)  
Google Scholar: [Author Only Title Only Author and Title](#)
- Jelinkova, A, Malinska, K., Simon, S., Kleine-Vehn, J., Parezova, M., Pejchar, P., Kubes, M., Martinec, J., Friml, J., Zazimalova, E., et al. (2010). Probing plant membranes with FM dyes: tracking, dragging or blocking? *Plant J.* 61, 883-892.  
Pubmed: [Author and Title](#)  
Google Scholar: [Author Only Title Only Author and Title](#)
- Jha, S.G., Larson, E.R., Humble, J., Domozych, D.S., Barrington, D.S., and Tierney, M.L. (2018). Vacuolar Protein Sorting 26C encodes an evolutionarily conserved large retromer subunit in eukaryotes that is important for root hair growth in *Arabidopsis thaliana*. *Plant J.* 94, 595-611.  
Pubmed: [Author and Title](#)  
Google Scholar: [Author Only Title Only Author and Title](#)
- Jones, D.S., Yuan, J., Smith, B.E., Willoughby, A.C., Kumimoto, E.L., and Kessler, S.A. (2017). MILDEWRESISTANCE LOCUS O function in pollen tube reception is linked to its oligomerization and subcellular distribution. *Plant Physiol.* 175, 172-185.  
Pubmed: [Author and Title](#)  
Google Scholar: [Author Only Title Only Author and Title](#)
- Koh, S., Andre, A., Edwards, H., Ehrhardt, D., and Somerville, S. (2005). *Arabidopsis thaliana* subcellular responses to compatible *Erysiphe cichoracearum* infections. *Plant J.* 44, 516-529.  
Pubmed: [Author and Title](#)  
Google Scholar: [Author Only Title Only Author and Title](#)
- Krinke, O., Ruelland, E., Valentová, O., Vergnolle, C., Renou, J.-P., Taconnat, L., Flemr, M., Burketová, L., and Zachowski, A. (2007). Phosphatidylinositol 4-kinase activation is an early response to salicylic acid in *Arabidopsis* suspension cells. *Plant Physiol.* 144, 1347-1359.  
Pubmed: [Author and Title](#)  
Google Scholar: [Author Only Title Only Author and Title](#)
- Krishnamoorthy, P., Sanchez-Rodriguez, C., Heilmann, I., and Persson, S. (2014). Regulatory roles of phosphoinositides in membrane trafficking and their potential impact on cell-wall synthesis and re-modelling. *Ann. Bot.* 114, 1049-1057.  
Pubmed: [Author and Title](#)  
Google Scholar: [Author Only Title Only Author and Title](#)
- Kusano, H., Testerink, C., Vermeer, J.E., Tsuge, T., Shimada, H., Oka, A., Munnik, T., and Aoyama, T. (2008). The *Arabidopsis* phosphatidylinositol phosphate 5-kinase PIP5K3 is a key regulator of root hair tip growth. *Plant Cell* 20, 367-380.  
Pubmed: [Author and Title](#)  
Google Scholar: [Author Only Title Only Author and Title](#)
- Kusch, S., and Panstruga, R. (2017). mlo-based resistance: an apparently universal "weapon" to defeat powdery mildew disease. *Mol. Plant-Microbe Interact.* 30, 179-189.  
Pubmed: [Author and Title](#)  
Google Scholar: [Author Only Title Only Author and Title](#)
- Kwaaitaal, M., Nielsen, M.E., Böhlenius, H., and Thordal-Christensen, H. (2017). The plant membrane surrounding powdery mildew haustoria shares properties with the endoplasmic reticulum membrane. *J. Exp. Bot.* 68, 5731-5743.  
Pubmed: [Author and Title](#)  
Google Scholar: [Author Only Title Only Author and Title](#)
- Lee, E., Vanneste, S., Pérez-Sancho, J., Benitez-Fuente, F., Strelau, M., Macho, A.P., Botella, M.A., Friml, J., and Rosado, A. (2019). Ionic stress enhances ER-PM connectivity via phosphoinositide-associated SYT1 contact site expansion in *Arabidopsis*. *Proceedings of the National Academy of Sciences* 116, 1420-1429.  
Pubmed: [Author and Title](#)  
Google Scholar: [Author Only Title Only Author and Title](#)
- Lee, Y., Kim, Y.W., Jeon, B.W., Park, K.Y., Suh, S.J., Seo, J., Kwak, J.M., Martinoia, E., Hwang, I., and Lee, Y. (2007). Phosphatidylinositol 4,5-bisphosphate is important for stomatal opening. *Plant J.* 52, 803-816.  
Pubmed: [Author and Title](#)  
Google Scholar: [Author Only Title Only Author and Title](#)
- Lefebvre, B., Batoko, H., Duby, G., and Boutry, M. (2004). Targeting of a *Nicotiana plumbaginifolia* H<sup>+</sup>-ATPase to the plasma membrane is not by default and requires cytosolic structural determinants. *Plant Cell* 16, 1772-1789.  
Pubmed: [Author and Title](#)  
Google Scholar: [Author Only Title Only Author and Title](#)
- Lenoir, M., and Overduin, M. (2013). PtdIns(4)P signalling and recognition systems. *Adv. Exp. Med. Biol.* 991, 59-83.  
Pubmed: [Author and Title](#)  
Google Scholar: [Author Only Title Only Author and Title](#)
- Littlefield, L.J., and Bracker, C.E. (1970). Continuity of host plasma membrane around haustoria of *Melampsora lini*. *Mycologia* 62, 609-614.

- Pubmed: [Author and Title](#)  
Google Scholar: [Author Only Title Only Author and Title](#)
- Liu, G., Greenshields, D.L., Sammynaiken, R., Hirji, R.N., Selvaraj, G., and Wei, Y. (2007a).** Targeted alterations in iron homeostasis underlie plant defense responses. *J. Cell Sci.* 120, 596-605.  
Pubmed: [Author and Title](#)  
Google Scholar: [Author Only Title Only Author and Title](#)
- Liu, G., Kennedy, R., Greenshields, D.L., Peng, G., Forseille, L., Selvaraj, G., and Wei, Y. (2007b).** Detached and attached *Arabidopsis* leaf assays reveal distinctive defense responses against hemibiotrophic *Colletotrichum* spp. *Mol. Plant-Microbe Interact.* 20, 1308-1319.  
Pubmed: [Author and Title](#)  
Google Scholar: [Author Only Title Only Author and Title](#)
- Liu, G., Ji, Y., Bhuiyan, N.H., Pilot, G., Selvaraj, G., Zou, J., and Wei, Y. (2010).** Amino acid homeostasis modulates salicylic acid-associated redox status and defense responses in *Arabidopsis*. *Plant Cell* 22, 3845-3863.  
Pubmed: [Author and Title](#)  
Google Scholar: [Author Only Title Only Author and Title](#)
- Lo Presti, L., Lanver, D., Schweizer, G., Tanaka, S., Liang, L., Tollot, M., Zuccaro, A., Reissmann, S., and Kahmann, R. (2015).** Fungal effectors and plant susceptibility. *Annu. Rev. Plant Biol.* 66, 513-545.  
Pubmed: [Author and Title](#)  
Google Scholar: [Author Only Title Only Author and Title](#)
- Love, M.I., Huber, W., and Anders, S. (2014).** Moderated estimation of fold change and dispersion for RNA-seq data with DESeq2. *Genome Biol.* 15, 1.  
Pubmed: [Author and Title](#)  
Google Scholar: [Author Only Title Only Author and Title](#)
- Makowski, S.L., Tran, T.T., and Field, S.J. (2017).** Emerging themes of regulation at the Golgi. *Curr. Opin. Cell Biol.* 45, 17-23.  
Pubmed: [Author and Title](#)  
Google Scholar: [Author Only Title Only Author and Title](#)
- Matsuoka, K., Bassham, D.C., Raikhel, N.V., and Nakamura, K. (1995).** Different sensitivity to wortmannin of two vacuolar sorting signals indicates the presence of distinct sorting machineries in tobacco cells. *J. Cell Biol.* 130, 1307-1318.  
Pubmed: [Author and Title](#)  
Google Scholar: [Author Only Title Only Author and Title](#)
- Mei, Y., Jia, W.-J., Chu, Y.-J., and Xue, H.-W. (2012).** *Arabidopsis* phosphatidylinositol monophosphate 5-kinase 2 is involved in root gravitropism through regulation of polar auxin transport by affecting the cycling of PIN proteins. *Cell Res.* 22, 581-597.  
Pubmed: [Author and Title](#)  
Google Scholar: [Author Only Title Only Author and Title](#)
- Micali, C.O., Neumann, U., Grunewald, D., Panstruga, R., and O'Connell, R. (2011).** Biogenesis of a specialized plant-fungal interface during host cell internalization of *Golovinomyces orontii* haustoria. *Cell Microbiol.* 13, 210-226.  
Pubmed: [Author and Title](#)  
Google Scholar: [Author Only Title Only Author and Title](#)
- Miklis, M., Consonni, C., Bhat, R.A., Lipka, V., Schulze-Lefert, P., and Panstruga, R. (2007).** Barley MLO modulates actin-dependent and actin-independent antifungal defense pathways at the cell periphery. *Plant Physiol.* 144, 1132-1143.  
Pubmed: [Author and Title](#)  
Google Scholar: [Author Only Title Only Author and Title](#)
- Morejohn, L.C. (1991).** The molecular pharmacology of plant tubulin and microtubules. In *The Cytoskeletal Basis of Plant Growth and Form*, C.W. Loyd, ed (London: Academic), pp. 29-43.  
Pubmed: [Author and Title](#)  
Google Scholar: [Author Only Title Only Author and Title](#)
- Moseley, J.B., and Goode, B.L. (2006).** The yeast actin cytoskeleton: from cellular function to biochemical mechanism. *Microbiol. Mol. Biol. Rev.* 70, 605-645.  
Pubmed: [Author and Title](#)  
Google Scholar: [Author Only Title Only Author and Title](#)
- Mueller-Roeber, B., and Pical, C. (2002).** Inositol phospholipid metabolism in *Arabidopsis*. Characterized and putative isoforms of inositol phospholipid kinase and phosphoinositide-specific phospholipase C. *Plant Physiol.* 130, 22-46.  
Pubmed: [Author and Title](#)  
Google Scholar: [Author Only Title Only Author and Title](#)
- Munnik, T., and Vermeer, J.E. (2010).** Osmotic stress-induced phosphoinositide and inositol phosphate signalling in plants. *Plant Cell Environ.* 33, 655-669.  
Pubmed: [Author and Title](#)  
Google Scholar: [Author Only Title Only Author and Title](#)
- Munnik, T., and Nielsen, E. (2011).** Green light for polyphosphoinositide signals in plants. *Curr. Opin. Plant Biol.* 14, 489-497.  
Pubmed: [Author and Title](#)



Google Scholar: [Author Only](#) [Title Only](#) [Author and Title](#)

**Nakanishi, S., Catt, K.J., and Balla, T. (1995).** A wortmannin-sensitive phosphatidylinositol 4-kinase that regulates hormone-sensitive pools of inositolphospholipids. *Proc. Natl. Acad. Sci. USA* 92, 5317-5321.

Pubmed: [Author and Title](#)

Google Scholar: [Author Only](#) [Title Only](#) [Author and Title](#)

**Nelson, B.K., Cai, X., and Nebenführ, A. (2007).** A multicolored set of in vivo organelle markers for co-localization studies in *Arabidopsis* and other plants. *Plant J.* 51, 1126-1136.

Pubmed: [Author and Title](#)

Google Scholar: [Author Only](#) [Title Only](#) [Author and Title](#)

**Nielsen, M.E., Feechan, A., Bohlenius, H., Ueda, T., and Thordal-Christensen, H. (2012).** *Arabidopsis* ARF-GTP exchange factor, GNOM, mediates transport required for innate immunity and focal accumulation of syntaxin PEN1. *Proc. Natl. Acad. Sci. USA* 109, 11443-11448.

Pubmed: [Author and Title](#)

Google Scholar: [Author Only](#) [Title Only](#) [Author and Title](#)

**Noack, L.C., and Jaillais, Y. (2017).** Precision targeting by phosphoinositides: how PIs direct endomembrane trafficking in plants. *Curr. Opin. Plant Biol.* 40, 22-33.

Pubmed: [Author and Title](#)

Google Scholar: [Author Only](#) [Title Only](#) [Author and Title](#)

**Nomura, K., Mecey, C., Lee, Y.-N., Imboden, L.A., Chang, J.H., and He, S.Y. (2011).** Effector-triggered immunity blocks pathogen degradation of an immunity-associated vesicle traffic regulator in *Arabidopsis*. *Proc. Natl. Acad. Sci. USA* 108, 10774-10779.

Pubmed: [Author and Title](#)

Google Scholar: [Author Only](#) [Title Only](#) [Author and Title](#)

**Ohtani, Y., Irie, T., Uekama, K., Fukunaga, K., and Pitha, J. (1989).** Differential effects of  $\alpha$ -,  $\beta$ - and  $\gamma$ -cyclodextrins on human erythrocytes. *Eur. J. Biochem.* 186, 17-22.

Pubmed: [Author and Title](#)

Google Scholar: [Author Only](#) [Title Only](#) [Author and Title](#)

**Opalski, K.S., Schultheiss, H., Kogel, K.H., and Hückelhoven, R. (2005).** The receptor-like MLO protein and the RAC/ROP family G-protein RACB modulate actin reorganization in barley attacked by the biotrophic powdery mildew fungus *Blumeria graminis* f.sp. *hordei*. *Plant J.* 41, 291-303.

Pubmed: [Author and Title](#)

Google Scholar: [Author Only](#) [Title Only](#) [Author and Title](#)

**Pertea, M., Pertea, G.M., Antonescu, C.M., Chang, T.-C., Mendell, J.T., and Salzberg, S.L. (2015).** StringTie enables improved reconstruction of a transcriptome from RNA-seq reads. *Nature Biotechnol.* 33, 290.

Pubmed: [Author and Title](#)

Google Scholar: [Author Only](#) [Title Only](#) [Author and Title](#)

**Pike, L.J., and Miller, J.M. (1998).** Cholesterol depletion delocalizes phosphatidylinositol bisphosphate and inhibits hormone-stimulated phosphatidylinositol turnover. *J. Biol. Chem.* 273, 22298-22304.

Pubmed: [Author and Title](#)

Google Scholar: [Author Only](#) [Title Only](#) [Author and Title](#)

**Platre, M.P., and Jaillais, Y. (2016).** Guidelines for the use of protein domains in acidic phospholipid imaging. *Methods Mol. Biol.* 1376, 175-194.

Pubmed: [Author and Title](#)

Google Scholar: [Author Only](#) [Title Only](#) [Author and Title](#)

**Pollard, T.D. (2007).** Regulation of actin filament assembly by Arp2/3 complex and formins. *Annu. Rev. Biophys. Biomol. Struct.* 36, 451-477.

Pubmed: [Author and Title](#)

Google Scholar: [Author Only](#) [Title Only](#) [Author and Title](#)

**Richter, S., Kientz, M., Brumm, S., Nielsen, M.E., Park, M., Gavidia, R., Krause, C., Voss, U., Beckmann, H., Mayer, U., et al. (2014).** Delivery of endocytosed proteins to the cell-division plane requires change of pathway from recycling to secretion. *eLife* 3, e02131.

Pubmed: [Author and Title](#)

Google Scholar: [Author Only](#) [Title Only](#) [Author and Title](#)

**Roberts, A.M., Mackie, A.J., Hathaway, V., Callow, J.A., and Green, J.R. (1993).** Molecular differentiation in the extrahaustorial membrane of pea powdery mildew haustoria at early and late stages of development. *Physiol. Mol. Plant Pathol.* 43, 147-160.

Pubmed: [Author and Title](#)

Google Scholar: [Author Only](#) [Title Only](#) [Author and Title](#)

**Saarikangas, J., Zhao, H., and Lappalainen, P. (2010).** Regulation of the actin cytoskeleton-plasma membrane interplay by phosphoinositides. *Physiol. Rev.* 90, 259-289.

Pubmed: [Author and Title](#)

Google Scholar: [Author Only](#) [Title Only](#) [Author and Title](#)

**Scheler, B., Schnepf, V., Galgenmüller, C., Ranf, S., and Hückelhoven, R. (2016).** Barley disease susceptibility factor RACB acts in epidermal cell polarity and positioning of the nucleus. *J. Exp. Bot.* 67, 3263-3275.

- Pubmed: [Author and Title](#)  
Google Scholar: [Author Only Title Only Author and Title](#)
- Schmidt, S.M., and Panstruga, R. (2007).** Cytoskeleton functions in plant-microbe interactions. *Physiol. Mol. Plant Pathol.* 71, 135-148.  
Pubmed: [Author and Title](#)  
Google Scholar: [Author Only Title Only Author and Title](#)
- Senju, Y., and Lappalainen, P. (2019).** Regulation of actin dynamics by PI(4,5)P2 in cell migration and endocytosis. *Curr. Opin. Cell Biol.* 56, 7-13.  
Pubmed: [Author and Title](#)  
Google Scholar: [Author Only Title Only Author and Title](#)
- Shimada, T.L., Betsuyaku, S., Inada, N., Ebine, K., Fujimoto, M., Uemura, T., Takano, Y., Fukuda, H., Nakano, A., and Ueda, T. (2019).** Enrichment of phosphatidylinositol 4,5-bisphosphate in the extra-invasive hyphal membrane promotes *Colletotrichum* infection of *Arabidopsis thaliana*. *Plant Cell Physiol.* 60, 1514-1524.  
Pubmed: [Author and Title](#)  
Google Scholar: [Author Only Title Only Author and Title](#)
- Simon, M.L., Platre, M.P., Marquès-Bueno, M.M., Armengot, L., Stanislas, T., Bayle, V., Caillaud, M.-C., and Jaillais, Y. (2016).** A PI4P-driven electrostatic field controls cell membrane identity and signaling in plants. *Nature plants* 2, 16089.  
Pubmed: [Author and Title](#)  
Google Scholar: [Author Only Title Only Author and Title](#)
- Simon, M.L., Platre, M.P., Assil, S., van Wijk, R., Chen, W.Y., Chory, J., Dreux, M., Munnik, T., and Jaillais, Y. (2014).** A multi-colour/multi-affinity marker set to visualize phosphoinositide dynamics in *Arabidopsis*. *Plant J.* 77, 322-337.  
Pubmed: [Author and Title](#)  
Google Scholar: [Author Only Title Only Author and Title](#)
- Sousa, E., Kost, B., and Malhó, R. (2008).** *Arabidopsis* phosphatidylinositol-4-monophosphate 5-kinase 4 regulates pollen tube growth and polarity by modulating membrane recycling. *Plant Cell* 20, 3050-3064.  
Pubmed: [Author and Title](#)  
Google Scholar: [Author Only Title Only Author and Title](#)
- Spector, I., Shochet, N.R., Kashman, Y., and Groweiss, A. (1983).** Latrunculins: novel marine toxins that disrupt microfilament organization in cultured cells. *Science* 219, 493-495.  
Pubmed: [Author and Title](#)  
Google Scholar: [Author Only Title Only Author and Title](#)
- Spencer-Phillips, P., and Gay, J. (1981).** Domains of ATPase in plasma membranes and transport through infected plant cells. *New Phytol.* 89, 393-400.  
Pubmed: [Author and Title](#)  
Google Scholar: [Author Only Title Only Author and Title](#)
- Stanislas, T., Hüser, A., Barbosa, I.C., Kiefer, C.S., Brackmann, K., Pietra, S., Gustavsson, A., Zourelidou, M., Schwechheimer, C., and Grebe, M. (2015).** *Arabidopsis* D6PK is a lipid domain-dependent mediator of root epidermal planar polarity. *Nature plants* 1, 15162.  
Pubmed: [Author and Title](#)  
Google Scholar: [Author Only Title Only Author and Title](#)
- Stenzel, I., Ischebeck, T., König, S., Holubowska, A., Sporysz, M., Hause, B., and Heilmann, I. (2008).** The type B phosphatidylinositol-4-phosphate 5-kinase 3 is essential for root hair formation in *Arabidopsis thaliana*. *Plant Cell* 20, 124-141.  
Pubmed: [Author and Title](#)  
Google Scholar: [Author Only Title Only Author and Title](#)
- Tan, X., Thapa, N., Choi, S., and Anderson, R.A. (2015).** Emerging roles of PtdIns(4,5)P2 - beyond the plasma membrane. *J. Cell Sci.* 128, 4047-4056.  
Pubmed: [Author and Title](#)  
Google Scholar: [Author Only Title Only Author and Title](#)
- Tejos, R., Sauer, M., Vanneste, S., Palacios-Gomez, M., Li, H., Heilmann, M., van Wijk, R., Vermeer, J.E., Heilmann, I., Munnik, T., et al. (2014).** Bipolar plasma membrane distribution of phosphoinositides and their requirement for auxin-mediated cell polarity and patterning in *Arabidopsis*. *Plant Cell* 26, 2114-2128.  
Pubmed: [Author and Title](#)  
Google Scholar: [Author Only Title Only Author and Title](#)
- Toker, A. (1998).** The synthesis and cellular roles of phosphatidylinositol 4,5-bisphosphate. *Curr. Opin. Cell Biol.* 10, 254-261.  
Pubmed: [Author and Title](#)  
Google Scholar: [Author Only Title Only Author and Title](#)
- Trapnell, C., Roberts, A., Goff, L., Pertea, G., Kim, D., Kelley, D.R., Pimentel, H., Salzberg, S.L., Rinn, J.L., and Pachter, L. (2012).** Differential gene and transcript expression analysis of RNA-seq experiments with TopHat and Cufflinks. *Nature Protoc.* 7, 562.  
Pubmed: [Author and Title](#)  
Google Scholar: [Author Only Title Only Author and Title](#)
- Tsuda, K., Mine, A., Bethke, G., Igarashi, D., Botanga, C.J., Tsuda, Y., Glazebrook, J., Sato, M., and Katagiri, F. (2013).** Dual regulation of gene expression mediated by extended MAPK activation and salicylic acid contributes to robust innate immunity in *Arabidopsis*



**thaliana.** *PLoS Genet.* **9**, e1004015.

Pubmed: [Author and Title](#)

Google Scholar: [Author Only Title Only Author and Title](#)

**van Leeuwen, W., Vermeer, J.E., Gadella, T.W., and Munnik, T. (2007).** Visualization of phosphatidylinositol 4,5-bisphosphate in the plasma membrane of suspension-cultured tobacco BY-2 cells and whole *Arabidopsis* seedlings. *Plant J.* **52**, 1014-1026.

Pubmed: [Author and Title](#)

Google Scholar: [Author Only Title Only Author and Title](#)

**Van Meer, G., Voelker, D.R., and Feigenson, G.W. (2008).** Membrane lipids: where they are and how they behave. *Nature Rev. Mol. Cell Biol.* **9**, 112-124.

Pubmed: [Author and Title](#)

Google Scholar: [Author Only Title Only Author and Title](#)

**Vermeer, J.E., Thole, J.M., Goedhart, J., Nielsen, E., Munnik, T., and Gadella, T.W. (2009).** Imaging phosphatidylinositol 4-phosphate dynamics in living plant cells. *Plant J.* **57**, 356-372.

Pubmed: [Author and Title](#)

Google Scholar: [Author Only Title Only Author and Title](#)

**Vermeer, J.E., van Leeuwen, W., Tobena-Santamaria, R., Laxalt, A.M., Jones, D.R., Divecha, N., Gadella, T.W., Jr., and Munnik, T. (2006).** Visualization of PtdIns3P dynamics in living plant cells. *Plant J.* **47**, 687-700.

Pubmed: [Author and Title](#)

Google Scholar: [Author Only Title Only Author and Title](#)

**Voegelé, R.T., and Mendgen, K. (2003).** Rust haustoria: nutrient uptake and beyond. *New Phytol.* **159**, 93-100.

Pubmed: [Author and Title](#)

Google Scholar: [Author Only Title Only Author and Title](#)

**Wang, W., Devoto, A., Turner, J.G., and Xiao, S. (2007).** Expression of the membrane-associated resistance protein RPW8 enhances basal defense against biotrophic pathogens. *Mol. Plant-Microbe Interact.* **20**, 966-976.

Pubmed: [Author and Title](#)

Google Scholar: [Author Only Title Only Author and Title](#)

**Wang, W., Wen, Y., Berkey, R., and Xiao, S. (2009).** Specific targeting of the *Arabidopsis* resistance protein RPW8.2 to the interfacial membrane encasing the fungal Haustorium renders broad-spectrum resistance to powdery mildew. *Plant Cell* **21**, 2898-2913.

Pubmed: [Author and Title](#)

Google Scholar: [Author Only Title Only Author and Title](#)

**Wang, Y.S., Yoo, C.M., and Blancaflor, E.B. (2008).** Improved imaging of actin filaments in transgenic *Arabidopsis* plants expressing a green fluorescent protein fusion to the C- and N-termini of the fimbrin actin-binding domain 2. *New Phytol.* **177**, 525-536.

Pubmed: [Author and Title](#)

Google Scholar: [Author Only Title Only Author and Title](#)

**Williams, M.E., Torabinejad, J., Cohick, E., Parker, K., Drake, E.J., Thompson, J.E., Hortter, M., and DeWald, D.B. (2005).** Mutations in the *Arabidopsis* phosphoinositide phosphatase gene SAC9 lead to overaccumulation of PtdIns(4,5)P<sub>2</sub> and constitutive expression of the stress-response pathway. *Plant Physiol.* **138**, 686-700.

Pubmed: [Author and Title](#)

Google Scholar: [Author Only Title Only Author and Title](#)

**Yang, G., Tang, L., Gong, Y., Xie, J., Fu, Y., Jiang, D., Li, G., Collinge, D.B., Chen, W., and Cheng, J. (2018).** A cerato-platanin protein SsCP1 targets plant PR1 and contributes to virulence of *Sclerotinia sclerotiorum*. *New Phytol.* **217**, 739-755.

Pubmed: [Author and Title](#)

Google Scholar: [Author Only Title Only Author and Title](#)

**Yang, L., Qin, L., Liu, G., Peremyslov, V.V., Dolja, V.V., and Wei, Y. (2014).** Myosins XI modulate host cellular responses and penetration resistance to fungal pathogens. *Proc. Natl. Acad. Sci. USA* **111**, 13996-14001.

Pubmed: [Author and Title](#)

Google Scholar: [Author Only Title Only Author and Title](#)

**Yi, M., and Valent, B. (2013).** Communication between filamentous pathogens and plants at the biotrophic interface. *Annu. Rev. Phytopathol.* **51**, 587-611.

Pubmed: [Author and Title](#)

Google Scholar: [Author Only Title Only Author and Title](#)

**Zhang, X., Henriques, R., Lin, S.-S., Niu, Q.-W., and Chua, N.-H. (2006).** Agrobacterium-mediated transformation of *Arabidopsis thaliana* using the floral dip method. *Nature Protoc.* **1**, 641-646.

Pubmed: [Author and Title](#)

Google Scholar: [Author Only Title Only Author and Title](#)

**Specific Recruitment of Phosphoinositide Species to the Plant-Pathogen Interfacial Membrane Underlies Arabidopsis Susceptibility to Fungal Infection**

Li Qin, Zhuqing Zhou, Qiang Li, Chun Zhai, Lijiang Liu, Teagen D Quilichini, Peng Gao, Sharon A Kessler, Yvon Jaillais, Raju Datla, Gary Peng, Daoquan Xiang and Yangdou Wei

*Plant Cell*; originally published online March 10, 2020;

DOI 10.1105/tpc.19.00970

This information is current as of March 10, 2020

<b>Supplemental Data</b>	<a href="/content/suppl/2020/03/10/tpc.19.00970.DC1.html">/content/suppl/2020/03/10/tpc.19.00970.DC1.html</a>
<b>Permissions</b>	<a href="https://www.copyright.com/ccc/openurl.do?sid=pd_hw1532298X&amp;issn=1532298X&amp;WT.mc_id=pd_hw1532298X">https://www.copyright.com/ccc/openurl.do?sid=pd_hw1532298X&amp;issn=1532298X&amp;WT.mc_id=pd_hw1532298X</a>
<b>eTOCs</b>	Sign up for eTOCs at: <a href="http://www.plantcell.org/cgi/alerts/ctmain">http://www.plantcell.org/cgi/alerts/ctmain</a>
<b>CiteTrack Alerts</b>	Sign up for CiteTrack Alerts at: <a href="http://www.plantcell.org/cgi/alerts/ctmain">http://www.plantcell.org/cgi/alerts/ctmain</a>
<b>Subscription Information</b>	Subscription Information for <i>The Plant Cell</i> and <i>Plant Physiology</i> is available at: <a href="http://www.aspb.org/publications/subscriptions.cfm">http://www.aspb.org/publications/subscriptions.cfm</a>